INSIGHTS INTO THE METABOLIC REGULATION OF GROWTH AND PROLIFERATION IN SACCHAROMYCES CEREVISIAE

APPROVED BY SUPERVISORY COMMITTEE

Benjamin Tu, Ph.D.

Yi Liu, Ph.D.

Ralph DeBerardinis, M.D., Ph.D.

Bing Li, Ph.D.

Elliott Ross, Ph.D.

DEDICATION

To my parents, husband and baby for their love and support

To my mentor and committee members for their guidance

INSIGHTS INTO THE METABOLIC REGULATION OF GROWTH AND PROLIFERATION IN SACCHAROMYCES CEREVISIAE

by

LING CAI

DISSERTATION

Presented to the Faculty of the Graduate School of Biomedical Sciences

The University of Texas Southwestern Medical Center at Dallas

In Partial Fulfillment of the Requirements

For the Degree of

DOCTOR OF PHILOSOPHY

The University of Texas Southwestern Medical Center at Dallas

Dallas, Texas

December, 2013

INSIGHTS INTO THE METABOLIC REGULATION OF GROWTH AND PROLIFERATION IN SACCHAROMYCES CEREVISIAE

Ling Cai

The University of Texas Southwestern Medical Center at Dallas, 2013

Supervising Professor: Benjamin P. Tu, Ph.D.

Cells needs to gauge their capacity to grow based on nutrient availability, and adopt different metabolic strategies for optimal growth and survival. We have investigated the molecular mechanism of how growth decisions are made based on metabolic status and how metabolic enzymes are regulated by nutrient availability.

In the first part of this study, we report that acetyl-CoA is the downstream metabolite of carbon sources that represents a critical metabolic signal for growth and proliferation. Upon entry into growth, intracellular acetyl-CoA levels increase substantially and consequently induce the Gcn5p/SAGA-catalyzed acetylation of histones at genes important

for growth, thereby enabling their rapid transcription and commitment to growth. Acetyl-CoA functions as a carbon-source rheostat that signals the initiation of the cellular growth program by promoting the acetylation of histones specifically at growth genes.

In the second part of the study, we report the dynamic modification of ribosome biogenesis transcription factor Ifh1p regulated by different metabolic cues. Ribosome biogenesis requires an enormous commitment of energy and resources in growing cells. We show that Ifh1p is dynamically acetylated and phosphorylated as a function of the growth state of cells. Ifh1p is acetylated at numerous sites in its N-terminal region by Gcn5p and deacetylated by NAD^+-dependent deacetylases of the sirtuin family. Acetylation of Ifh1p is responsive to intracellular acetyl-CoA levels and serves to regulate the stability of Ifh1p. The phosphorylation of Ifh1p is mediated by Protein Kinase A and is dependent on TORC1 signaling. Instead of modulating overall rates of RP gene transcription or growth, these nutrient-responsive modifications of Ifh1p play a more prominent role in the regulation of cellular replicative lifespan.

Finally, we report the different roles of acetyl-CoA synthetases Acs1p and Acs2p in yeast metabolism. While Acs2p is important for rapid growth in glucose medium, Acs1p has unique roles in more challenging growth conditions. It is important for yeast metabolic cycling and is recruited to foci structure near mitochondria that might be involved in shuttling acetyl-CoA into the mitochondria during hypoxia.

TABLE OF CONTENTS

PRIOR PUBLICATIONS

1: Marin-Valencia I, Yang C, Mashimo T, Cho S, Baek H, Yang XL, Rajagopalan KN, Maddie M, Vemireddy V, Zhao Z, Cai L, Good L, Tu BP, Hatanpaa KJ, Mickey BE, Matés JM, Pascual JM, Maher EA, Malloy CR, Deberardinis RJ, Bachoo RM. Analysis of tumor metabolism reveals mitochondrial glucose oxidation in genetically diverse human glioblastomas in the mouse brain in vivo. *Cell Metabolism*. 2012 Jun 6; 15(6):827-37

2: Cai L, Tu BP. Driving the cell cycle through metabolism. *Annual Review of Cell and Developmental Biology*. 2012; 28:59-87

3: Zhang L, Das P, Schmolke M, Manicassamy B, Wang Y, Deng X, Cai L, Tu BP, Forst CV, Roth MG, Levy DE, García-Sastre A, de Brabander J, Phillips MA, Fontoura BM. Inhibition of pyrimidine synthesis reverses viral virulence factor-mediated block of mRNA nuclear export. *Journal of Cell Biology*. 2012 Feb 6; 196(3):315-26.

4: Cai L, Tu BP. Acetyl-CoA drives the transcriptional growth program in yeast. *Cell Cycle*. 2011 Sep 15; 10(18):3045-6

5: Cai L, Sutter BM, Li B, Tu BP. Acetyl-CoA induces cell growth and proliferation by promoting the acetylation of histones at growth genes. *Molecular Cell*. 2011 May 20; 42(4):426-37

LIST OF FIGURES

LIST OF TABLES

LIST OF DEFINITIONS

Abbreviation	Definition
2PG	2-phosphoglycerate
3PG	3-phosphoglycerate
ACS	Acetyl-CoA Synthetase
ADH	Alcoholdehydrogenase
ALD	Aldehydehydrogenase
AMPK	AMP-activated protein kinase
ATP	adenosine triphosphate
BPG	1,3-bisphosphoglycerate
CCCP	Carbonyl cyanide m-chlorophenyl hydrazone
ChIP	chromatin immunoprecipitation
CHX	Cycloheximide
DHAP	dihydroxyacetone phosphate
dO2	Dissolved Oxygen
DOC	deoxycholic acid
EDTA	ethylenediaminetetraacetic acid
EGTA	ethylene glycol tetraacetic acid
ER	endoplasmic reticulum
F6P	fructose-6-phosphate
FADH2	reduced flavin adenine dinucleotide
FBP	fructose-1,6-bisphosphate

FDR	false discovery rate
G3P	glyceraldehyde-3-phosphate
G6P	glucose-6-phosphate
GFP	green fluorescent protein
HST	Homologue of Sir Two
IP	immunoprecipitation
Kd	dissociation constant
LC-MS/MS	Liquid chromatography-tandem mass spectrometry
NAD	Nicotinamide Adenine Dinucleotide
NADH	reduced nicotinamide adenine dinucleotide
NADP	Nicotinamide Adenine Dinucleotide Phosphate
NADPH	reduced nicotinamide adenine dinucleotide phosphate
OX	Oxidative
PCR	polymerase chain reaction
PEP	phosphoenolpyruvate
PKA	Protein Kinase A
PMSF	phenylmethanesulfonylfluoride
PPase	Phosphatase
qPCR	real-time PCR
RB	Reductive Building
RC	Reductive Charging
ribi genes	ribosome biogenesis genes

RLS	replicative lifespan
RP genes	Ribosomal Protein
SAGA	Spt-Ada-Gcn5-acetyltransferase
SAM	S-Adenosyl Methionine
SD	Synthethic medium with D-glucose
TCA	TriChloroacetic Acid
TCA	Tricarboxylic Acid Cycle (citric acid cycle)
TOR	Target of Rapamycin
ts	temperature sensitive
UDP-glucose	Uridine DiPhosphate glucose.
WT	Wild Type
YMC	Yeast Metabolic Cycle
YPD	Yeast extract Peptone medium with D-glucose
YPGE	Yeast extract Peptone medium with Glycerol and Ethanol

CHAPTER ONE – Introduction

The Yeast Metabolic Cycle

When prototrophic budding yeast cells are cultured in a chemostat under continuous glucose limited growth, they become highly synchronized and exhibit oscillations in oxygen consumption coupled to their cell cycle (Figure 1.1). The gene expression and metabolic profiles have been previously characterized and revealed that different transcription program and metabolic activities are temporally compartmentalized into different phases of these cycles (Tu et al., 2005; Tu et al., 2007) (Figure 1.1). Thus these cycles have been termed as the Yeast Metabolic Cycle (YMC).

The growth pattern in a YMC is different from a traditional batch culture used in the laboratory. Cells grown in YPD batch culture experience several phases of growth as the cell density increases. After inoculation, there is a lag phase when cells adapt to the nutrient abundant environment. Then during the first exponential growth phase, yeast cells preferentially use glucose fermentation to support rapid cell growth while accumulating ethanol and acetate as glycolytic products. When glucose is exhausted, yeast cells undergo a diauxic shift to switch their metabolism to using the fermentation products in the second exponential growth phase. However, the speed of proliferation slows down after diauxic shift and cells also turn on their stress resistance program. Finally, when nutrients are depleted, cells exit from cell cycle and enter quiescent phase.

In contrast, the chemostat provides a constant growth environment with fixed pH, oxygen supply, cell density, and constant rate for nutrient addition as well as waste removal (Novick and Szilard, 1950). The highly synchronized cells under steady state growth

continuously transition between three phases, OX (oxidative), RB (reductive, building) and RC (reductive, charging) (Tu et al., 2005) .

Based on the transcription profiles, the OX phase can be likened to growth phase or G1 phase of the cell cycle. During this time the cells experience a sharp increase in mitochondrial respiration and this is accompanied by rapid induction of genes involved in ribosomal biogenesis and amino acid biosynthesis, particularly sulfur metabolism. Then as the cells slow down their oxygen consumption, they enter RB phase during which cell division takes place. Cell cycle genes including those that encode cyclins, histones and spindle poles are turned on while at the same time, mitochondrial gene transcripts are also abundantly detected. After RB phase, the cells enter RC phase which can be likened to G0 phase. The oxygen consumption rate is relatively low in RC phase and the transcription program in this phase are composed of stress response genes including heat shock proteins genes, autophagy genes, vacuolar genes and ubiquitin/proteasome genes (Tu et al., 2005).

From the metabolic profiling study we also learned that different metabolites fluctuate across the cycle too. In the OX growth phase with robust mitochondrial respiration, acetyl-CoA and NADP(H) levels peak as a result of active carbon metabolism. During RB phase, cells engage in nucleotide production to meet the need in DNA replication and S-adenosylmethionine (SAM) levels are also increase. And during the quiescent like RC phase, cells stock up glucose in the form of trehalose and glycogen to increase stress resistance and prepare for the next burst of growth in the following OX phase (Tu et al., 2007).

Central Carbon Metabolism in Yeast

When cells exit from the quiescent like RC phase, a sharp increase in oxygen consumption marks the onset of OX growth phase of the YMC. During this transition, glucose transporters are highly expressed and cells also break down their carbon reserve in the form of trehalose and glycogen to supply a big bolus of glucose that supports rapid cell growth during this phase. Glucose is central to carbon metabolism. Glucose not only fuels glycolysis and the tricarboxylic acid (TCA) cycle for the production of ATP but also enters the pentose phosphate pathway to produce ribose sugars that are needed for DNA and RNA synthesis (Figure1.2). The pentose phosphate pathway also produces reduced Nicotinamide Adenine Dinucleotide Phosphate (NADPH), which is required for fatty acid and sterol biosynthesis as well as other biosynthetic processes. Metabolic intermediates from glycolysis and the TCA cycle also branch into many other biosynthetic and metabolic pathways (DeBerardinis et al., 2008). Glucose is also the precursor for many sugars involved in numerous glycosylation modifications that function along the secretory pathway or at the cell surface (Helenius and Aebi, 2001) (Figure 1.2). However, when glucose is depleted, the previous accumulated glycolytic product ethanol and acetate become the main carbon source for the cell. Ethanol will first be converted into acetaldehyde through the reaction of alcohol dehydrogenase (ADH), and acetaldehyde will be converted into acetate through aldehyde dehydrogenase (ALD). Acetate is used to produce acetyl-CoA in the cytosol through acetyl-CoA synthetase using energy from ATP hydrolysis. Cytosolic acetyl-CoA can be transported into mitochondria or feed into glyoxylate cycle for anabolic reactions, or act as an acetyl donor to acetylate proteins such as histones.

Growth Program in Yeast

Observations from a wide spectrum of organisms suggest that attainment of a critical cell size is a prerequisite for the onset of the cell cycle (Hartwell and Unger, 1977) . In yeast, entry into the cell cycle typically depends on a period of growth and expansion to increase cell size, in preparation for the division process (Jorgensen and Tyers, 2004). While metabolism provides fuel and building blocks, ribosomes are the main builder for constructing new proteins for the growing cell. Ribosome biogenesis, the generation of ribosome, is a monumental task that is dependent on hundreds of proteins and an enormous commitment of energy and resources.

The synthesis of new ribosomes involves transcription of rDNA, ribosomal protein (RP) genes and genes encoding accessory factors for rRNA processing and ribosome assembly, collectively called ribosome biogenesis (ribi) genes (Zaman et al., 2008). In rapidly growing cells, the majority of cellular transcriptional activity is devoted to ribosome biogenesis (Warner, 1999). 60% of total transcription is devoted to ribosomal RNA, and 50% of RNA polymerase II transcription and 90% of mRNA splicing are devoted to ribosomal proteins (RPs) (Warner, 1999). Thus, a yeast cell must be able to assess that it is metabolically competent to meet the budget of ribosome biogenesis before making such a commitment (Figure 1.3). Although ribosome biogenesis is known to be regulated by nutrient-sensing signal transduction pathways such as the TORC1 (Target of Rapamycin) and PKA (Protein Kinase A) pathways, the precise manner by which key nutritional cues are relayed to the ribosome biogenesis machinery has not been fully elucidated (Zaman et al., 2008).

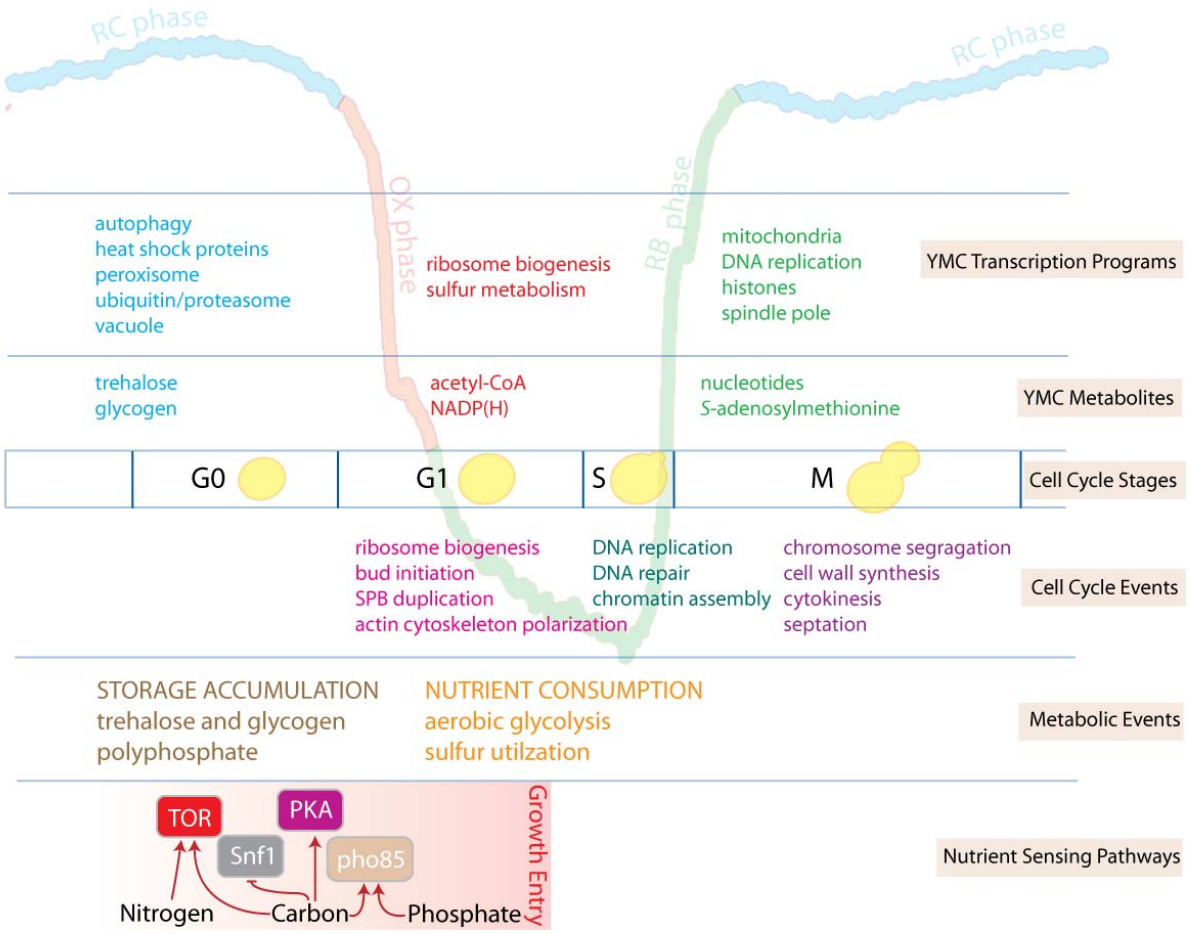

Figure 1.1. The Yeast Metabolic Cycle
Snapshot of the changes in metabolism that occur as a function of the cell cycle in budding yeast. Depiction of when key gene expression programs, metabolites, cell cycle events, and metabolic events are thought to be active or upregulated with respect to cell cycle stage (G0, G1, S, and M) and metabolic cycle phase OX (growth), RB (division), and RC (survival/quiescence). The YMC trace represents absolute dissolved oxygen concentrations in the growth medium—a drop in dO2 is indicative of oxygen consumption.

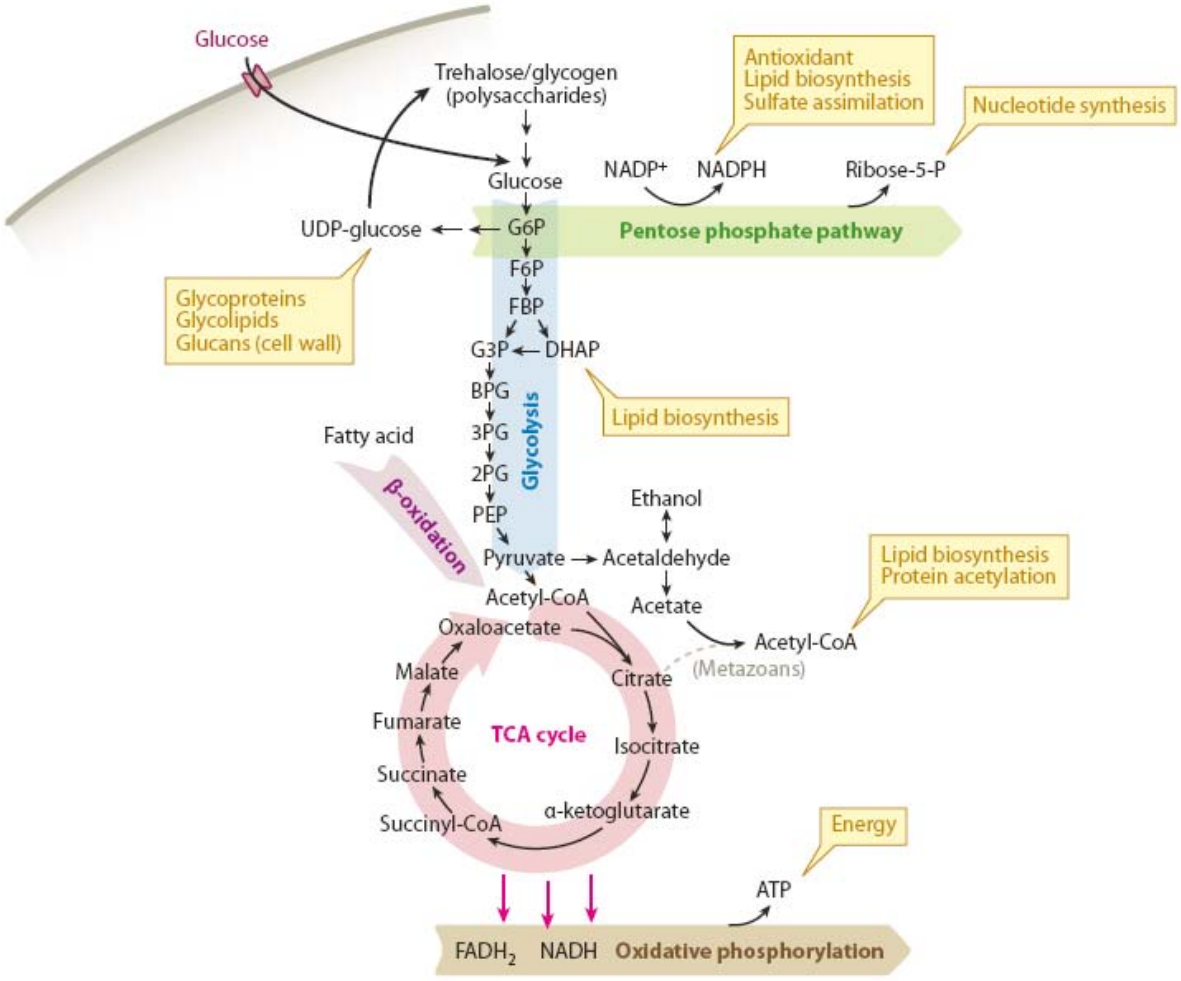

Figure 1.2 Major metabolic pathways of glucose and carbon utilization in yeast.
Glucose is transported into the cell from external sources or released from storage carbohydrates such as trehalose and glycogen. Glucose can be used for glycosylation of lipids and proteins and can be turned into components of the cell wall. Catabolism of glucose through the pentose phosphate pathway, glycolysis, and tricarboxylic acid (TCA) cycle provides essential metabolites that are building blocks of lipids and nucleic acids. Glucose catabolism also provides reducing power for biosynthetic reactions and production of ATP through oxidative phosphorylation. Abbreviations: 2PG, 2-phosphoglycerate; 3PG, 3-phosphoglycerate; BPG, 1,3-bisphosphoglycerate; DHAP, dihydroxyacetone phosphate; F6P, fructose-6-phosphate; FADH2, reduced flavin adenine dinucleotide; FBP, fructose-1,6-bisphosphate; G3P, glyceraldehyde-3-phosphate; G6P, glucose-6-phosphate; NADH, reduced nicotinamide adenine dinucleotide; NADPH, reduced nicotinamide adenine dinucleotide phosphate; PEP, phosphoenolpyruvate; UDP-glucose, uridine diphosphate glucose.

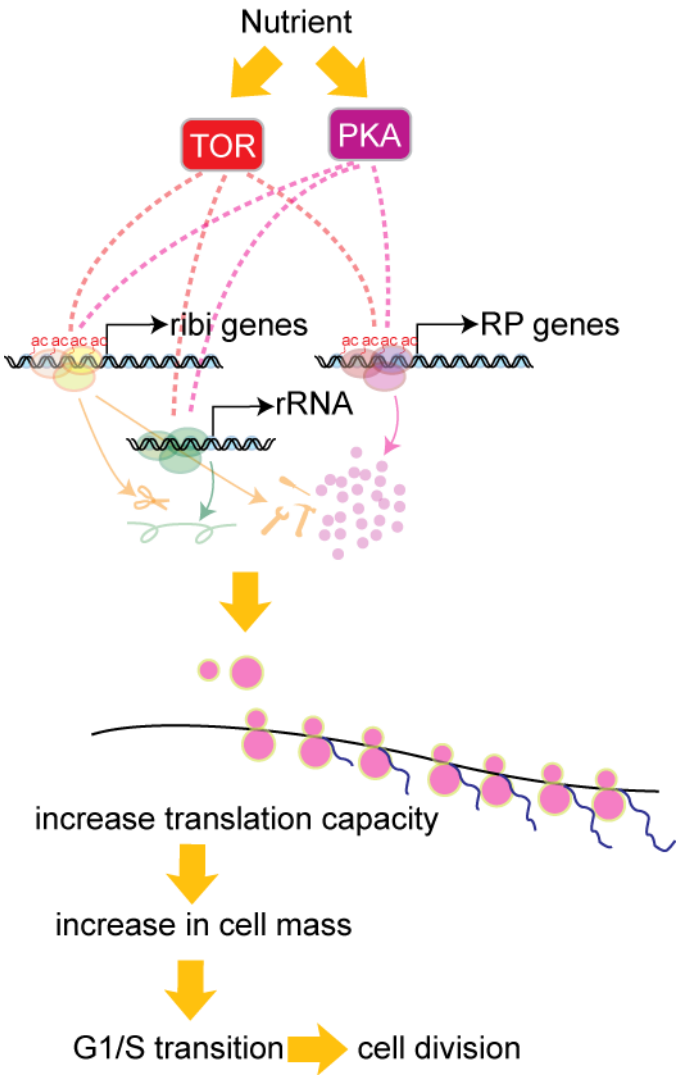

Figure 1.3 Ribosome biogenesis is critical for cell growth and proliferation.
Ribosome biogenesis is controlled by the target of rapamycin (TOR) and protein kinase A (PKA) nutrient-sensing pathways. Transcription of cohorts of ribosomal protein (RP) genes and ribosome biogenesis (ribi) genes, as well as rRNA, are concurrently regulated by specific transcription factors downstream of TORC1 and PKA signaling. As a result of the increase in translation capacity, the cell increases in mass and size until it is ready to go through division. The transcription factor Ifh1p is an essential regulator of ribosomal protein (RP) genes.

CHAPTER TWO

Histone Acetylation by SAGA during Rapid Cell Growth

Acetyl-CoA Is a Metabolite of Carbon Sources that Induces Entry into Growth

What are the metabolic and nutritional cues that induce yeast cells to enter growth? To address this question using the YMC, we observed that the addition of select carbon sources can induce metabolically cycling cells to prematurely exit the RC quiescent-like phase and immediately enter the OX growth phase. Such "phase advancement" into growth is accompanied by a burst of mitochondrial respiration and the induction of growth genes that are typical of a normal OX phase (Chen et al., 2007; Tu and McKnight, 2009). Soon afterwards, cells begin the division process and normal metabolic cycles resume. Not only can addition of glucose, galactose and fatty acid induce such phase advancement, the end products of glycolysis, including lactate, ethanol and acetate can also trigger cells to enter growth (Figure 2.1A).

Since ethanol and acetate must be converted to acetyl-CoA during the course of their metabolism (Figure 2.1B). And it is generally recognized in the field that glucose represents the key metabolic signal for various nutrient sensing pathways involving Ras, PKA, Snf1 (the yeast AMPK) and TORC1 (Glucose-sensing and -signaling mechanisms in yeast). To test whether the conversion of acetate to glucose via the glyoxylate cycle was important for the growth induction, we blocked the glyoxylate cycle by deleting the key enzyme isocitrate lyase (Icl1p). Interestingly, this mutant can still undergo yeast metabolic cycle without a

functional glyoxylate cycle and premature entry into OX growth phase from RC quiescent-like phase can still be induced by addition of acetate (Figure 2.2).

We suspected that acetyl-CoA itself might represent a metabolic signal to enter growth. We confirmed the previous metabolite investigations of YMC, which revealed that acetyl-CoA is one of the most dynamically oscillating metabolites that peak during the OX growth phase (Figure 2.3A). Moreover, in cells from batch culture, we found the levels of acetyl-CoA are higher in rapidly growing exponential phase cells compared to slow-growing cells entering stationary phase (Figure 2.3B). These data revealed that a substantial increase in intracellular acetyl-CoA is associated with and may be required for, entry into growth.

How may acetyl-CoA function as a signal for growth? It is not only a central intermediate in carbon metabolism for energy production through TCA cycle or for biosynthetic reactions that generate lipid and sterols, it is also an acetyl donor for acetylation reactions. We hypothesized that certain protein acetylation events might be sensitive to intracellular levels of acetyl-CoA and these events may function in growth regulation so that the metabolic status of the cell could be conveyed in the form of post-translational modification to regulate cellular activities. To test this hypothesis, we performed an unbiased proteomic approach in search of proteins that might become acetylated only upon entry into the OX growth phase of YMC in tune with the increase in intracellular acetyl-CoA levels (Figure 2.4A). In the middle of quiescent-like RC phase we spiked in ^{13}C acetate and this induced rapid entry into growth as revealed by the immediate drop in dissolved oxygen levels. Metabolites were extracted from cells collected at 1.5min interval during this process and acetyl-CoA levels were measured by LC-MS/MS. We were able to detect robust acetyl-

CoA production from the exogenous ^{13}C acetate at just 0.5min after it was added to the cells. Interestingly, from the ^{12}C acetate measurement, we found that the production of acetyl-CoA from endogenous ^{12}C was also stimulated in this phase advance event, suggesting there may be some positive feedback mechanism to produce more acetyl-CoA (Figure 2.4B). Cells were collected during the phase advancement and used for proteomic screen for newly acetylated proteins during entry into growth (Figure 2.4A)

SAGA Components Are Acetylated by Gcn5p upon Entry into Growth

One of the proteins identified in the proteomic screen was Spt7p, a component of the SAGA (Spt-Ada-Gcn5-Acetyltransferase) transcriptional coactivator complex (Grant et al., 1997). To test if the acetylation of Spt7p was dynamic and correlated with the fluctuation in acetyl-CoA levels across the YMC, we epitope tagged Spt7p and immunoprecipitated SAGA across the YMC to assess its acetylation state (Figure 2.5). We confirmed that Spt7p was acetylated and discovered that two other proteins (Ada3p, Sgf73p) within the SAGA complex were dynamically acetylated during the OX phase precisely when intracellular acetyl-CoA levels increased (Figure 2.5). The cyclic acetylation of Ada3p and Sgf73p (the yeast homolog of Ataxin-7) was more dynamic than that of Spt7p (Figure 2.5), and the steady-state abundance of SAGA remained largely unchanged as a function of the YMC (Figure 2.6). In support of these data, previous studies also detected acetylation of yeast Spt7p and Sgf73p and human Ada3p within SAGA (Gamper et al., 2009; Mischerikow et al., 2009).

The Gcn5p acetyltransferase is a component of SAGA (Brownell et al., 1996; Grant et al., 1997), suggesting it might be responsible for acetylation of proteins within the complex. Indeed, we confirmed that Spt7p, Sgf73p, and Ada3p were no longer acetylated in a gcn5Δ mutant (Figure 2.7), despite still being present within a SAGA complex lacking Gcn5p (Wu and Winston, 2002) (Figure 2.8). Moreover, incubation of purified SAGA with acetyl-CoA resulted in hyperacetylation of Sgf73p (Figure 2.9), while the acetylation state of other proteins within SAGA remained largely unchanged (Figure 2.9). These data suggest that Sgf73p in particular can be acetylated at many sites and that its acetylation might be particularly sensitive to acetyl-CoA fluctuations.

To find out the function of these acetylation marks, we tried to make acetylation defective mutants for each of these SAGA components. We performed our acetylation site mapping experiment by mass spectrometry and referenced a proteomic paper which also identified acetylation of the same SAGA components (Mischerikow et al., 2009). Multiple lysines within these proteins were confirmed to be sites of acetylation by mutation to arginine (Figure 2.10). Interestingly, although the six lysine to alanine mutations in Sgf73p almost eliminated acetylation on Sgf73p in YPD batch culture, when cells were collected from YMC, there is little change in the acetylation of Sgf73p in this mutant (Figure 2.10).

Induction of Histone Acetylation upon Entry into Growth

Since SAGA functions as a histone acetyltransferase (Grant et al., 1997; Lee and Workman, 2007; Suka et al., 2001), we next tested whether the acetylation of particular sites on histones might occur in tune with the increase in acetyl-CoA concentration upon entry

into the OX growth phase. Strikingly, we observed that the acetylation of many sites on histone H3 (K9, K14, K18, K23, K27, K56) and histone H4 (K5, K8, K12) was highly periodic over the YMC. All of these sites, with the exception of H3K56 and H4K16, were acetylated beginning in the OX growth phase, which is precisely when acetyl-CoA levels within the cell increase substantially (Figure 2.11). H3K56 acetylation takes place at later timepoints during the temporal window of the YMC when cell division occurs (Figure 2.11) (Tu et al., 2005). These data confirmed that H3K56 acetylation occurs during S phase and function in cell cycle (Masumoto et al., 2005; Xu et al., 2005). Interestingly, H3K4 trimethylation, which is a mark associated with active transcription (Pokholok et al., 2005), did not fluctuate significantly at the bulk level during YMC (Figure 2.11). As SAGA has been implicated in the acetylation of many of these sites on H3 that increase in OX phase (Grant et al., 1997; Grant et al., 1999), these data reveal that Gcn5p-containing SAGA might specifically acetylates H3 only following the burst of acetyl-CoA production that is concomitant with entry into growth.

SAGA and Acetylated Histones at Growth Genes upon Entry into Growth

Since growth genes such as ribosomal protein genes are highly expressed during growth. High levels of histone acetylation could be occurring at these growth genes. Therefore we next looked at whether SAGA might be recruited to acetylate H3 at growth genes during OX phase of the YMC. It has been previously reported in the literature that many growth genes expressed in OX phase as well as stress genes expressed in RC phase are identified as SAGA/Gcn5p targets (Huisinga and Pugh, 2004; Robert et al., 2004). We chose

several SAGA target genes that are induced during the RC phase (*STI1*, *ARO9*) and several targets that are induced during the OX phase of the YMC (*RPS11B*, *RPL33B*, *SHM2*) to determine whether they might be regulated by SAGA-catalyzed histone acetylation during the YMC (Huisinga and Pugh, 2004; Robert et al., 2004). We performed chromatin immunoprecipitation (ChIP) analysis to quantitate SAGA binding and histone acetylation at these target genes in either OX or RC phase (Figure 2.12). We confirmed that SAGA preferentially bound OX phase targets during OX phase and RC phase targets during RC phase (Figure 2.12A). H3K9, H3K14, H3K18, H3K23, and H3K27 were significantly acetylated at the OX phase SAGA targets specifically during OX phase, perhaps as expected. In striking contrast, for RC phase SAGA targets, there was no significant increase in H3 acetylation in either RC phase or OX phase (Figure 2.12A). These data suggest that acetyl-CoA enables SAGA to acetylate histones specifically at OX phase growth genes to facilitate enhanced transcription. In support of this idea, the transcripts of OX phase genes peak very sharply in the midst of the respiratory burst, and H3 acetylation has been shown to correlate with transcription rate (Figure 2.12B) (Kurdistani et al., 2004; Pokholok et al., 2005; Tu et al., 2005). It is worth noting that several acetylated sites on H4 were also present at ribosomal genes during OX phase (Figure 2.13). And these H4 sites are acetylated by acetyltransferase NuA4. We will discuss later how NuA4 might be downstream of SAGA.

Having established that induction of histone acetylation occurs at several growth genes upon entry into growth, we next performed ChIP-seq analysis to assess the genome-wide locations of H3K9 acetylation, a highly cyclic OX phase histone modification catalyzed by SAGA (Grant et al., 1999; Zhang et al., 1998) (Figure 2.14). Substantially more genomic

regions containing acetylated-H3K9 were observed in OX phase compared to RC phase (Figures 2.14A and 2.14B), in agreement with western analysis (Figure 2.11). Strikingly, H3K9 acetylation was present almost exclusively at growth genes (e.g., ribosome biogenesis, translation, amino acid metabolism), specifically during OX phase (Figures 2.14A and 2.14B and Figure 2.15). Many chromosomal locations containing H3K9 acetylation correlated well with SAGA binding, especially at ribosomal genes (Figures 2.14A and 2.14C). In contrast, many fewer genomic regions containing H3K9 acetylation were detected in RC phase (Figure 2.14B), despite the fact that >43% of all periodic YMC genes are expressed in RC phase (Tu et al., 2005). Moreover, the majority of regions bound by SAGA in the RC phase were not associated with a corresponding increase in H3K9 acetylation (Figure 2.14A). Collectively, these data strongly suggest that histone acetylation induced by acetyl-CoA is rate limiting primarily for the transcription of OX phase growth genes, whereas RC phase genes are much less dependent on histone acetylation for activation.

Acetyl-CoA Drives Cell Growth through Gcn5p and SAGA

Multiple lines of genetic evidence substantiate our findings that acetyl-CoA sets in motion a series of acetylation events to enable cellular commitment to growth. Bulk histone acetylation was previously found to be compromised in yeast containing mutations in acetyl-CoA synthetase enzymes that control acetyl-CoA flux (Takahashi et al., 2006). Furthermore, a synthetic genetic interaction between a temperature-sensitive mutation in acetyl-CoA synthetase (*acs2-ts*) and *gcn5*Δ has been reported (Takahashi et al., 2006). Notably, we observed that a *gcn5*Δ mutant exhibited slow growth and did not undergo the synchronized

bursts of respiratory growth that are a hallmark of metabolic cycles, in contrast to mutants lacking other acetyltransferases (Figures 2.16). A catalytically inactive Gcn5p point mutant (E173Q) also exhibited a severe cycling phenotype (Figures 2.17) (Trievel et al., 1999). Moreover, an acs1Δ mutant, which lacks the acetyl-CoA synthetase expressed under glucose-poor conditions (van den Berg et al., 1996), did not undergo metabolic cycles (Figure 2.16B). How might the acetylation of Sgf73p, Ada3p, and Spt7p by Gcn5p affect the SAGA complex and its ability to acetylate histones at growth genes? We have already shown that the composition of SAGA remains unchanged across the YMC (Figure 2.6). We also attempted to test whether the acetylation of SAGA enhances its activity as a histone acetyltransferase but we did not detect differences in its ability to acetylate free histones or core nucleosomes in vitro. This could be due to the robust auto acetylation of SAGA in vitro (Figure 2.9). We wanted to use acetylation defective mutants to study the mechanism but the mutations we introduced to SAGA components were unable to eliminate the acetylation on SAGA detected by western blot, such mutants are still substantially acetylated in the suboptimal growth condition in YMC and the residual acetylation might be sufficient for regulating SAGA (Figure 2.10).

Therefore, we took some alternative approaches. First, we made deletion mutants of the acetylated SAGA components and observed a growth defect (Figure 2.18A). *spt7Δ* is very sick because without this scaffolding protein the SAGA complex falls apart. However, the composition of SAGA was not affected in *ada3*Δ and *sgf73*Δ mutants (Figure 2.18B). Interestingly, *sgf73*Δ mutant exhibited slow defects in H3 acetylation, and abnormal metabolic cycles (Figures 2.18C and 2.18D). Although Sgf73p is also required for histone

deubiquitylation catalyzed by SAGA (Kohler et al., 2008), this activity does not appear critical for entry into growth, as the *ubp8*Δ mutant exhibited normal growth and more normal metabolic cycles (Figure 2.19). In addition, the *ada3*Δ mutant, which completely eliminates acetylation of Spt7p and Sgf73p (Figure 2.20), also exhibited slow growth, defects in H3 acetylation, and abnormal cycles (Figures 2.18C and 2.18D).

The second alternative approach we have taken is by constructing a diploid strain expressing one copy of wild-type (WT) Gcn5p and one copy of a catalytically inactive Gcn5p (E173Q) mutant, each marked with its own epitope tag. Interestingly, we observed that the catalytically inactive Gcn5p was present within a SAGA complex that did not appear to be acetylated, while as expected WT Gcn5p was present within a SAGA complex that is acetylated (Figure 2.21). This diploid strain expressing two different alleles of Gcn5p was able to undergo normal metabolic cycles, and so we tested whether the acetylation of SAGA might influence its ability to be recruited to particular genes. We observed that while both acetylated and deacetylated SAGA were present at an RC phase gene during RC phase, the acetylated form of SAGA (as pulled down using WT Gcn5p) exhibited increased binding to a ribosomal gene during the OX growth phase (Figure 2.21). These data suggest that the Gcn5p-catalyzed acetylation of SAGA components might function to aid its recruitment to certain classes of genes, in particular the OX phase growth genes. In this experiment, we cannot exclude the possibility that Gcn5p-dependent acetylation of a chromosome-bound target might be required for the stabilization of SAGA on chromatin. Moreover, it is possible that some of the acetylation sites within SAGA could be a coincidental consequence of having an acetyltransferase enzyme situated within a complex of proteins that is activated in

response to a burst of acetyl-CoA production. Nonetheless, previous studies on the role of Ada3p and the observation that the acetylation of SAGA components Spt7p and Sgf73p is dependent on Ada3p (Figure 2.20) suggest the possibility that acetylation of SAGA could function to stimulate its nucleosomal acetyltransferase activity and perhaps its activation or recruitment to growth genes (Balasubramanian et al., 2002; Wu et al., 1999).

Gcn5p is Important for Acetyl-CoA Driven Growth Gene Expression

To test whether Gcn5p is important for inducing growth gene expression during growth induction, we added ^{13}C acetate to WT and *gcn5*Δ cells from the chemostat and measured acetyl-CoA production, histone acetylation and expression of selected OX phase growth genes as well as quiescent RC phase genes during a 22 minute time course (Figure 2.22A). Although no difference of ^{13}C acetyl-CoA production from exogenous acetate or ^{12}C acetyl-CoA production from endogenous carbon sources was detected (Figure 2.22C), acetate induced increase in H3 acetylation was impaired (Figure 2.22B) and growth gene induction was compromised (Figure 2.22D), while the expression pattern quiescent phase gene *ARO9* remains unchanged (Figure 2.22D). Moreover, the increase in bulk levels of H4 acetylation in response to acetyl-CoA is also dependent on Gcn5p (Figure 2.22B), suggesting the activity of the NuA4 acetyltranferase complex can be influenced by SAGA in some instances.

In addition to the three components within SAGA complex, we have found a few more Gcn5p targets dynamically acetylated across the YMC in tune with acetyl-CoA levels such as Snf2p (Figure 2.23) and Ifh1p (discussed in the next chapter). However, it needs to be pointed out that such dynamic acetylation property is not found for all the acetylated

proteins (Figure 2.23). As we have shown that H4 acetylation by NuA4 acetyltransferase complex is dynamic in the YMC but is dependent on Gcn5p, we have also found Yng2p, a component of NuA4 is also acetylated by the levels remain constant across YMC. So how and why could the Gcn5p containing SAGA complex acetylate its substrates in response to increase in acetyl-CoA concentration? Based on previous in vitro Kd (~8.5 mM) and Km (~2.5 mM) measurements for Gcn5p (Berndsen and Denu, 2008; Langer et al., 2002), our estimates of intracellular acetyl-CoA concentration across the YMC (~3–30 mM) indicate it is conceivable that the activity of SAGA could be regulated in vivo by physiological fluctuations of acetyl-CoA (Figure 2.24). Accordingly, the observation that a catalytically inactive point mutant of Gcn5p fails to undergo the bursts of growth that are a hallmark of the YMC is consistent with a critical role for Gcn5p in driving cell growth (Figure 2.17).Moreover, we observed that the A190T mutant, which increases its affinity for acetyl-CoA by ~10-fold from 8.5 to 0.56 mM (Langer et al., 2002), exhibits a temperature-sensitive growth defect on acetate as the carbon source, suggesting that Gcn5p might be finely tuned to sense and respond to a higher threshold of acetyl-CoA levels in vivo (Figure 2.25). However, the kinetic parameters for Gcn5p are comparable to those measured for other acetyltransferases such as Esa1p (Berndsen and Denu, 2008). In contrast to this observation, the increase in H4 acetylation catalyzed by the Esa1p-containing NuA4 complex in response to acetyl-CoA is dependent on Gcn5p (Figure 2.22B), indicating the in vivo behavior of acetyltransferases in relation to changes in acetyl-CoA substrate levels might not be immediately predictable from estimates of their kinetic parameters alone. Regardless, multiple lines of evidence strongly indicate that Gcn5p-containing SAGA distinctively

acetylates substrates in vivo in response to the burst of acetyl-CoA production that accompanies entry into growth. As such, acetyl-CoA triggers a series of acetylation events within SAGA and at histone tail surrounding growth genes, thereby enabling rapid gene activation and consequent commitment to growth. Future studies will be required to resolve the molecular changes to the SAGA complex following acetylation and how they affect its function and recruitment to particular classes of genes, as well as the basis for its ability to acetylate substrates in tune with increases in intracellular acetyl-CoA levels.

Hight Resolution ChIP-seq and RNA-seq Across YMC

We have also conducted high temporal resolution RNA-seq and ChIP-seq for H3K9ac across 16 timepoints from the yeast metabolic cycle (Figure 2.26). The results revealed that the epigenetic profile over the YMC is highly dynamic (Figure 2.27). These high resolution data have led us to intriguing observations on how gene expression is precisely orchestrated temporally. For example, we found that the distinct sub-steps of the ribosome biogenesis process are efficiently regulated in the OX growth phase of the YMC. The ribi genes that encode accessory factors for ribosome assembly and rRNA processing are turned on just about 5 mins before the ribosomal protein (RP) genes are expressed (Figure 2.28). Such data support a “just in time supply chain” model in which yeast cells prepare the ribosomal assembly factors and ribosomal RNA just ahead of the ribosome structural proteins and amino acid biosynthetic pathways to maximize efficiency of ribosome biogenesis and translation. In agreement with the RNA-seq data, our H3K9ac ChIP-seq data also revealed robust regulation of ribi and RP genes (Figure 2.29). Interestingly, H3K9ac

marks on the promoter of ribi genes appear to be more transient compared to the RP genes. In collaboration with Zheng Kuang in Jef Boeke's lab at Johns Hopkins University, we have interrogated the genome-wide occupancy profiles for many more different epigenetic marks on histones as well as for chromatin modifiers.

Summary

Our data have revealed one of the elusive mechanisms by which carbon sources trigger growth and raise the possibility that the products of glycolytic metabolism (e.g., ethanol, acetate, lactate) may be important activators of growth within microbial communities and cancerous tumors (Sonveaux et al., 2008). In addition, genetic alterations that cause a net accumulation of intracellular acetyl-CoA may enhance cellular proliferative capacity. As protein acetylation has also been linked to metabolism in several previous studies (Choudhary et al., 2009; Friis et al., 2009; Takahashi et al., 2006; Wang et al., 2010; Wellen et al., 2009; Zhao et al., 2010), we predict that a similar control of gene expression and protein activities with respect to intracellular acetyl-CoA levels might represent a widely conserved mechanism by which cell growth and proliferation are coordinated with metabolic state.

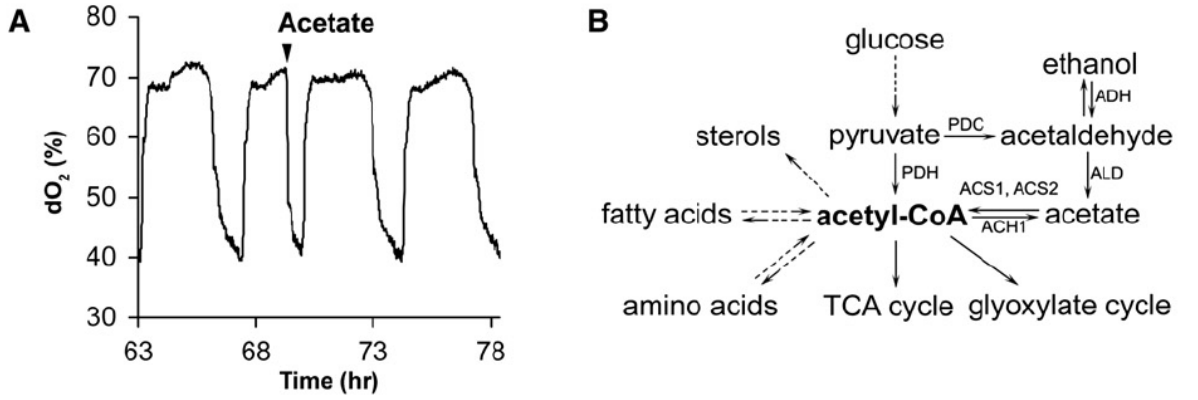

Figure 2.1 Entry into the OX, growth phase of the YMC can be induced by addition of various carbon sources. To our knowledge, sugars like glucose and galactose as well as fatty acid can readily trigger cells in the RC quiescent-like phase to prematurely enter growth phase. Interestingly, metabolites downstream of glycolysis or fatty acid catabolism such as ethanol, acetaldehyde, acetate and lactate can also induce such phase advancement.
(A) Phase advancement induced by addition of acetate (1mM). The transition of RC phase to OX phase is characterized by a burst of mitochondrial respiration which rapidly consumes dissolved oxygen in the medium.
(B) Yeast pathways that synthesize and consume acetyl-CoA. Acetyl-CoA is a central metabolite that connects carbon catabolism to anabolism.

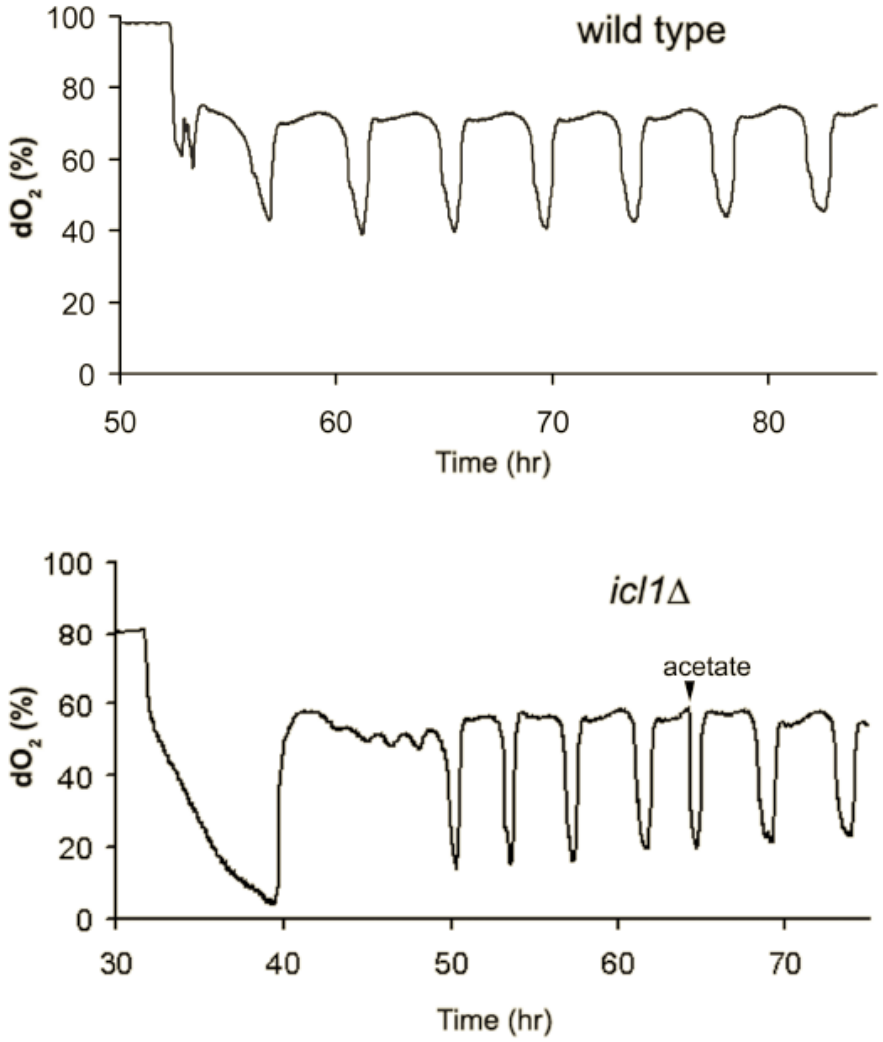

Figure 2.2 Acetate can still induce entry into growth in *icl1*Δ YMC. Isocitrate lyase (Icl1p) catalyzes the formation of succinate and glyoxylate from isocitrate, a key reaction of the glyoxylate cycle. Products of glyoxylate cycle can be used in gluconeogenesis for the generation of glucose. *icl1*Δ mutant that lacks a functional glyoxylate cycle can still be induced into OX growth phase by acetate, suggesting that acetyl-CoA itself and not its conversion to glucose, can act as a growth signal.

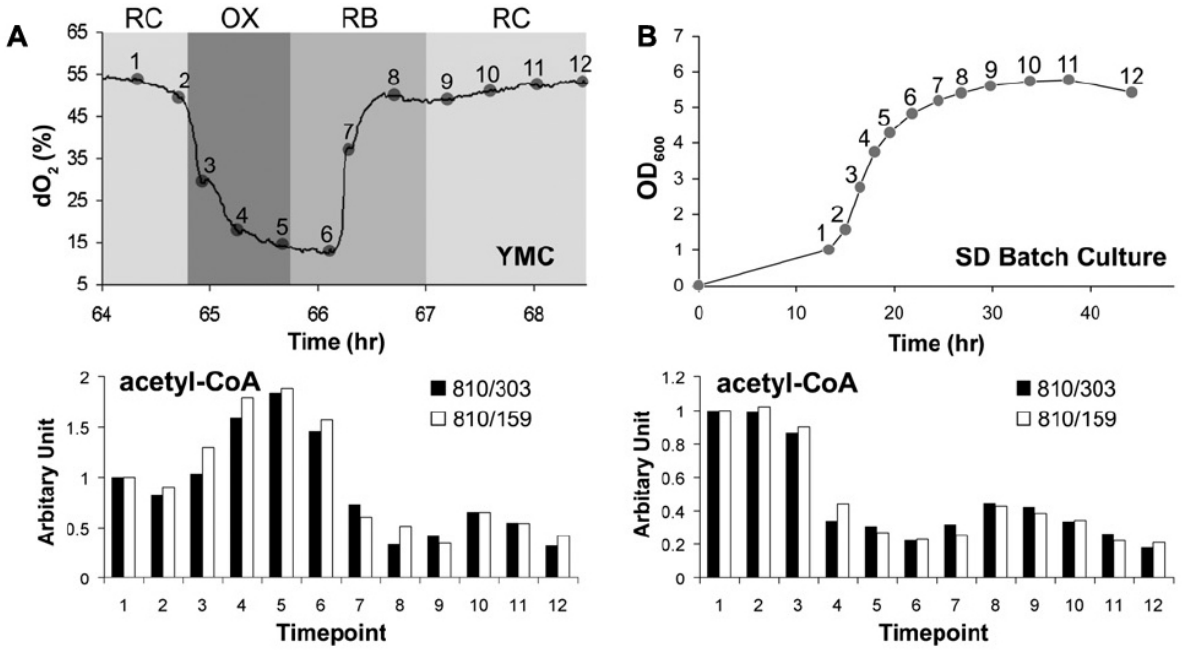

Figure 2.3 Levels of acetyl-CoA are associated with growth rate.
(A) Upregulation of acetyl-CoA production upon entry into the OX growth phase. Metabolites were extracted from cells harvested at the indicated 12 time points across one cycle. Acetyl-CoA levels were measured by LC-MS/MS using multiple reaction monitoring (MRM) and quantitating two specific daughter fragments for acetyl-CoA (303, 159 Da) as described previously (Tu et al., 2007). Data were normalized against the first time point.
(B) Acetyl-CoA levels correlate with growth rate in batch culture. Metabolites were extracted from an equivalent number of cells collected at the specified time points during batch culture growth in SD minimal media. Note that acetyl-CoA levels are significantly higher in exponential phase compared to stationary phase.

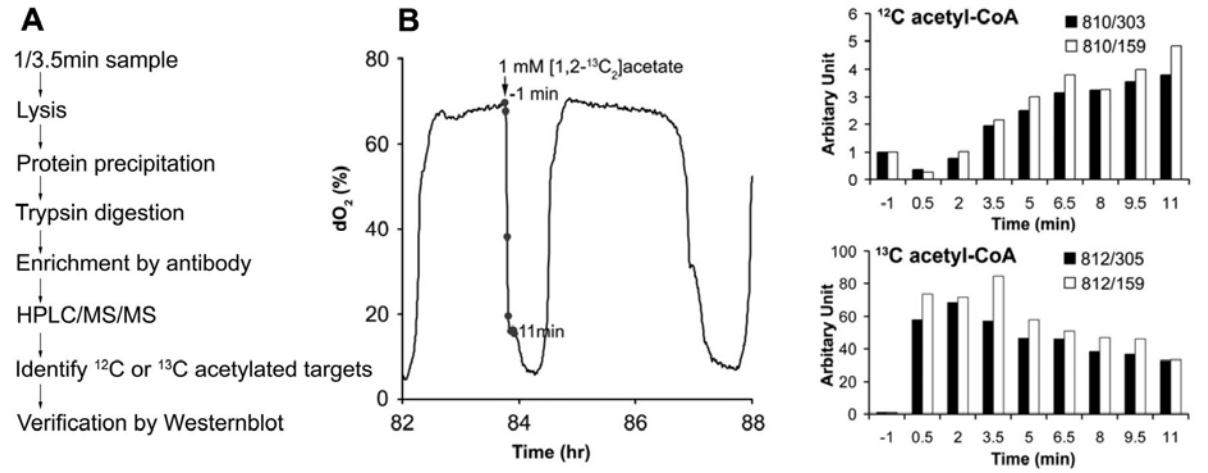

Figure 2.4 Screen for protein acetylation events when cells enter growth

(A) Schematic flowchart of screen process.

(B) Acetate-induced entry into growth is accompanied by a significant increase in intracellular acetyl-CoA. Metabolites were extracted from cells collected at 1.5 min intervals following addition of 13C-labeled acetate to cells in RC phase. ^{12}C and ^{13}C acetyl-CoA were quantitated by LC-MS/MS. ^{13}C acetate was quickly converted to ^{13}C acetyl-CoA, and ^{12}C acetyl-CoA from endogenous, unlabeled carbon sources also increased in response to the stimulus.

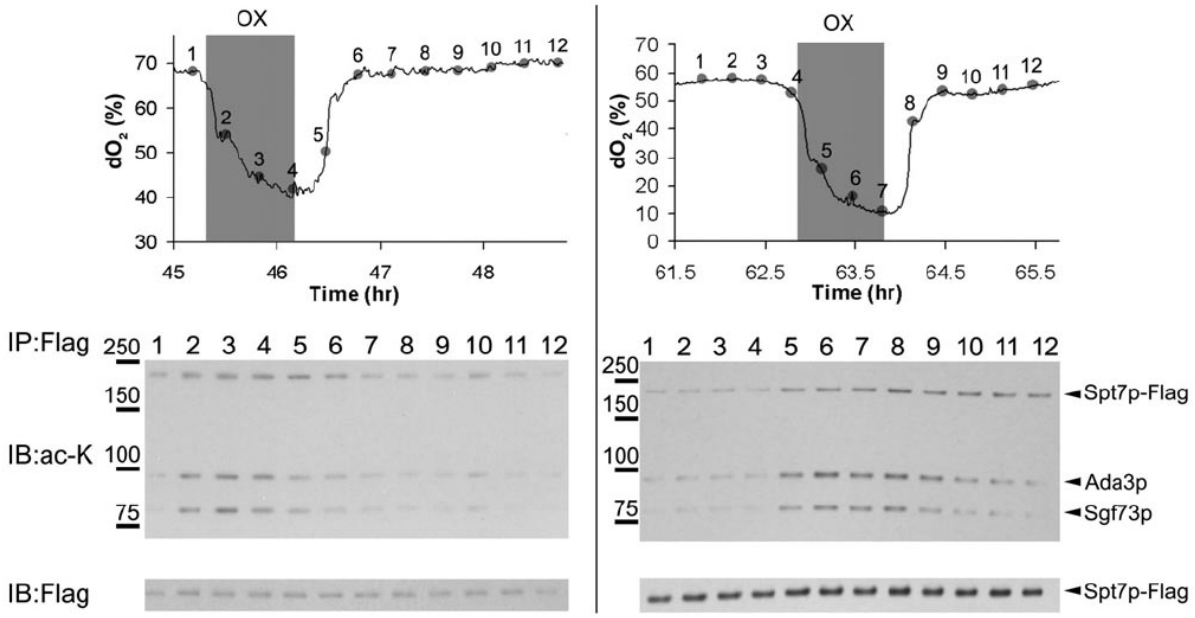

Figure 2.5 Dynamic acetylation of SAGA components across YMC. SAGA was immunoprecipitated from a SPT7-FLAG strain across 12 time points of the YMC, and protein acetylation was detected by western blot using an anti-acetyllysine antibody. Spt7p, Ada3p, and Sgf73p were found to be dynamically acetylated over theYMC with the highest levels in the OX growth phase, when acetyl-CoA levels increase substantially (Figure 2.3A). Data from two independent metabolic cycle experiments are shown.

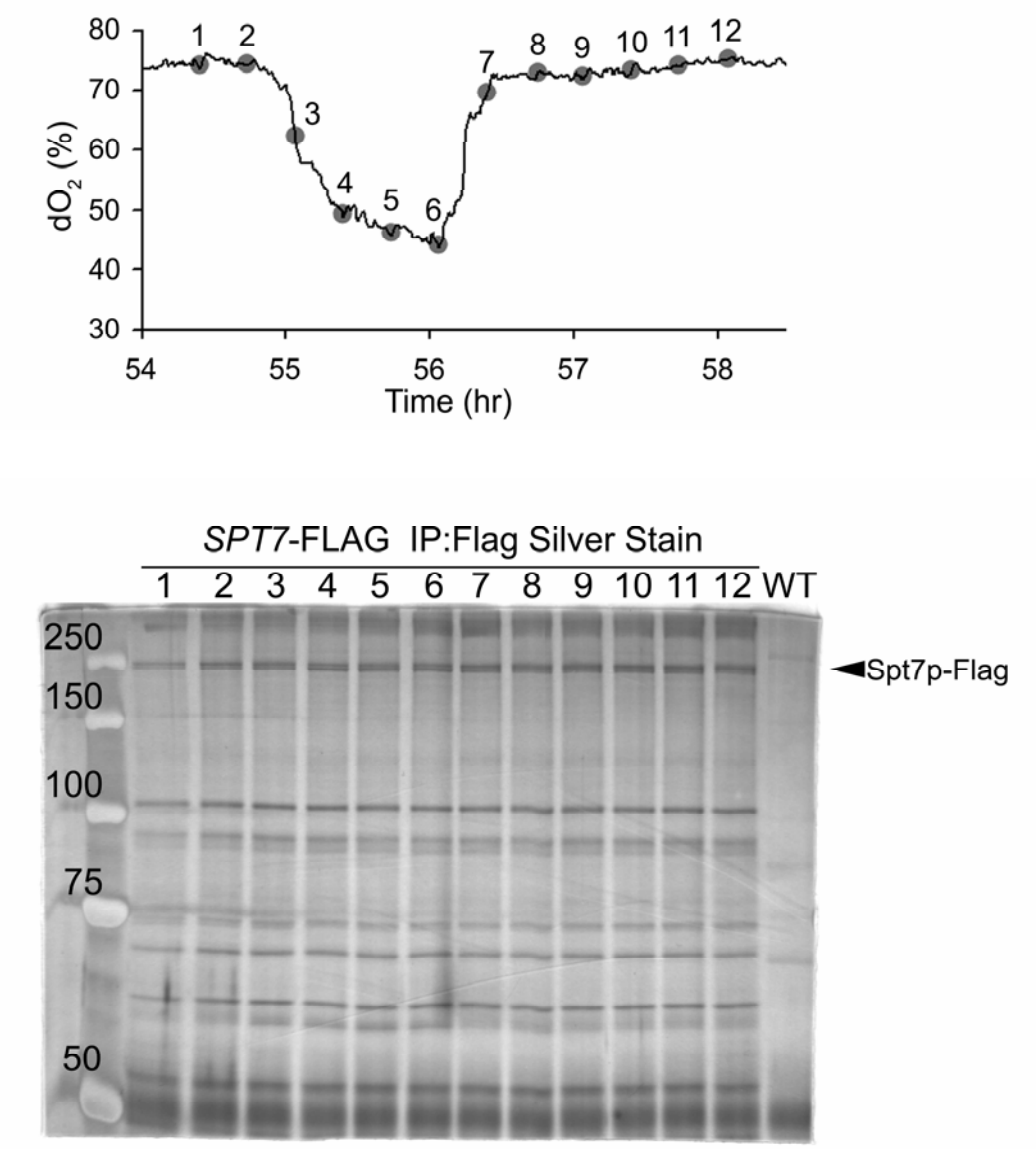

Figure 2.6 SAGA composition remained unchanged across the YMC. SAGA was immunoprecipitated from a SPT7-FLAG strain at the indicated 12 time points across one metabolic cycle. Proteins associated with the beads were separated by SDS-PAGE and silver-stained. An untagged, WT strain was used as a negative control. Note the lack of significant changes in the proteins co-immunoprecipitating with Spt7p across the YMC.

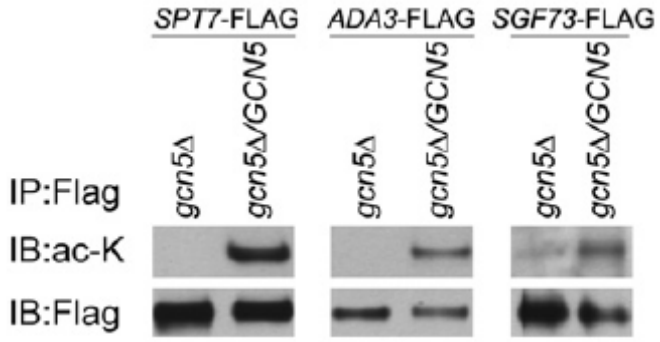

Figure 2.7 Acetylation of SAGA components is dependent on Gcn5p. Strains expressing C-terminally FLAG-tagged versions of either SPT7, ADA3, or SGF73 in a haploid *gcn5*Δ background were constructed. Proteins were immunoprecipitated from cells grown to log phase using a FLAG antibody, and then acetylation state was detected by western blot. After mating to a WT *GCN5* haploid, acetylation of each of the three proteins was restored in the resulting diploid.

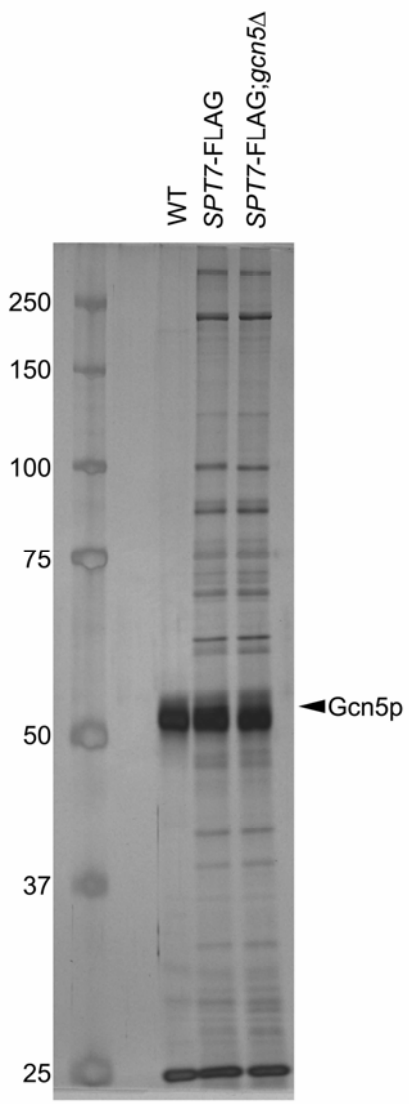

Figure 2.8 SAGA composition remained largely unchanged in *gcn5*Δ
SAGA was immunoprecipitated from either a WT or *gcn5*Δ strain expressing Spt7-FLAG, from cells grown to log phase in YPD. Note that the SAGA complex remains intact in a *gcn5*Δ mutant, in agreement with previous studies (Wu and Winston, 2002). The band that corresponds to Gcn5p partially overlaps with the ~50 kDa heavy chain.

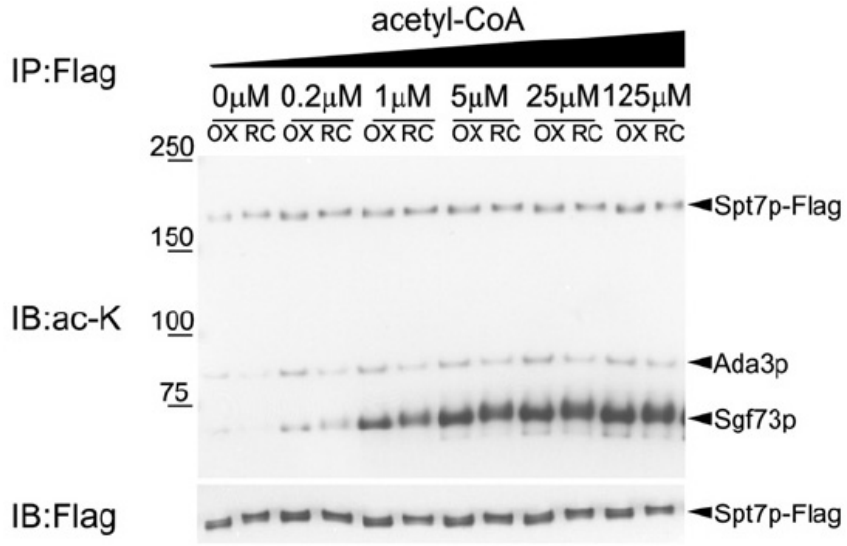

Figure 2.9 Sgf73p is hyperacetylated upon incubation of SAGA with acetyl-CoA in vitro. Immunopurified SAGA complex from the OX or RC phase of the YMC was incubated with the indicated concentrations of acetyl-CoA for 30 min at 30ºC. The acetylation state of SAGA components was monitored by western blot. Note that Sgf73p within SAGA becomes hyperacetylated, suggesting there are many lysine residues that can be acetylated in response to acetyl-CoA.

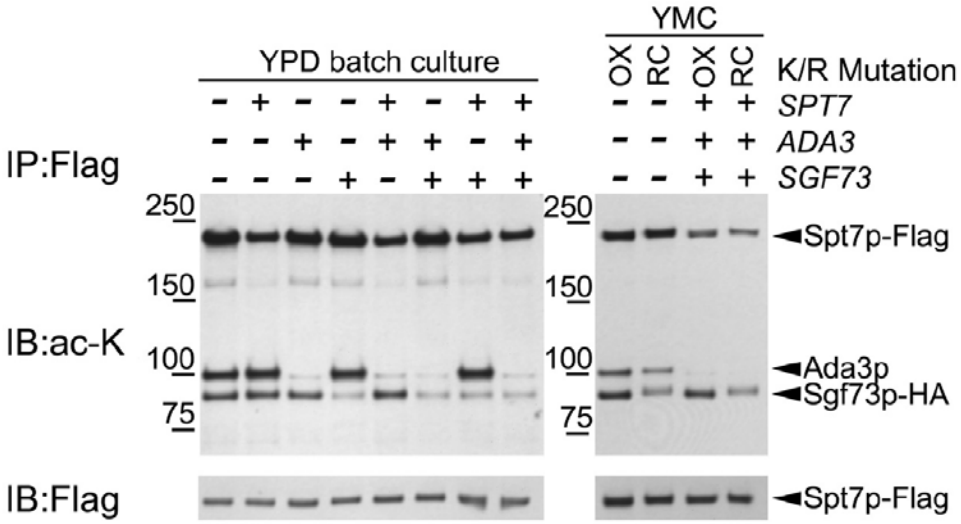

Figure 2.10 SAGA components are acetylated at many lysine residues.
Mutants were constructed in a *SPT7*-FLAG, *SGF73*-HA strain, according to sites identified by LC-MS/MS and by a previous study (Mischerikow et al., 2009). K603 and 607 on Spt7p; K183 on Ada3p; and K171, 199, 211, 224, 288, and 300 on Sgf73p were mutated to arginine separately or in combination as indicated. The resulting consequences on acetylation of SAGA were determined by immunoprecipitating SAGA from either a log phase YPD batch culture (left) or OX or RC phase of the YMC (right), followed by western analysis.

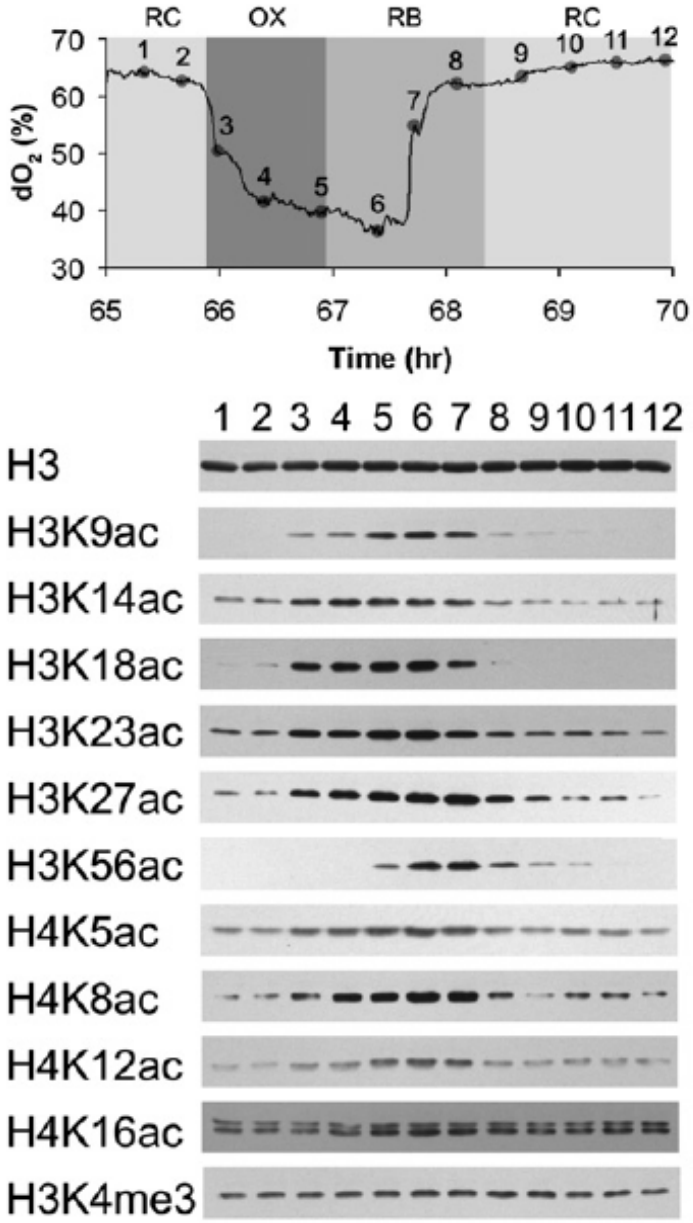

Figure 2.11 Induction of Histone Acetylation upon Entry into Growth. Protein extracts were prepared across 12 time points of one metabolic cycle for bulk analysis of histone modifications. Western blots were performed using highly specific antibodies recognizing the indicated modifications on histone H3 or H4. Acetylation of H3K9, H3K14, H3K18, H3K23, H3K27, and H4K5, H4K8, H4K12 increased substantially in tune with the increase in acetyl-CoA that accompanies entry into the OX growth phase. Acetylation of H3K56 increased at later time points in RB phase during the time of cell division. H3K4 trimethylation remained largely unchanged as a function of the YMC as assayed at the bulk level.

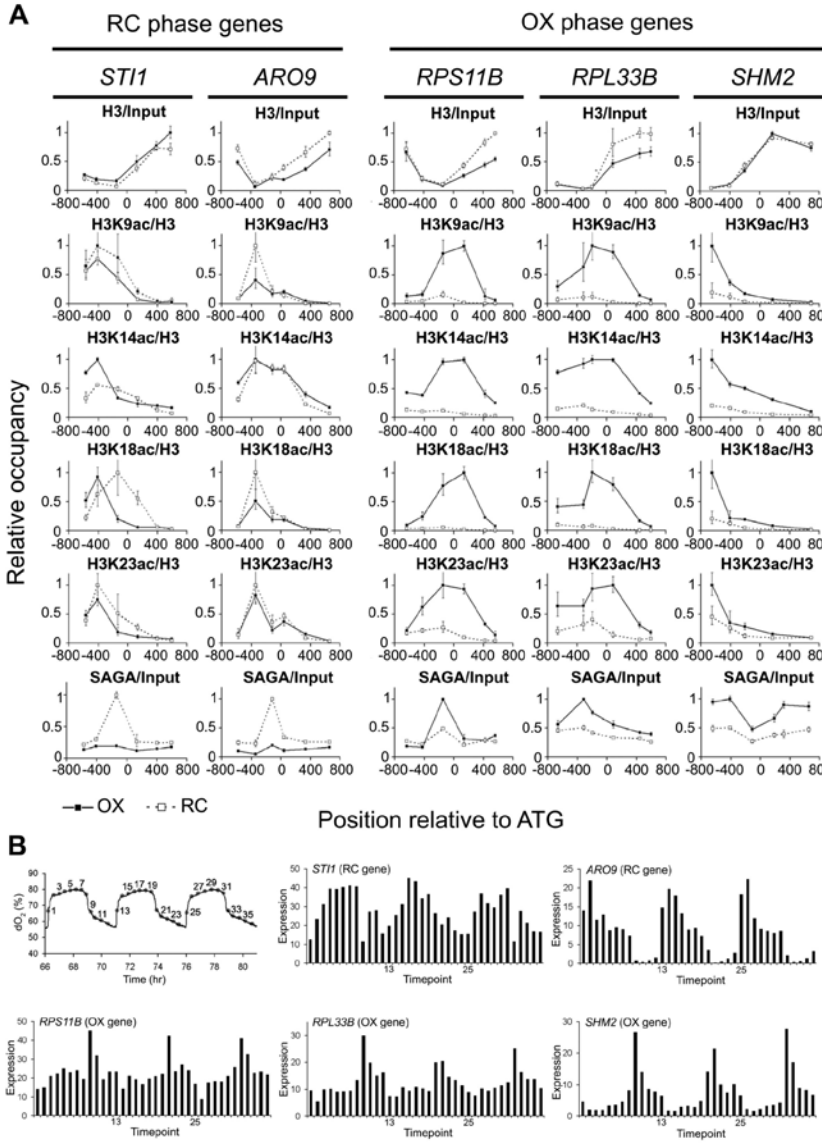

Figure 2.12 SAGA and Acetylated Histones Are Present at Growth Genes upon Entry into Growth

(A) ChIP was performed to quantitate SAGA binding and histone acetylation at previously identified SAGA target genes that peak during either RC phase (*STI1, ARO9*) or OX phase (*RPS11B, RPL33B, SHM2*). SPT7-FLAG cells were crosslinked for ChIP analysis in early OX phase corresponding to time point 3 and in early RC phase corresponding to time point 9 (Figure 2.11). Histones at these OX phase genes are significantly acetylated upon gene activation, in contrast to RC phase genes.

(B) YMC expression profiles of SAGA target genes from RC and OX Phase used for ChIP analysis. Expression data are from 36 time points over three consecutive metabolic cycles as reported previously (Tu et al., 2005).

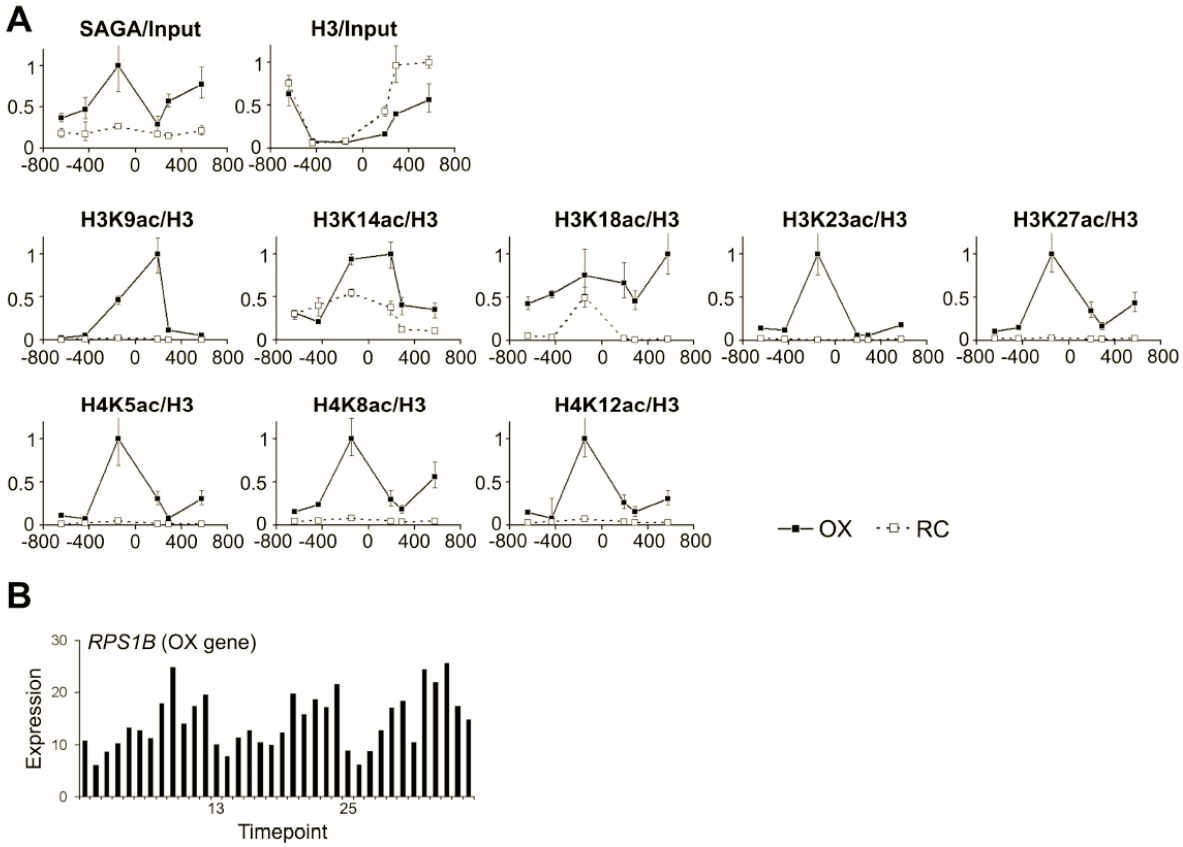

Figure 2.13 Several sites on H4 at Ribosomal Genes are also Acetylated upon Entry into Growth

(A) ChIP analysis surveying abundance of SAGA and the indicated acetylated sites on H3 or H4 at *RPS1B* (another SAGA target highly expressed in OX phase of the YMC) during OX and RC phase.

(B) YMC expression profile of *RPS1B* taken from (Tu et al., 2005). Note that acetylation of both H3 and H4 was observed at this ribosomal gene during OX phase.

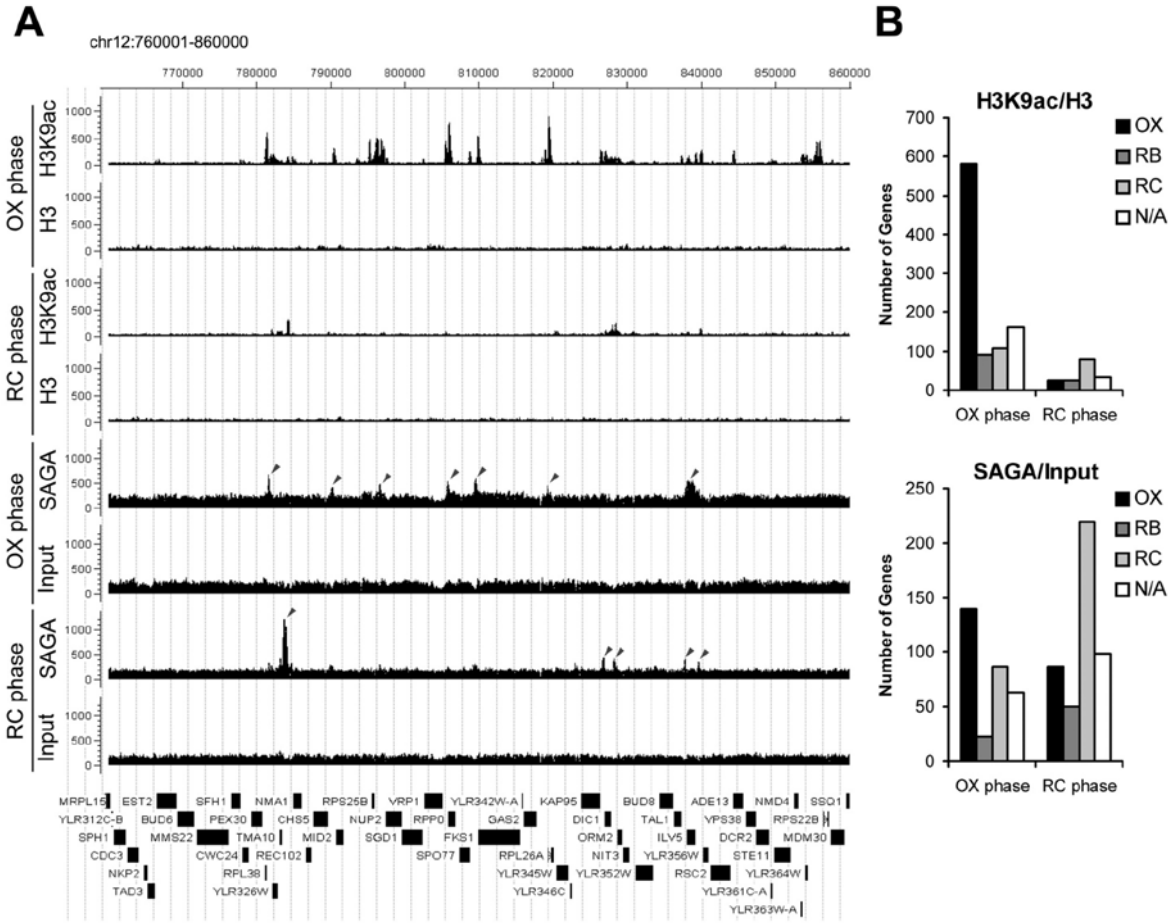

C

Genes occupied by H3K9ac

	FUNCTIONAL CATEGORY	P-value
OX phase	ribosome biogenesis	2.7E-66
	translation	7.5E-10
	nucleic acid binding	3.7E-08
	amino acid metabolism	2.2E-07
	RNA processing	1.3E-05
RC phase	electron transport	2.3E-05
	respiration	5.3E-05
	oxidation of fatty acids	1.3E-03
	lipid, fatty acid and isoprenoid metabolism	2.9E-03
	tricarboxylic-acid pathway	7.9E-03

Genes occupied by SAGA

	FUNCTIONAL CATEGORY	P-value
OX phase	ribosome biogenesis	2.4E-21
	glycolysis and gluconeogenesis	5.6E-06
	amino acid metabolism	1.2E-05
	metabolism of energy reserves	6.8E-03
	C-compound and carbohydrate metabolism	8.2E-03
RC phase	C-compound and carbohydrate metabolism	3.7E-12
	stress response	6.1E-08
	glycolysis and gluconeogenesis	8.6E-08
	protein folding and stabilization	7.7E-06
	transported compounds	2.0E-05

Figure 2.14 Genome-wide Analysis reveals that Histone H3 at Growth Genes Becomes Acetylated upon Entry into Growth.

(A) ChIP-seq analysis was performed to reveal genomic regions occupied by H3K9ac and SAGA at a time point in either early OX or early RC phase, as in Figure 2.11. Sequencing data were analyzed and displayed using CisGenome (Ji et al., 2008). The arrows mark peaks associated with the following genes (maximal YMC phase of expression in parentheses): SAGA OX phase, *RPL38* (OX), *MID2* (OX), *RPS25B* (OX), *RPP0* (OX), *FKS1* (OX),

RPL26A (OX), and *ILV5* (OX); SAGA RC phase, *TMA10* (RC), *KAP95* (OX), *DIC1* (RC), *TAL1* (N/A), and *ILV5* (OX). The temporal expression profiles of these genes across the YMC were highly consistent with these ChIP-seq data (Figure 2.14). Note that H3K9ac peaks are much more frequent and significant in OX phase compared to RC phase. Many SAGA binding sites in OX phase corresponded directly to significant regions of H3K9 acetylation, while many SAGA binding sites in RC phase did not.

(B) YMC phase distribution of genes occupied by H3K9 acetylation or SAGA in either early OX or RC phase. Many more genomic regions of H3K9 acetylation were present in OX phase (n = 942) compared to RC phase (n = 161) at the same level of statistical significance. H3K9 acetylation was present almost exclusively at OX phase growth genes, specifically during OX phase (p value < 9.8×10^{140}). As determined previously by microarray analysis, there are 1016 OX, 975 RB, and 1508 RC phase genes in the YMC (Tu et al., 2005).

(C) Functional categories of genes occupied by H3K9 acetylation or SAGA as determined by MIPS (Munich Information Center for Protein Sequences) functional classification. The genes called by each ChIP-seq experiment were used to identify overrepresented gene functions (the top 100 genes are listed in tables 2.1 -2.4). Note that genes involved in ribosome biogenesis were found to be the most significant group of H3K9ac and SAGA targets. Genes involved in translation, amino acid metabolism, and rRNA processing which are also critical for growth are also highly overrepresented.

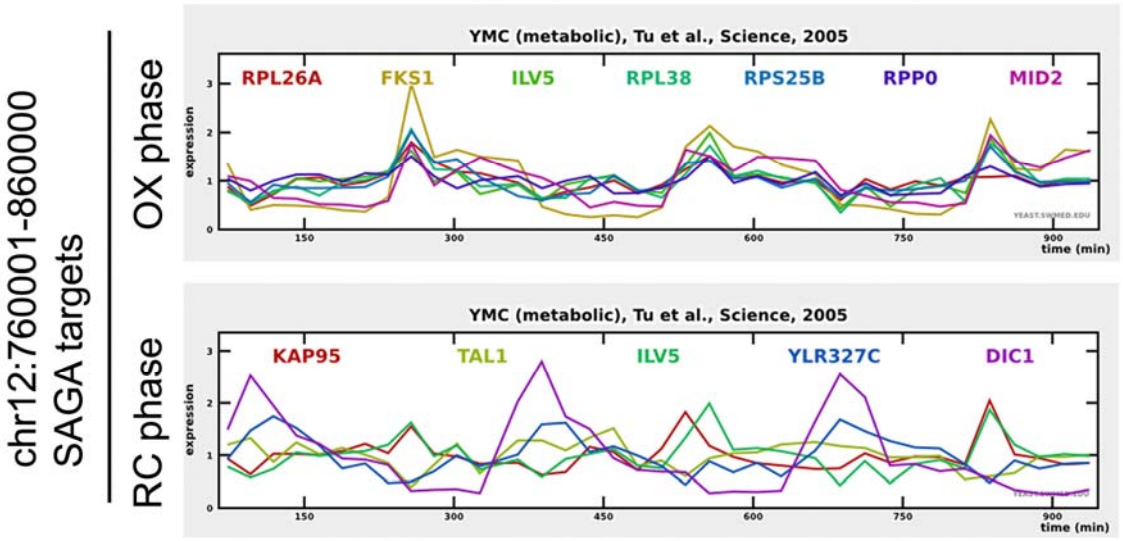

Figure 2.15. YMC Expression Profiles of Genes Marked in the ChIP-Seq Data Shown in Figure 2.14.

Expression data are from 36 time points over 3 consecutive metabolic cycles as reported previously (Tu et al., 2005) Expression data were displayed using SCEPTRANS - www.sceptrans.org

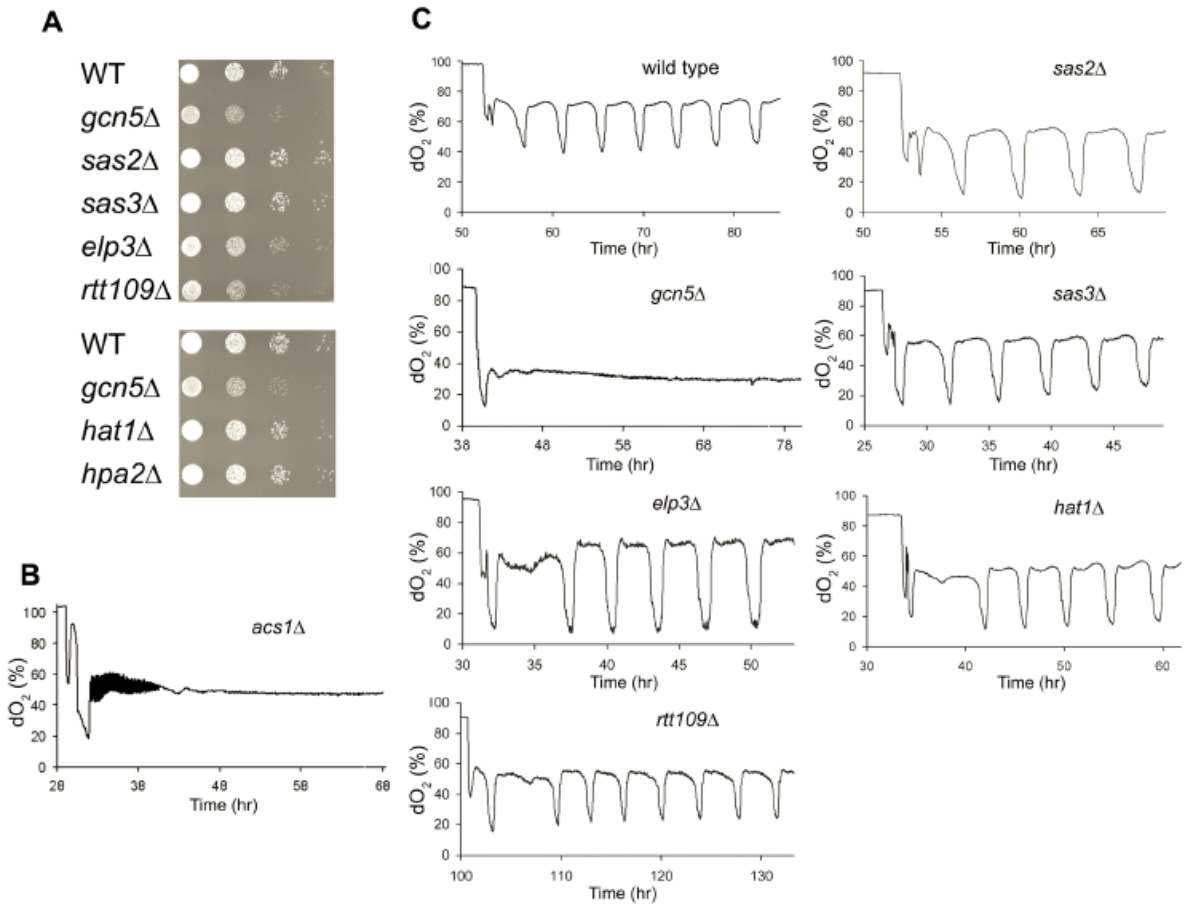

Figure 2.16 Gcn5p is an Acetyltransferase that is required for both Optimal Growth and Metabolic Cycling

(A) Serial dilutions of the indicated non-essential acetyltransferase gene deletion mutants were grown on SD minimal media at 30°C.

(B) The *acs1*Δ mutant, which lacks the acetyl-CoA synthetase expressed under nutrient-poor conditions, cannot undergo metabolic cycles, despite normal growth on SD media (data not shown). This observation supports a critical role for acetyl-CoA in the establishment of the synchronized bursts of growth that are a hallmark of the YMC.

(C) Representative YMC traces of select deletion mutants. Note that the *gcn5*Δ mutant was completely unable to undergo the synchronized bursts of respiratory growth that are a hallmark of the YMC. While *gcn5*Δ, *elp3*Δ, and *rtt109*Δ each compromised growth on SD, only *gcn5*Δ could not undergo metabolic cycles.

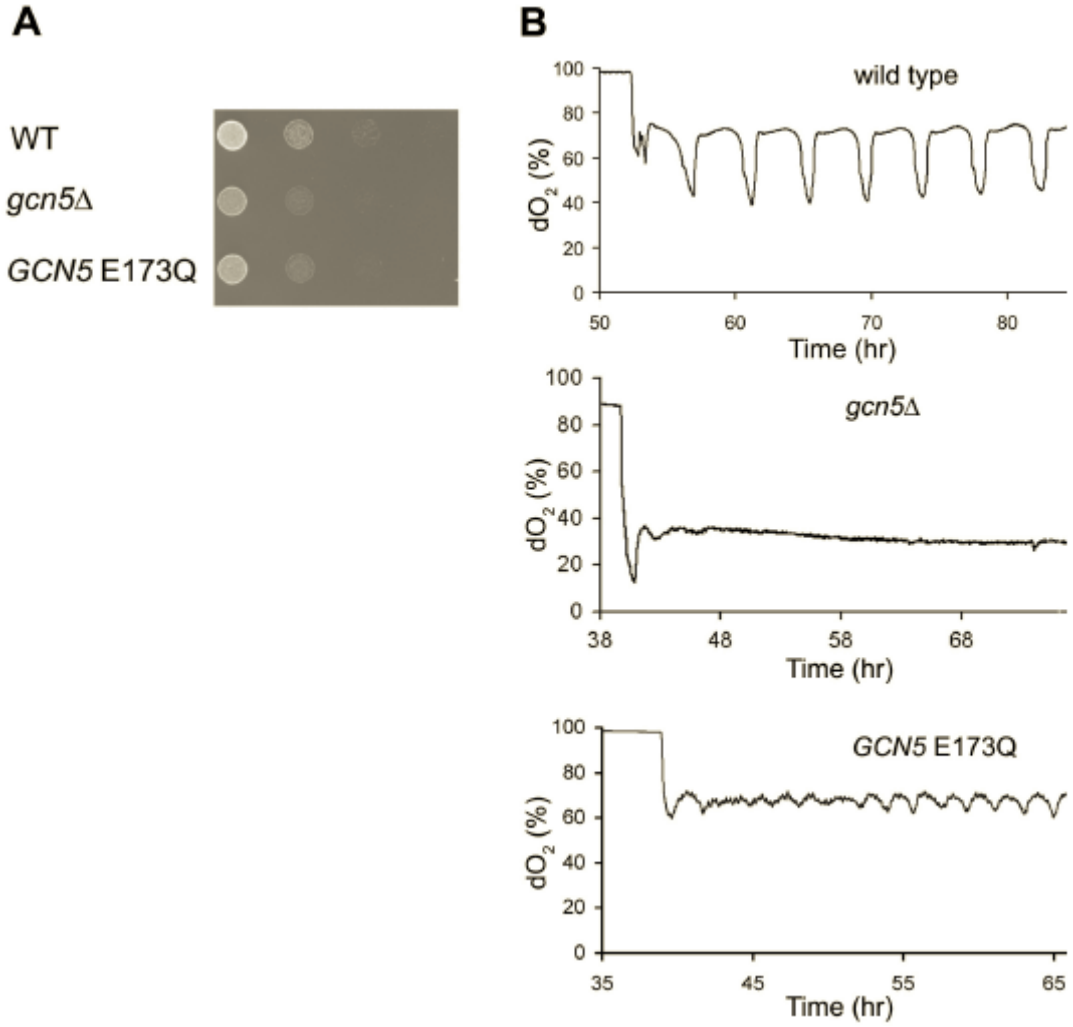

Figure 2.17. Both gcn5Δ and a Catalytically Inactive E173Q Mutant Exhibit Growth Defects and Severe Metabolic Cycling Phenotypes
(A) Serial dilutions of wild-type, *gcn5*Δ and *GCN5* E173Q strains grown on SD minimal media.
(B) YMC traces for the *gcn5*Δ and *GCN5* E173Q mutants.

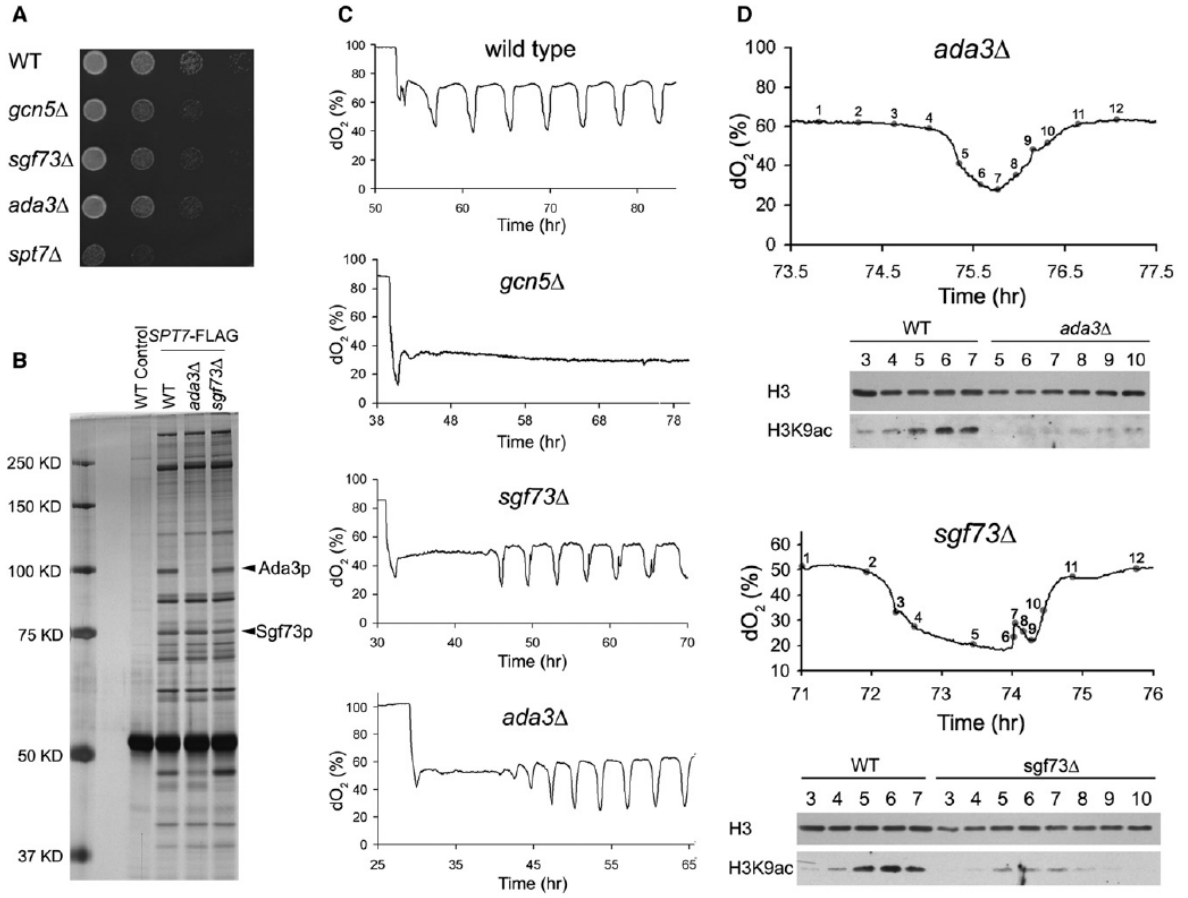

Figure 2.18 Deletion Mutants of the Acetylated SAGA Components Result in Slow Growth, Reduced H3 Acetylation, and Abnormal Metabolic Cycles

(A) Serial dilutions of the indicated strains were grown on SD minimal media at 30°C.

(B) Composition of the SAGA complex in WT, *ada3*Δ or *sgf73*Δ strains.

(C) YMC traces of the indicated strains. Note that the *ada3*Δ or *sgf73*Δ mutants experience a long delay (>10 hr) before they start cycling.

(D *ada3*Δ and *sgf73*Δ strains have significantly reduced H3K9 acetylation at OX, RB phase time points compared to WT. Note that ada3D exhibited a shorter OX phase compared to WT, while *sgf73*Δ exhibited an abnormal RB phase during which cells exhibit a second burst of oxygen consumption.

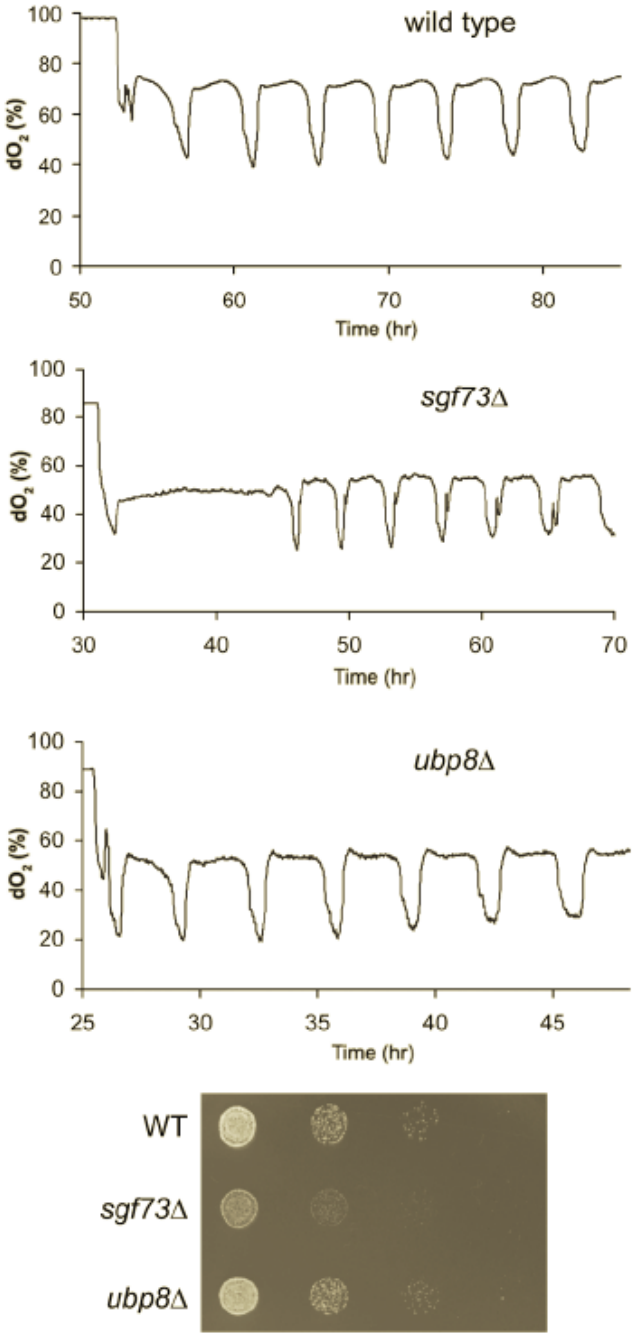

Figure 2.19 Growth and YMC Profiles for the *sgf73*Δ and *ubp8*Δ Mutants
For the *sgf73*Δ mutant, there were reproducible delays (>10 h) in the onset of cycling followed by short, abnormal bursts of oxygen consumption in the midst of the RB phases. In contrast, a *ubp8*Δ mutant which lacks the SAGA deubiquitination component (Henry et al., 2003) exhibited more normal metabolic cycles as well as normal growth on SD, suggesting that the histone deubiquitylase activity of SAGA is not critical for entry into growth.

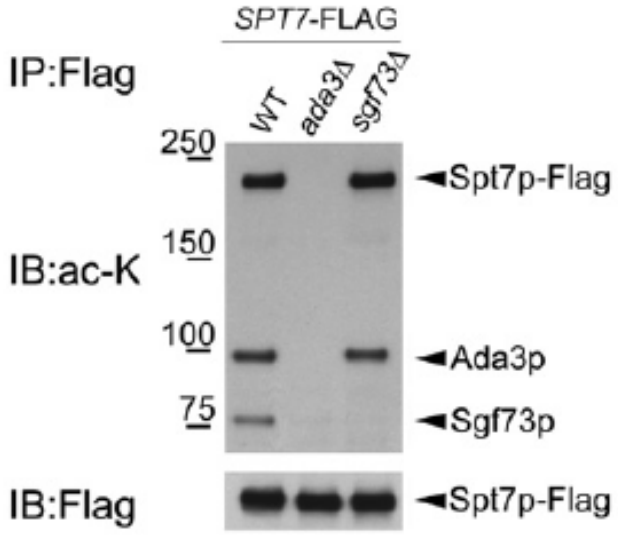

Figure 2.20 The acetylation of SAGA components is dependent on Ada3p.
The acetylation status of SAGA components are determined as described in the indicated strains

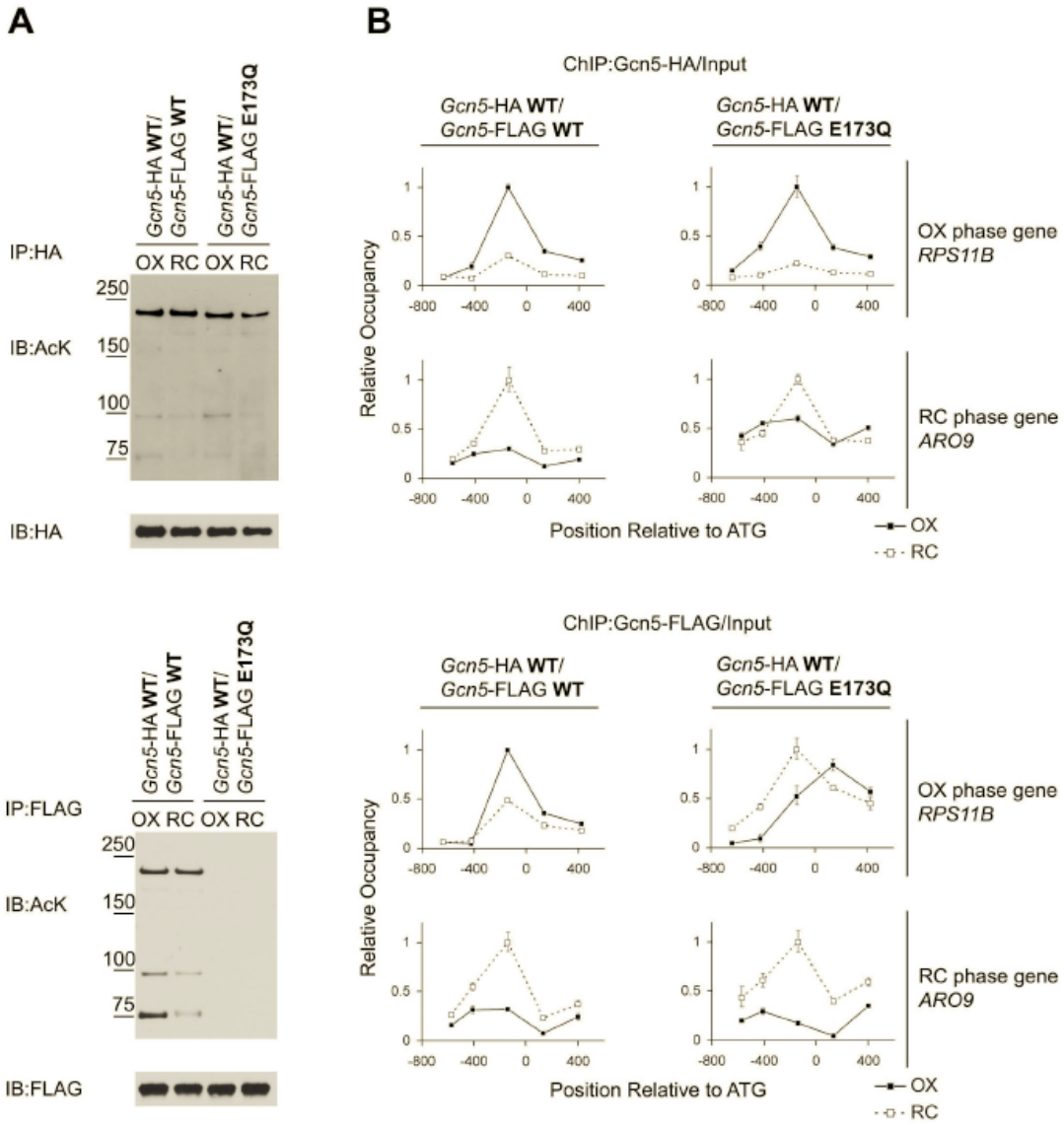

Figure 2.21. The Acetylation of SAGA Enables Recruitment to Growth Genes

(A) In the presence of a catalytically inactive Gcn5p (E173Q), the SAGA complex is not acetylated. Diploid strains expressing the indicated tagged versions of either a WT or a catalytically inactive Gcn5p were constructed and used to immunoprecipitate the SAGA complex during either the OX or RC phase. Note that Gcn5p E173Q pulls down a SAGA that is not acetylated. The integrity of the SAGA complex is not dependent on Gcn5p (Figure 2.8), in agreement with previous studies (Wu and Winston, 2002).

(B) The deacetylated form of SAGA can be recruited to an RC phase gene, but not to an OX phase growth gene. ChIP experiments were performed as described in Figure 2.12 to assess whether acetylated or deacetylated SAGA can bind to a representative RC phase gene (*ARO9*) or OX phase gene (*RPS11B*) during either OX or RC phase. Note that deacetylated SAGA is present at the RC phase gene during RC phase, but not at the OX phase gene during OX phase.

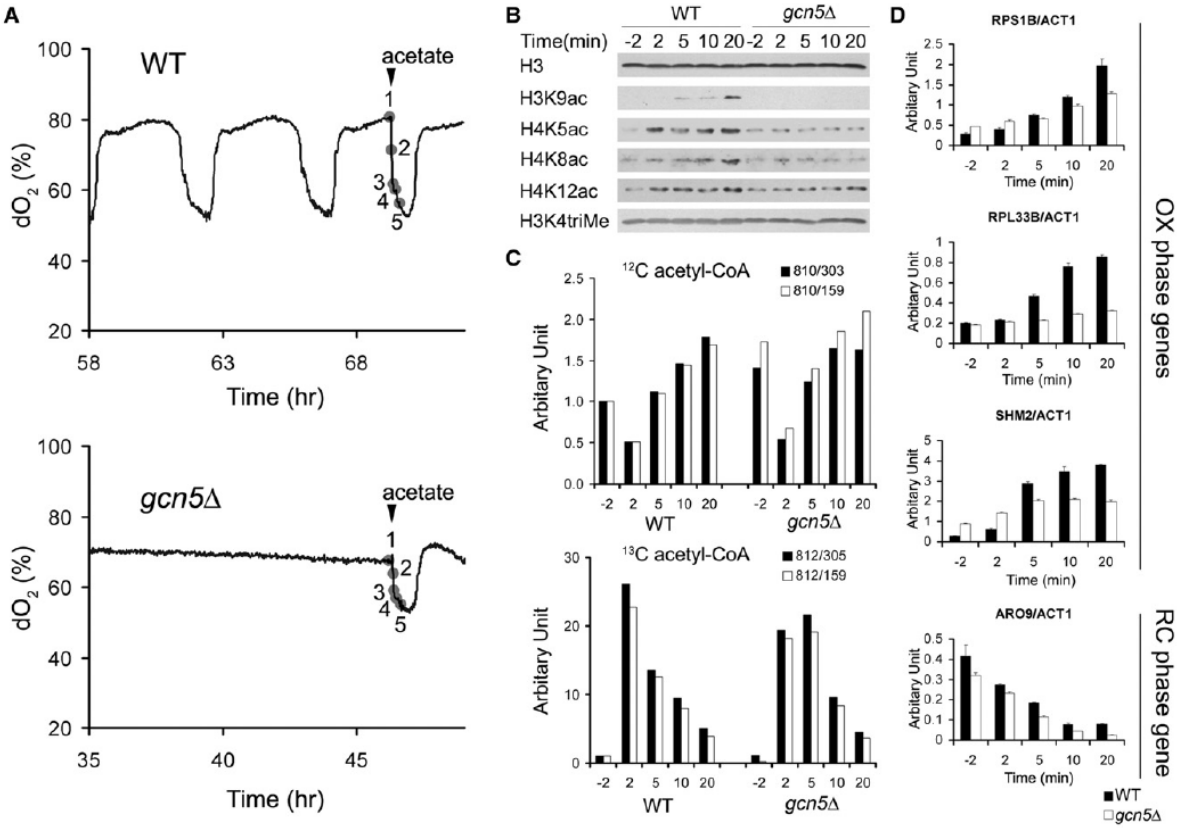

Figure 2.22. Acetyl-CoA-Induced Histone Acetylation and Growth Gene Expression Are Driven by Gcn5p and SAGA

(A) Acetate was added to WT or *gcn5*Δ cells during continuous growth to provide a burst of acetyl-CoA. Samples were harvested at the five indicated time points (2 min before, and 2, 5, 10, and 20 min after acetate dosing).

(B) H3K9 acetylation and H4 acetylation increase in response to acetate addition in WT cells but not in gcn5D cells.

(C) 13C acetate is converted to 13C acetyl-CoA and stimulates 12C acetyl-CoA production in both WT and *gcn5*Δ cells.

(D) *gcn5*Δ cells exhibit much slower induction of growth genes in response to acetate addition. Transcript levels of representative genes highly expressed in the OX growth phase (*RPS1B, RPL33B, SHM2*) or RC quiescent-like phase (*ARO9*) were measured by real-time PCR and normalized against actin (*ACT1*) transcript levels. Note that despite the defect in growth gene induction, transcript levels of the RC phase gene ARO9 still decreased with similar kinetics in the *gcn5*Δ mutant. Error bars denote standard deviation for triplicate experiments.

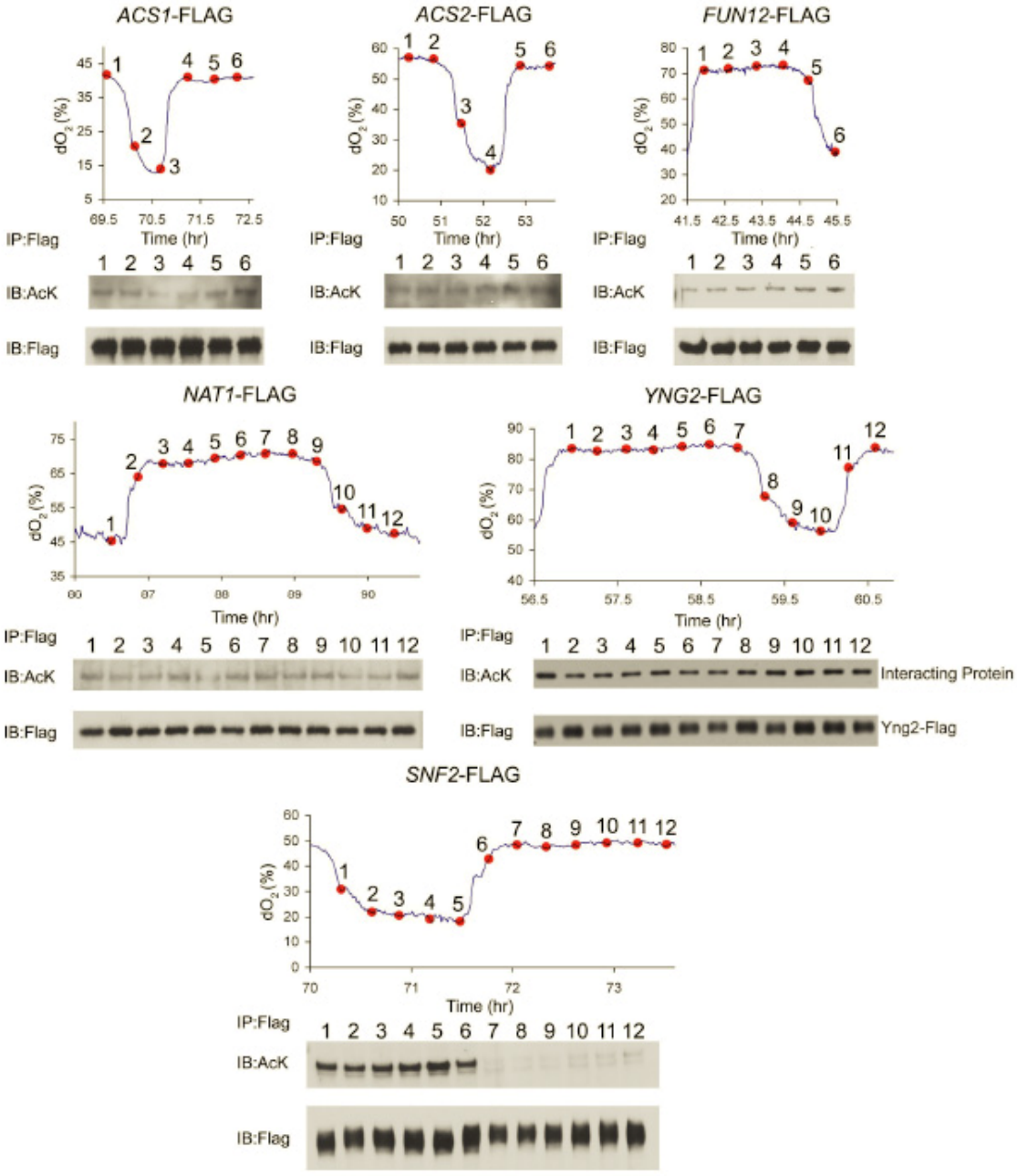

Figure 2.23 Not all Acetylated Proteins are Dynamically Acetylated across the YMC
The indicated proteins were tagged and then immunoprecipitated across the YMC to assess acetylation status as described in Figure 2A. Note that Snf2p, another Gcn5p substrate (Kim et al., 2010), is also dynamically acetylated across the YMC. In contrast, Acs1p, Acs2p, Fun12p, and Nat1p are acetylated but their acetylation is not dynamic across the YMC. Moreover, the NuA4 complex was immunoprecipitated across the YMC using a YNG2-FLAG strain. A coimmunoprecipitating protein of ~100 kDa is acetylated but its acetylation state did not change significantly as a function of the YMC.

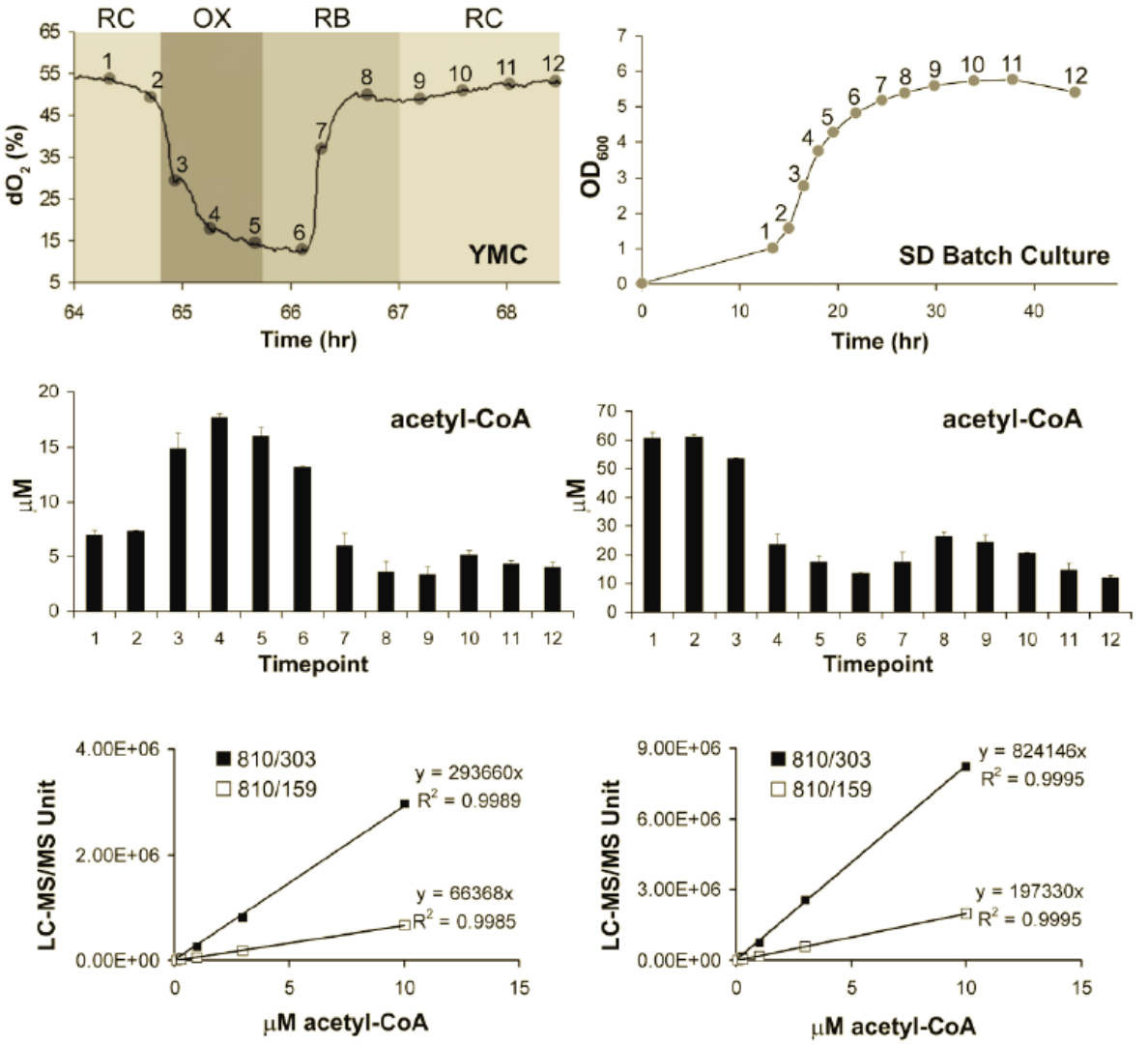

Figure 2.24. Estimates of In vivo Acetyl-CoA Concentrations in Yeast
The in vivo intracellular concentration of acetyl-CoA (average of the cell population, across the YMC and during batch culture growth) was calculated based on LC-MS/MS standard curves constructed using pure acetyl-CoA (Sigma). Values deduced from two daughter fragments of acetyl-CoA (303, 159 Da) were averaged. The estimation of acetyl-CoA concentration assumes 100% extraction of acetyl-CoA and a haploid cell volume of ~42 fl (Jorgensen et al., 2002). As only ~40-50% of the cell population enters cell division in each permissive window of the YMC under these continuous growth conditions (Tu et al., 2005), we estimate that acetyl-CoA may fluctuate between a low of ~3 µM in RC phase to over ~30 µM in OX phase cells that commit to growth. The Kd of acetyl-CoA binding to Gcn5p was previously measured to be ~8.5 µM (Langer et al., 2002), suggesting it is highly probable that Gcn5p activity is regulated by physiological fluctuations in acetyl-CoA.

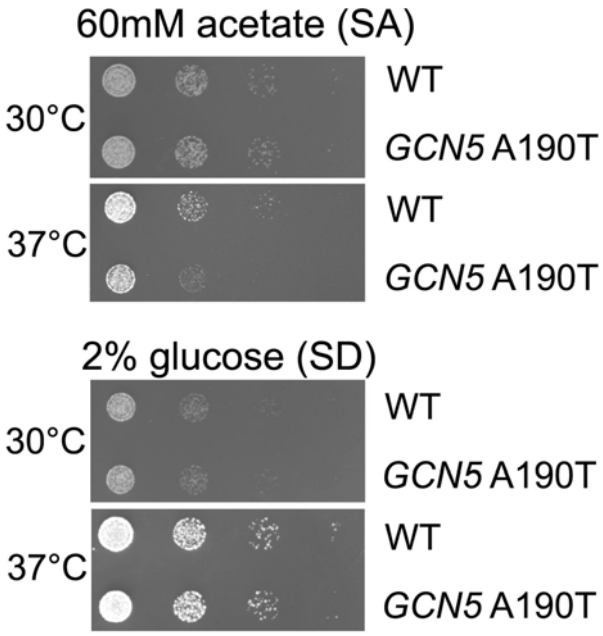

Figure 2.25 Temperature sensitive growth phenotype of Kd mutant *GCN5 A190T* on minimal medium with 60mM acetate (SA).

This mutant has a lower Kd for acetyl-CoA (0.56μM compared to 8.5μM for wild type, (Langer et al., 2002), thus increasing the affinity of the enzyme for acetyl-CoA by ~10), and exhibits a growth defect on acetate (SA) at 37°C but not 30°C. However, *GCN5* A190T cells exhibited normal growth on minimal medium with 2% glucose at 30°C and 37°C. Pictures of each plate were taken at different times due to different growth rates. In addition, *GCN5 A190T* cells exhibited normal metabolic cycles at 30°C (data not shown).

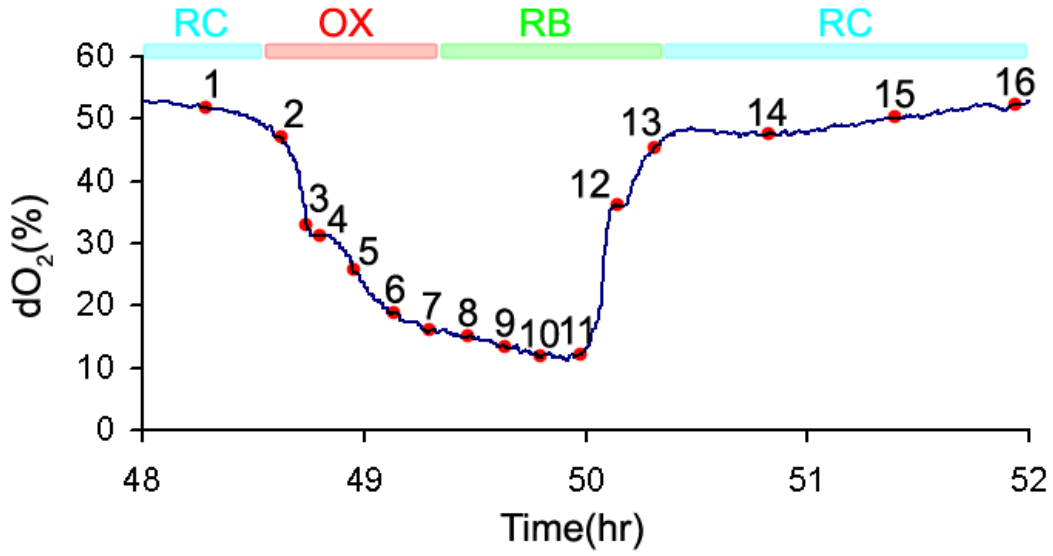

Figure 2.26 Timepoint collections over theYMC for RNA-seq and H3K9ac ChIP-seq
16 timepoints were collected over a YMC from CEN.PK alpha strain. The OX, RB and RC phases of the YMC was marked on top of the trace. Specific times of collection are listed in Table 2.5. Note that the intervals between timepoints were spaced differently in order to capture more dynamic changes in the OX and RB phase.

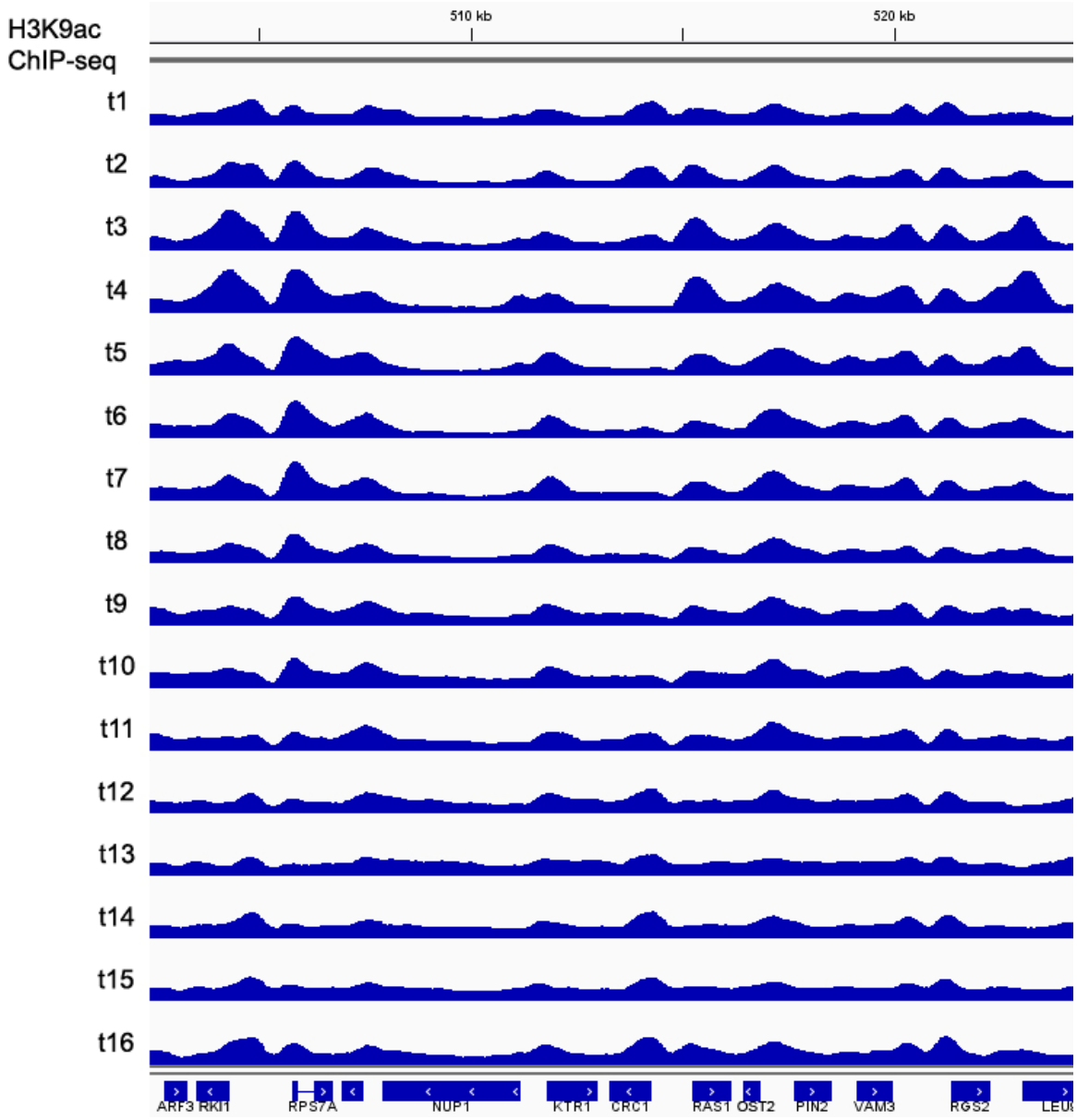

Figure 2.27 Snapshot of H3K9ac ChIP-seq over 16 timepoints from the YMC
H3K9ac occupancy was viewed in the integrated genome viewer (IGV). Note that most of the peaks were dynamically changing over the 16 timepoints. In agreement with the previous observation that histone acetylation is regulated by acetyl-CoA levels, the overall magnitude of the peaks from OX phase (t2-t7) is higher than in the RC phase (t1, t14-t16).

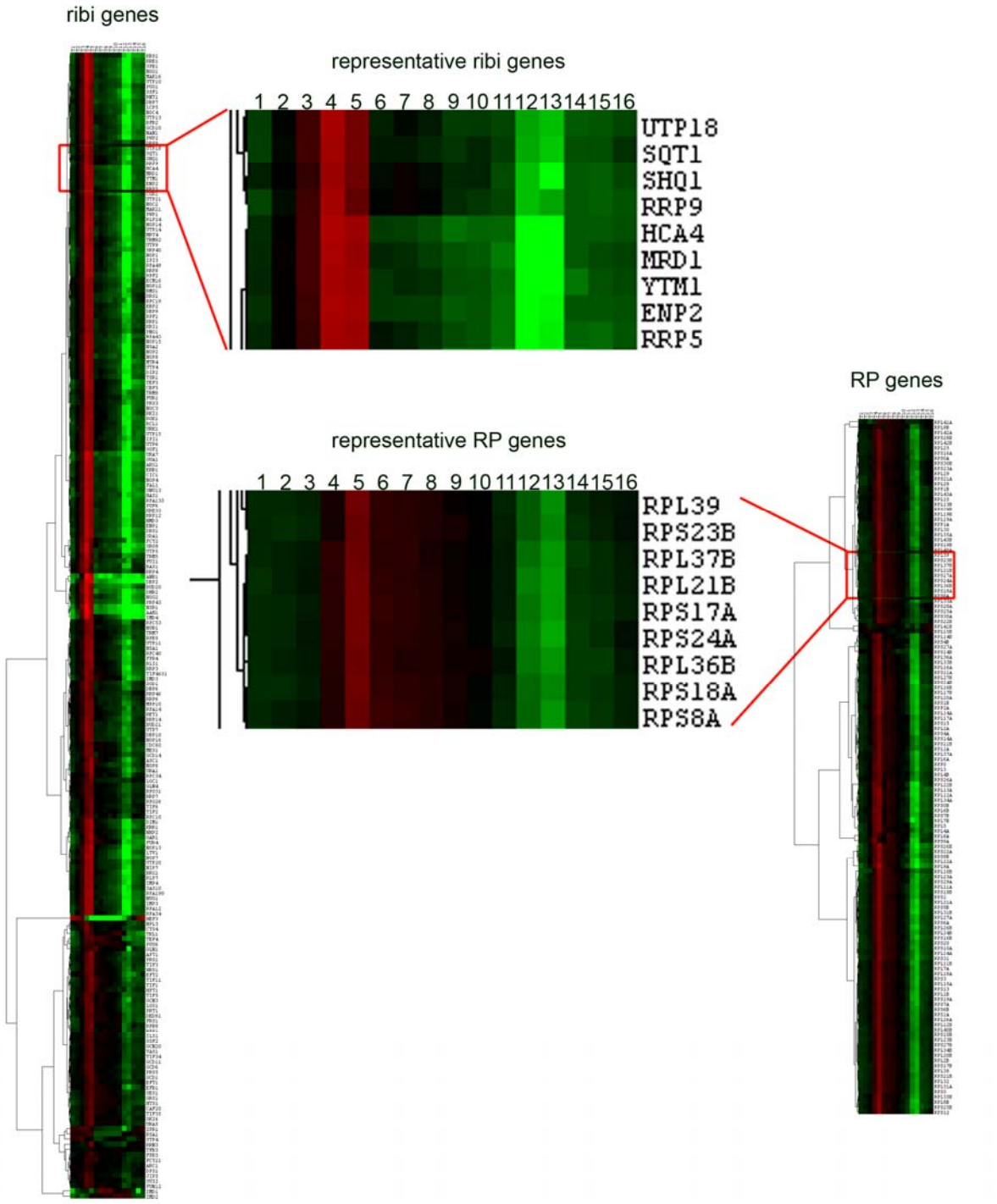

Figure 2.28 "just in time" regulation of ribi and RP gene expression
Expression profiles of ~240 ribi genes and ~140 RP genes were retrieved from the RNA-seq data and clustered to generate heatmaps. Expression of ribi genes started to increase from timepoint 3 and peak at timepoint 4 while expression of RP genes increase from timepoint 4 and peak at timepoint 5. The time difference between t3 and t4 is less than 5 min.

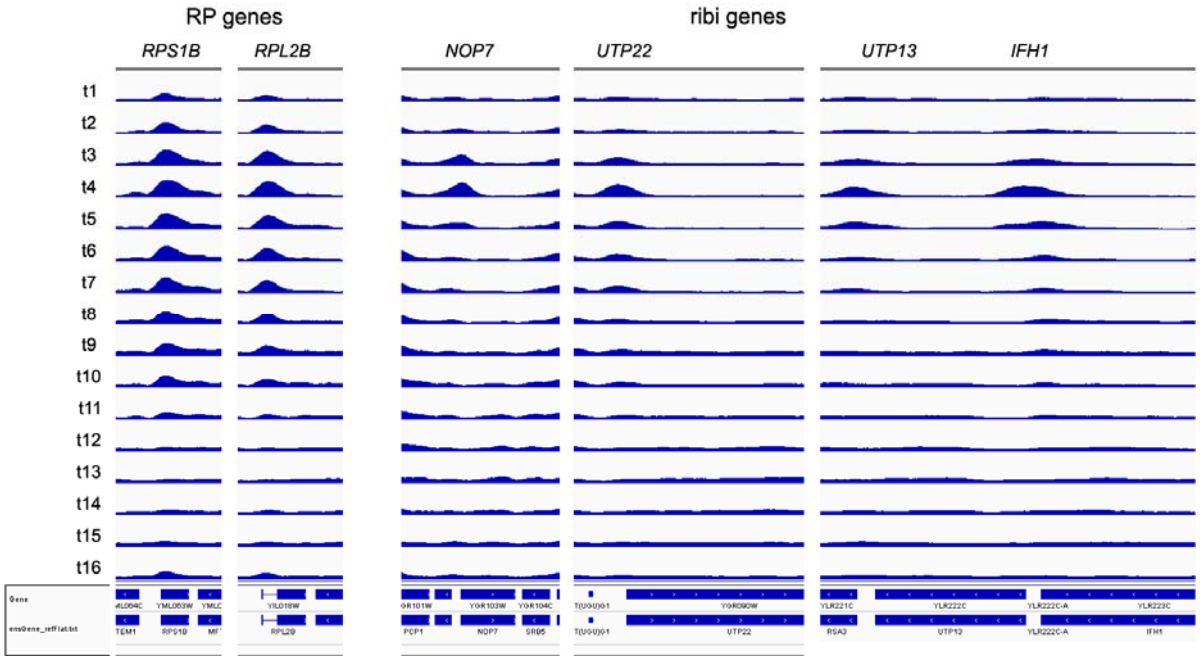

Figure 2.29 H3K9ac ChIP-seq profiles of representative RP and ribi genes

H3K9ac occupancy on promoters of representative RP and ribi genes were viewed from the Integrated Genome Viewer (IGV). H3K9ac marks on RP and ribi genes increase robustly during OX phase (t2-t7) in tune with the increasing acetyl-CoA levels. H3K9ac marks on ribi genes however, seems to be more transient than on RP genes.

Table 2.1. The top 100 peaks in OX phase for H3K9ac/H3 ranked by p-value/number of reads, as called by CLC Genomics Workbench. Note the abundance of ribosomal genes and other genes important for growth.

	Chr	start	end	Standard Name	Systematic Name	YMC phase	Description
1	chr5	269972	270061	RPL34A	YER056C-A	OX	Protein component of the large (60S) ribosomal subunit, nearly identical to Rpl34Bp and has similarity to rat L34 ribosomal protein
2	chr2	168421	168509	RPL19B	YBL027W	OX	Protein component of the large (60S) ribosomal subunit, nearly identical to Rpl19Ap and has similarity to rat L19 ribosomal protein
3	chr10	75001	75046	RPS22A	YJL190C	OX	Protein component of the small (40S) ribosomal subunit
4	chr7	439039	439105	RPL30	YGL030W	OX	Protein component of the large (60S) ribosomal subunit, has similarity to rat L30 ribosomal protein
5	chr6	223881	223972	YFR032C-B	YFR032C-B	N/A	Putative protein of unknown function
6	chr12	282219	282342	BUD20	YLR074C	OX	Protein involved in bud-site selection
7	chr5	101216	101278	CUP5	YEL027W	OX	Proteolipid subunit of the vacuolar H(+)-ATPase V0 sector (subunit c; dicyclohexylcarbodiimide binding subunit)
8	chr4	308505	308569	RPL13A	YDL082W	OX	Protein component of the large (60S) ribosomal subunit, nearly identical to Rpl13Bp
9	chr16	75714	75811	RPL36B	YPL249C-A	OX	Protein component of the large (60S) ribosomal subunit, nearly identical to Rpl36Ap and has similarity to rat L36 ribosomal protein
10	chr3	178098	178181	RPS14A	YCR031C	OX	Ribosomal protein 59 of the small subunit, required for ribosome assembly and 20S pre-rRNA processing
11	chr12	722060	722182	ATP14	YLR295C	RB	Subunit h of the F0 sector of mitochondrial F1F0 ATP synthase, which is a large, evolutionarily conserved enzyme complex required for ATP synthesis
12	chr12	796046	796119	RPS25B	YLR333C	OX	Protein component of the small (40S) ribosomal subunit
13	chr15	960073	960182	RPA43	YOR340C	OX	RNA polymerase I subunit A43
14	chr2	606220	606308	RPL21A	YBR191W	OX	Protein component of the large (60S) ribosomal subunit, nearly identical to Rpl21Bp and has similarity to rat L21 ribosomal protein
15	chr15	254273	254355	RPP2A	YOL039W	OX	Ribosomal protein P2 alpha, a component of the ribosomal stalk, which is involved in the interaction between translational elongation factors and the ribosome
16	chr16	588122	588206	YPR013C	YPR013C	OX	Putative zinc finger protein
17	chr3	124898	125000	YCR007C	YCR007C	N/A	Putative integral membrane protein, member of DUP240 gene family
18	chr7	558474	558595	CAX4	YGR036C	OX	Dolichyl pyrophosphate (Dol-P-P) phosphatase with a luminally oriented active site in the ER, cleaves the anhydride linkage in Dol-P-P
19	chr2	89312	89413	YBL071C-B	YBL071C-B	N/A	Putative protein of unknown function
20	chr4	1301663	1301754	RPL12B	YDR418W	OX	Protein component of the large (60S) ribosomal subunit, nearly identical to Rpl12Ap
21	chr15	968482	968539	YOR342C	YOR342C	OX	Putative protein of unknown function
22	chr7	1065783	1065888	BIO2	YGR286C	N/A	Biotin synthase, catalyzes the conversion of dethiobiotin to biotin, which is the last step of the biotin biosynthesis pathway
23	chr11	431290	431470	RPL14A	YKL006W	OX	N-terminally acetylated protein component of the large (60S) ribosomal subunit, nearly identical to Rpl14Bp and has similarity to rat L14 ribosomal protein
24	chr15	867786	867844	YOR293C-A	YOR293C-A	N/A	Putative protein of unknown function
25	chr12	260308	260406	REX2	YLR059C	OX	3'-5' RNA exonuclease
26	chr9	98846	98861	RPL16A	YIL133C	OX	N-terminally acetylated protein component of the large (60S) ribosomal subunit, binds to 5.8 S rRNA
27	chr11	556940	557207	KTR2	YKR061W	OX	Mannosyltransferase involved in N-linked protein glycosylation
28	chr8	75422	75498	RPS20	YHL015W	OX	Protein component of the small (40S) ribosomal subunit
29	chr12	499138	499211	RPS31	YLR167W	OX	Fusion protein that is cleaved to yield a ribosomal protein of the small (40S) subunit and ubiquitin
30	chr5	15404	15464	DLD3	YEL071W	RB	D-lactate dehydrogenase, part of the retrograde regulon which consists of genes whose expression is stimulated by damage to mitochondria
31	chr15	93863	93877	RPL18A	YOL120C	OX	Protein component of the large (60S) ribosomal subunit, identical to Rpl18Bp and has similarity to rat L18 ribosomal protein
32	chr15	79819	80326	RPL25	YOL127W	OX	Primary rRNA-binding ribosomal protein component of the large (60S) ribosomal subunit, has similarity to E. coli L23 and rat L23a ribosomal proteins
33	chr14	331270	331329	RPL42A	YNL162W	OX	Protein component of the large (60S) ribosomal subunit, identical to Rpl42Bp and has similarity to rat L44 ribosomal protein
34	chr5	53030	53114	RPL12A	YEL054C	OX	Protein component of the large (60S) ribosomal subunit, nearly identical to Rpl12Bp
35	chr12	1028905	1028982	RPL6B	YLR448W	OX	Protein component of the large (60S) ribosomal subunit, has similarity to Rpl6Ap and to rat L6 ribosomal protein
36	chr15	1043733	1043766	GDH1	YOR375C	OX	NADP(+)-dependent glutamate dehydrogenase, synthesizes glutamate from ammonia and alpha-ketoglutarate
37	chr5	423773	423832	RPS26B	YER131W	OX	Protein component of the small (40S) ribosomal subunit
38	chr12	781947	782109	YLR326W	YLR326W	OX	Putative protein of unknown function, predicted to be palmitoylated
39	chr13	551172	551266	RPL13B	YMR142C	OX	Protein component of the large (60S) ribosomal subunit, nearly identical to Rpl13Ap
40	chr13	651304	651385	RPL36A	YMR194W	OX	N-terminally acetylated protein component of the large (60S) ribosomal subunit, nearly identical to Rpl36Bp and has similarity to rat L36 ribosomal protein
41	chr16	481477	481566	EGD1	YPL037C	OX	Subunit beta1 of the nascent polypeptide-associated complex (NAC) involved in protein targeting, associated with cytoplasmic ribosomes
42	chr7	325256	325409	TOS8	YGL096W	RC	Homeodomain-containing protein and putative transcription factor found associated with chromatin
43	chr2	549300	549380	RPB5	YBR154C	OX	RNA polymerase subunit ABC27, common to RNA polymerases I, II, and III
44	chr4	364754	364780	LHP1	YDL051W	OX	RNA binding protein required for maturation of tRNA and U6 snRNA precursors
45	chr11	383070	383182	MAE1	YKL029C	OX	Mitochondrial malic enzyme, catalyzes the oxidative decarboxylation of malate to pyruvate, which is a key intermediate in sugar metabolism and a precursor for synthesis of several amino acids
46	chr14	663046	663097	TIM23	YNR017W	RB	Essential component of the Translocase of the Inner Mitochondrial membrane (TIM23 complex)
47	chr15	779430	779472	RPL33B	YOR234C	OX	Ribosomal protein L37 of the large (60S) ribosomal subunit, nearly identical to Rpl33Ap and has similarity to rat L35a
48	chr14	302684	302765	RPS3	YNL178W	OX	Protein component of the small (40S) ribosomal subunit, has apurinic/apyrimidinic (AP) endonuclease activity
49	chr13	753176	753705	RPL20A	YMR242C	OX	Protein component of the large (60S) ribosomal subunit, nearly identical to Rpl20Bp and has similarity to rat L18a ribosomal protein
50	chr16	405898	406017	RPL21B	YPL079W	OX	Protein component of the large (60S) ribosomal subunit, nearly identical to Rpl21Ap and has similarity to rat L21 ribosomal protein
51	chr12	855207	855374	RPS22B	YLR367W	OX	Protein component of the small (40S) ribosomal subunit
52	chr12	931797	931872	RPL31B	YLR406C	OX	Protein component of the large (60S) ribosomal subunit, nearly identical to Rpl31Ap and has similarity to rat L31 ribosomal protein
53	chr4	1490617	1490679	SNA2	YDR525W-A	RC	Protein of unknown function, has similarity to Pmp3p, which is involved in cation transport
54	chr14	499639	499724	RPL9B	YNL067W	OX	Protein component of the large (60S) ribosomal subunit, nearly identical to Rpl9Ap and has similarity to E. coli L6 and rat L9 ribosomal proteins
55	chr11	335022	335102	TMA19	YKL056C	OX	Protein that associates with ribosomes
56	chr7	677325	677435	TPC1	YGR096W	OX	Mitochondrial membrane transporter that mediates uptake of the essential cofactor thiamine pyrophosphate (ThPP) into mitochondria
57	chr2	785494	785654	CTP1	YBR291C	OX	Mitochondrial inner membrane citrate transporter, member of the mitochondrial carrier family

58	chr12	522855	522947	RPL37A	YLR185W	OX	Protein component of the large (60S) ribosomal subunit, has similarity to Rpl37Bp and to rat L37 ribosomal protein
59	chr13	226023	226097	RPS17A	YML024W	OX	Ribosomal protein 51 (rp51) of the small (40s) subunit
60	chr4	341062	341135	RPS29B	YDL061C	OX	Protein component of the small (40S) ribosomal subunit
61	chr12	673265	673312	RPS28B	YLR264W	OX	Protein component of the small (40S) ribosomal subunit
62	chr8	382551	382624	RPL42B	YHR141C	OX	Protein component of the large (60S) ribosomal subunit, identical to Rpl42Ap and has similarity to rat L44
63	chr4	117655	117743	RPL35A	YDL191W	OX	Protein component of the large (60S) ribosomal subunit, identical to Rpl35Bp and has similarity to rat L35 ribosomal protein
64	chr13	535007	535085	RRB1	YMR131C	OX	Essential nuclear protein involved in early steps of ribosome biogenesis
65	chr2	45693	45774	RPL32	YBL092W	OX	Protein component of the large (60S) ribosomal subunit, has similarity to rat L32 ribosomal protein
66	chr7	738588	738709	PPT1	YGR123C	OX	Protein serine/threonine phosphatase with similarity to human phosphatase PP5
67	chr16	576476	576575	SUT2	YPR009W	OX	Putative transcription factor
68	chr13	732332	732416	RPS10B	YMR230W	OX	Protein component of the small (40S) ribosomal subunit
69	chr13	123891	123953	RPL6A	YML073C	OX	N-terminally acetylated protein component of the large (60S) ribosomal subunit, has similarity to Rpl6Bp and to rat L6 ribosomal protein
70	chr7	879770	879865	HIP1	YGR191W	OX	High-affinity histidine permease, also involved in the transport of manganese ions
71	chr10	703043	703101	RPS4A	YJR145C	OX	Protein component of the small (40S) ribosomal subunit
72	chr8	505488	505562	RPS4B	YHR203C	OX	Protein component of the small (40S) ribosomal subunit
73	chr15	1010737	1010829	VTS1	YOR359W	OX	Post-transcriptional gene regulator, flap-structured DNA-binding and RNA-binding protein
74	chr4	1239533	1239623	RPP2B	YDR382W	OX	Ribosomal protein P2 beta, a component of the ribosomal stalk, which is involved in the interaction between translational elongation factors and the ribosome
75	chr12	819321	819396	RPL26A	YLR344W	OX	Protein component of the large (60S) ribosomal subunit, nearly identical to Rpl26Bp and has similarity to E. coli L24 and rat L26 ribosomal proteins
76	chr12	264240	264293	YLR063W	YLR063W	OX	Putative S-adenosylmethionine-dependent methyltransferase
77	chr7	148850	148888	YGL188C-A	YGL188C-A	N/A	Putative protein of unknown function
78	chr5	306382	306475	RPS24A	YER074W	OX	Protein component of the small (40S) ribosomal subunit
79	chr13	558442	558527	TIF34	YMR146C	OX	eIF3i subunit of the core complex of translation initiation factor 3 (eIF3), which is essential for translation
80	chr9	188142	188236	LYS12	YIL094C	OX	Homo-isocitrate dehydrogenase, an NAD-linked mitochondrial enzyme required for the fourth step in the biosynthesis of lysine, in which homo-isocitrate is oxidatively decarboxylated to alpha-ketoadipate
81	chr11	109327	109413	RPL17A	YKL180W	OX	Protein component of the large (60S) ribosomal subunit, nearly identical to Rpl17Bp and has similarity to E. coli L22 and rat L17 ribosomal proteins
82	chr7	534686	534736	RPS25A	YGR027C	OX	Protein component of the small (40S) ribosomal subunit
83	chr4	1402016	1402089	RPL27B	YDR471W	OX	Protein component of the large (60S) ribosomal subunit, nearly identical to Rpl27Ap and has similarity to rat L27 ribosomal protein
84	chr4	1359897	1359982	RPS18A	YDR450W	OX	Protein component of the small (40S) ribosomal subunit
85	chr5	237628	237728	ERG28	YER044C	RC	Endoplasmic reticulum membrane protein, may facilitate protein-protein interactions between the Erg26p dehydrogenase and the Erg27p 3-ketoreductase and/or tether these enzymes to the ER
86	chr15	444785	444867	RPL3	YOR063W	OX	Protein component of the large (60S) ribosomal subunit, has similarity to E. coli L3 and rat L3 ribosomal proteins
87	chr7	311135	311225	RPL28	YGL103W	OX	Ribosomal protein of the large (60S) ribosomal subunit, has similarity to E. coli L15 and rat L27a ribosomal proteins
88	chr13	13655	13747	ERO1	YML130C	OX	Thiol oxidase required for oxidative protein folding in the endoplasmic reticulum
89	chr12	898283	898404	RPS29A	YLR388W	OX	Protein component of the small (40S) ribosomal subunit
90	chr10	119426	119462	YJL160C	YJL160C	RC	Putative protein of unknown function
91	chr10	608451	608530	RPL43B	YJR094W-A	OX	Protein component of the large (60S) ribosomal subunit, identical to Rpl43Ap and has similarity to rat L37a ribosomal protein
92	chr14	252030	252116	SSB2	YNL209W	OX	Cytoplasmic ATPase that is a ribosome-associated molecular chaperone, functions with J-protein partner Zuo1p
93	chr7	56023	56086	MTO1	YGL236C	RB	Mitochondrial protein, forms a heterodimer complex with Mss1p that performs the 5-carboxymethylaminomethyl modification of the wobble uridine base in mitochondrial tRNAs
94	chr10	180915	181028	YJL127C-B	YJL127C-B	N/A	Putative protein of unknown function
95	chr2	306865	306922	PDX3	YBR035C	N/A	Pyridoxine (pyridoxamine) phosphate oxidase, has homologs in E. coli and Myxococcus xanthus
96	chr12	1002017	1002101	ATG23	YLR431C	RC	Peripheral membrane protein required for the cytoplasm-to-vacuole targeting (Cvt) pathway and efficient macroautophagy
97	chr10	466544	466620	ESS1	YJR017C	N/A	Peptidylprolyl-cis/trans-isomerase (PPIase) specific for phosphorylated serine and threonine residues N-terminal to proline
98	chr4	322408	322521	RPL31A	YDL075W	OX	Protein component of the large (60S) ribosomal subunit, nearly identical to Rpl31Bp and has similarity to rat L31 ribosomal protein
99	chr7	920694	920779	RPS0A	YGR214W	OX	Protein component of the small (40S) ribosomal subunit, nearly identical to Rps0Bp
100	chr11	229526	229611	KTI12	YKL110C	OX	Protein that plays a role, with Elongator complex, in modification of wobble nucleosides in tRNA

Table2.2. The top 100 peaks in RC phase for H3K9ac/H3 ranked by p-value/number of reads, as called by CLC Genomics Workbench.

	Chr	start	end	Standard Name	Systematic Name	YMC phase	Description
1	chr4	915156	915211	HTA1	YDR225W	N/A	Histone H2A, core histone protein required for chromatin assembly and chromosome function
2	chr11	92619	92832	MTR2	YKL186C	RC	mRNA transport regulator, essential nuclear protein
3	chr4	599269	599336	RAD55	YDR076W	N/A	Protein that stimulates strand exchange by stabilizing the binding of Rad51p to single-stranded DNA
4	chr8	17297	17439	YHL042W	YHL042W	N/A	Putative protein of unknown function
5	chr4	135102	135148	INH1	YDL181W	RC	Protein that inhibits ATP hydrolysis by the F1F0-ATP synthase
6	chr3	123107	123229	CIT2	YCR005C	RB	Citrate synthase, catalyzes the condensation of acetyl coenzyme A and oxaloacetate to form citrate, peroxisomal isozyme involved in glyoxylate cycle
7	chr5	265045	265135	HIS1	YER055C	OX	ATP phosphoribosyltransferase, a hexameric enzyme, catalyzes the first step in histidine biosynthesis
8	chr4	679947	679987	ALT2	YDR111C	RC	Putative alanine transaminase (glutamic pyruvic transaminase)
9	chr10	181742	181974	YJL127C-B	YJL127C-B	N/A	Putative protein of unknown function
10	chr5	69506	69589	IES6	YEL044W	RC	Protein that associates with the INO80 chromatin remodeling complex under low-salt conditions
11	chr15	1044045	1044129	GDH1	YOR375C	OX	NADP(+)-dependent glutamate dehydrogenase, synthesizes glutamate from ammonia and alpha-ketoglutarate
12	chr13	759389	759483	FAA4	YMR246W	RC	Long chain fatty acyl-CoA synthetase, activates imported fatty acids with a preference for C12:0-C16:0 chain lengths
13	chr10	468553	468627	TES1	YJR019C	RC	Peroxisomal acyl-CoA thioesterase likely to be involved in fatty acid oxidation rather than fatty acid synthesis
14	chr4	1490569	1490644	SNA2	YDR525W-A	RC	Protein of unknown function, has similarity to Pmp3p, which is involved in cation transport
15	chr12	874722	874793	FBP1	YLR377C	RC	Fructose-1,6-bisphosphatase, key regulatory enzyme in the gluconeogenesis pathway, required for glucose metabolism
16	chr7	785414	785496	YGR146C-A	YGR146C-A	N/A	Putative protein of unknown function
17	chr8	297173	297190	HXT5	YHR096C	RC	Hexose transporter with moderate affinity for glucose, induced in the presence of non-fermentable carbon sources, induced by a decrease in growth rate
18	chr15	109020	109099	SHR5	YOL110W	RC	Subunit of a palmitoyltransferase, composed of Shr5p and Erf2p, that adds a palmitoyl lipid moiety to heterolipidated substrates such as Ras1p and Ras2p through a thioester linkage
19	chr11	389896	389959	GPX1	YKL026C	RC	Phospholipid hydroperoxide glutathione peroxidase induced by glucose starvation that protects cells from phospholipid hydroperoxides and nonphospholipid peroxides during oxidative stress
20	chr13	610945	611027	SIP18	YMR175W	RC	Phospholipid-binding protein
21	chr7	433711	433823	MIG1	YGL035C	RC	Transcription factor involved in glucose repression
22	chr16	195833	195905	UIP4	YPL186C	RC	Protein that interacts with Ulp1p, a Ubl (ubiquitin-like protein)-specific protease for Smt3p protein conjugates
23	chr2	741831	742010	FMP21	YBR269C	RC	Putative protein of unknown function
24	chr7	989463	989550	MGA1	YGR249W	RC	Protein similar to heat shock transcription factor
25	chr15	232041	232431	DDR2	YOL052C-A	N/A	Multistress response protein, expression is activated by a variety of xenobiotic agents and environmental or physiological stresses
26	chr4	977010	977095	SWM1	YDR260C	RC	Subunit of the anaphase-promoting complex, which is an E3 ubiquitin ligase that regulates the metaphase-anaphase transition and exit from mitosis
27	chr12	1011681	1011767	YLR437C	YLR437C	RC	Protein that regulates the nuclear localization of ribonucleotide reductase Rnr2p and Rnr4p subunits
28	chr7	849134	849206	ERG1	YGR175C	OX	Squalene epoxidase, catalyzes the epoxidation of squalene to 2,3-oxidosqualene
29	chr7	979743	979829	LSC2	YGR244C	RC	Beta subunit of succinyl-CoA ligase, which is a mitochondrial enzyme of the TCA cycle that catalyzes the nucleotide-dependent conversion of succinyl-CoA to succinate
30	chr15	216717	216784	GPD2	YOL059W	OX	NAD-dependent glycerol 3-phosphate dehydrogenase, homolog of Gpd1p, expression is controlled by an oxygen-independent signaling pathway required to regulate metabolism under anoxic conditions
31	chr16	900076	900168	SMX3	YPR182W	RC	Core Sm protein Sm F
32	chr14	198306	198374	ZWF1	YNL241C	N/A	Glucose-6-phosphate dehydrogenase (G6PD), catalyzes the first step of the pentose phosphate pathway
33	chr10	337585	337673	YJL052C-A	YJL052C-A	N/A	Putative protein of unknown function, identified based on comparison to related yeast species
34	chr12	322845	322922	YLR091W	YLR091W	RC	Protein of unknown function, required for mitochondrial genome maintenance
35	chr7	144462	144534	COX13	YGL191W	RB	Subunit VIa of cytochrome c oxidase, which is the terminal member of the mitochondrial inner membrane electron transport chain
36	chr12	341371	341466	YLR099W-A	YLR099W-A	N/A	Putative protein of unknown function
37	chr8	107811	107880	QCR10	YHR001W-A	RC	Subunit of the ubiqunol-cytochrome c oxidoreductase complex which includes Cobp, Rip1p, Cyt1p, Cor1p, Qcr2p, Qcr6p, Qcr7p, Qcr8p, Qcr9p, and Qcr10p
38	chr10	236902	236990	LSB6	YJL100W	RC	Type II phosphatidylinositol 4-kinase that binds Las17p, which is a homolog of human Wiskott-Aldrich Syndrome protein involved in actin patch assembly and actin polymerization
39	chr7	398319	398382	OLE1	YGL055W	RC	Delta(9) fatty acid desaturase, required for monounsaturated fatty acid synthesis and for normal distribution of mitochondria
40	chr16	615053	615157	ATH1	YPR026W	RC	Acid trehalase required for utilization of extracellular trehalose
41	chr13	167895	167957	YML054C-A	YML054C-A	N/A	Putative protein of unknown function
42	chr16	46809	46882	KEL3	YPL263C	OX	Cytoplasmic protein of unknown function
43	chr15	1039051	1039122	ALD4	YOR374W	RC	Mitochondrial aldehyde dehydrogenase, required for growth on ethanol and conversion of acetaldehyde to acetate
44	chr15	389242	389315	CRS5	YOR031W	RC	Copper-binding metallothionein, required for wild-type copper resistance
45	chr4	1496545	1496657	QCR7	YDR529C	RB	Subunit 7 of the ubiquinol cytochrome-c reductase complex, which is a component of the mitochondrial inner membrane electron transport chain
46	chr16	552061	552128	ULA1	YPL003W	RC	Protein that acts together with Uba3p to activate Rub1p before its conjugation to proteins (neddylation), which may play a role in protein degradation
47	chr13	625897	625983	YMR182W-A	YMR182W-A	N/A	Putative protein of unknown function
48	chr16	373531	373605	SSU1	YPL092W	RC	Plasma membrane sulfite pump involved in sulfite metabolism and required for efficient sulfite efflux
49	chr16	132599	132684	FLC1	YPL221W	OX	Putative FAD transporter
50	chr7	525438	525537	UGA1	YGR019W	RC	Gamma-aminobutyrate (GABA) transaminase (4-aminobutyrate aminotransferase) involved in the 4-aminobutyrate and glutamate degradation pathways
51	chr4	1459670	1459775	PSP1	YDR505C	RC	Asn and gln rich protein of unknown function
52	chr4	892349	892419	AHA1	YDR214W	RC	Co-chaperone that binds to Hsp82p and activates its ATPase activity
53	chr13	478127	478211	YMR105W-A	YMR105W-A	N/A	Putative protein of unknown function
54	chr16	198782	198871	YPL183W-A	YPL183W-A	RB	Protein involved translation

55	chr4	1233471	1233532	YDR379C-A	YDR379C-A	N/A	Protein involved in the assembly of the mitochondrial succinate dehydrogenase complex
56	chr15	154687	154773	MPD2	YOL088C	RC	Member of the protein disulfide isomerase (PDI) family, exhibits chaperone activity
57	chr10	452222	452232	YJR008W	YJR008W	RC	Putative protein of unknown function
58	chr7	909192	909311	YGR205W	YGR205W	RC	ATP-binding protein of unknown function
59	chr10	291362	291470	PRY1	YJL079C	RB	Protein of unknown function
60	chr16	822353	822464	ASN1	YPR145W	OX	Asparagine synthetase, isozyme of Asn2p
61	chr4	1166619	1166703	SVF1	YDR346C	N/A	Protein with a potential role in cell survival pathways, required for the diauxic growth shift
62	chr6	90549	90621	EPL1	YFL024C	RC	Component of NuA4, which is an essential histone H4/H2A acetyltransferase complex
63	chr16	30082	30155	ATP15	YPL271W	N/A	Epsilon subunit of the F1 sector of mitochondrial F1F0 ATP synthase, which is a large, evolutionarily conserved enzyme complex required for ATP synthesis
64	chr16	296762	296904	GIP3	YPL137C	OX	Glc7-interacting protein whose overexpression relocalizes Glc7p from the nucleus and prevents chromosome segregation
65	chr13	30163	30230	NDI1	YML120C	RB	NADH:ubiquinone oxidoreductase, transfers electrons from NADH to ubiquinone in the respiratory chain but does not pump protons
66	chr2	294070	294201	ETR1	YBR026C	RC	2-enoyl thioester reductase, member of the medium chain dehydrogenase/reductase family
67	chr13	253186	253265	YML007C-A	YML007C-A	N/A	Putative protein of unknown function
68	chr15	742093	742168	MGM1	YOR211C	OX	Mitochondrial GTPase, present in complex with Ugo1p and Fzo1p
69	chr8	370064	370127	IGO2	YHR132W-A	N/A	Protein required for initiation of G0 program
70	chr4	1059132	1059243	ATP5	YDR298C	RB	Subunit 5 of the stator stalk of mitochondrial F1F0 ATP synthase, which is an evolutionarily conserved enzyme complex required for ATP synthesis
71	chr11	143535	143628	PIR1	YKL164C	RC	O-glycosylated protein required for cell wall stability
72	chr4	699900	699990	YDR124W	YDR124W	OX	Putative protein of unknown function
73	chr13	391648	391858	SEN15	YMR059W	OX	Subunit of the tRNA splicing endonuclease, which is composed of Sen2p, Sen15p, Sen34p, and Sen54p
74	chr11	171466	171572	AVT3	YKL146W	N/A	Vacuolar transporter, exports large neutral amino acids from the vacuole
75	chr15	931023	931099	SNC2	YOR327C	RC	Vesicle membrane receptor protein (v-SNARE) involved in the fusion between Golgi-derived secretory vesicles with the plasma membrane
76	chr4	316624	316696	MDH3	YDL078C	RC	Peroxisomal malate dehydrogenase, catalyzes interconversion of malate and oxaloacetate
77	chr15	380933	381002	STI1	YOR027W	RC	Hsp90 cochaperone, interacts with the Ssa group of the cytosolic Hsp70 chaperones and activates Ssa1p ATPase activity
78	chr13	343847	343939	MIH1	YMR036C	RC	Protein tyrosine phosphatase involved in cell cycle control
79	chr4	1189492	1189591	YDR357C	YDR357C	RC	Protein of unknown function
80	chr4	1445904	1445989	ITR1	YDR497C	RC	Myo-inositol transporter with strong similarity to the minor myo-inositol transporter Itr2p, member of the sugar transporter superfamily
81	chr16	17250	17306	YPL277C	YPL277C	RC	Putative protein of unknown function
82	chr15	675526	675592	LAS17	YOR181W	RC	Actin assembly factor, activates the Arp2/3 protein complex that nucleates branched actin filaments
83	chr11	567414	567483	GPT2	YKR067W	RC	Glycerol-3-phosphate/dihydroxyacetone phosphate dual substrate-specific sn-1 acyltransferase located in lipid particles and the ER
84	chr7	554965	555078	TIM21	YGR033C	RC	Nonessential subunit of the Translocase of the Inner Mitochondrial membrane (TIM23 complex)
85	chr7	108087	108141	POX1	YGL205W	RC	Fatty-acyl coenzyme A oxidase, involved in the fatty acid beta-oxidation pathway
86	chr13	262863	262997	GLO1	YML004C	RC	Monomeric glyoxalase I, catalyzes the detoxification of methylglyoxal (a by-product of glycolysis) via condensation with glutathione to produce S-D-lactoylglutathione
87	chr13	649825	650066	MRPL24	YMR193W	RB	Mitochondrial ribosomal protein of the large subunit
88	chr4	1184417	1184562	TRP4	YDR354W	RC	Anthranilate phosphoribosyl transferase of the tryptophan biosynthetic pathway, catalyzes the phosphoribosylation of anthranilate, subject to the general control system of amino acid biosynthesis
89	chr10	204965	205016	MDV1	YJL112W	RB	Peripheral protein of the cytosolic face of the mitochondrial outer membrane, required for mitochondrial fission
90	chr7	581472	581570	NQM1	YGR043C	RC	Transaldolase of unknown function
91	chr16	299737	299844	ODC1	YPL134C	RB	Mitochondrial inner membrane transporter, exports 2-oxoadipate and 2-oxoglutarate from the mitochondrial matrix to the cytosol for lysine and glutamate biosynthesis and lysine catabolism
92	chr4	894407	894503	ADR1	YDR216W	RC	Carbon source-responsive zinc-finger transcription factor, required for transcription of the glucose-repressed gene ADH2, of peroxisomal protein genes
93	chr4	755186	755298	KGD2	YDR148C	RB	Dihydrolipoyl transsuccinylase, component of the mitochondrial alpha-ketoglutarate dehydrogenase complex
94	chr13	558849	558958	YMR147W	YMR147W	RC	Putative protein of unknown function
95	chr12	758840	758922	QNQ1	YLR312C	RC	Putative protein of unknown function
96	chr4	188509	188808	NOP14	YDL148C	OX	Nucleolar protein, forms a complex with Noc4p that mediates maturation and nuclear export of 40S ribosomal subunits
97	chr9	126193	126251	AYR1	YIL124W	RC	NADPH-dependent 1-acyl dihydroxyacetone phosphate reductase found in lipid particles, ER, and mitochondrial outer membrane
98	chr4	1443846	1443929	PUF6	YDR496C	OX	Pumilio-homology domain protein that binds the 3' UTR of ASH1 mRNA and represses its translation, resulting in proper asymmetric localization of ASH1 mRNA
99	chr13	192774	192854	CAT2	YML042W	RC	Carnitine acetyl-CoA transferase present in both mitochondria and peroxisomes, transfers activated acetyl groups to carnitine to form acetylcarnitine which can be shuttled across membranes
100	chr15	340110	340216	SGT2	YOR007C	RC	Glutamine-rich cytoplasmic protein that serves as a scaffold for binding Get4/5p and other proteins required to mediate posttranslational insertion of tail-anchored proteins into the ER membrane

Table 2.3. The top 100 peaks in OX phase for SAGA/Input ranked by max|FC|, as called by CisGenome (Ji et al., 2008). Note the abundance of ribosomal genes and other genes important for growth.

	Chr	start	end	Standard Name	Systematic Name	YMC phase	Description
1	chr7	398033	398061	SDS23	YGL056C	RC	One of two S. cerevisiae homologs (Sds23p and Sds24p) of the S. pombe Sds23 protein, which is implicated in APC/cyclosome regulation
2	chr11	666196	666524	YKR106W	YKR106W	N/A	Protein of unconfirmed function
3	chr12	1061443	1061547	YLR460C	YLR460C	N/A	Member of the quinone oxidoreductase family, up-regulated in response to the fungicide mancozeb
4	chr2	813136	813164	COS2	YBR302C	RC	Protein of unknown function, member of the DUP380 subfamily of conserved, often subtelomerically-encoded proteins
5	chr16	645534	645606	YPR036W-A	YPR036W-A	N/A	Protein of unknown function
6	chr5	69100	69180	GLY1	YEL046C	OX	Threonine aldolase, catalyzes the cleavage of L-allo-threonine and L-threonine to glycine
7	chr4	368976	369053	SIT4	YDL047W	N/A	Type 2A-related serine-threonine phosphatase that functions in the G1/S transition of the mitotic cycle
8	chr1	230037	230265	YAR075W	YAR075W	OX	Non-functional protein with homology IMP dehydrogenase
9	chr4	465291	465399	SNQ2	YDR011W	RC	Plasma membrane ATP-binding cassette (ABC) transporter, multidrug transporter involved in multidrug resistance and resistance to singlet oxygen species
10	chr8	562450	562612	YHR219W	YHR219W	N/A	Putative protein of unknown function with similarity to helicases
11	chr7	766247	766370	TPO2	YGR138C	OX	Polyamine transport protein specific for spermine
12	chr7	598982	599010	MUP1	YGR055W	OX	High affinity methionine permease, integral membrane protein with 13 putative membrane-spanning regions
13	chr4	132836	132932	LYS20	YDL182W	OX	Homocitrate synthase isozyme, catalyzes the condensation of acetyl-CoA and alpha-ketoglutarate to form homocitrate, which is the first step in the lysine biosynthesis pathway
14	chr7	483128	484428	YGL007C-A	YGL007C-A	N/A	Putative protein of unknown function, identified by gene-trapping, microarray-based expression analysis, and genome-wide homology searching
15	chr5	545299	545378	BMH1	YER177W	N/A	14-3-3 protein, major isoform
16	chr9	249154	249358	VHR1	YIL056W	RB	Transcriptional activator, required for the vitamin H-responsive element mediated induction of VHT1 and BIO5 in response to low biotin concentrations
17	chr5	85222	85431	UTR5	YEL035C	RC	Protein of unknown function
18	chr5	462003	462032	FTR1	YER145C	RB	High affinity iron permease involved in the transport of iron across the plasma membrane
19	chr11	630195	630284	PCK1	YKR097W	RB	Phosphoenolpyruvate carboxykinase, key enzyme in gluconeogenesis, catalyzes early reaction in carbohydrate biosynthesis, glucose represses transcription and accelerates mRNA degradation
20	chr4	1490021	1490494	SNA2	YDR525W-A	RC	Protein of unknown function, has similarity to Pmp3p, which is involved in cation transport
21	chr8	122389	122441	YHR007C-A	YHR007C-A	N/A	Putative protein of unknown function
22	chr10	236430	236475	GSH1	YJL101C	OX	Gamma glutamylcysteine synthetase catalyzes the first step in glutathione (GSH) biosynthesis
23	chr8	462156	462251	OYE2	YHR179W	OX	Conserved NADPH oxidoreductase containing flavin mononucleotide (FMN), homologous to Oye3p with different ligand binding and catalytic properties
24	chr12	370546	370617	CCW12	YLR110C	RC	Cell wall mannoprotein, mutants are defective in mating and agglutination, expression is downregulated by alpha-factor
25	chr11	230914	230959	HAP4	YKL109W	RB	Subunit of the heme-activated, glucose-repressed Hap2p/3p/4p/5p CCAAT-binding complex, a transcriptional activator and global regulator of respiratory gene expression
26	chr2	140475	140602	FUI1	YBL042C	OX	High affinity uridine permease, localizes to the plasma membrane
27	chr16	679061	679089	ROX1	YPR065W	OX	Heme-dependent repressor of hypoxic genes
28	chr7	271842	271885	MET13	YGL125W	RB	Major isozyme of methylenetetrahydrofolate reductase, catalyzes the reduction of 5,10-methylenetetrahydrofolate to 5-methyltetrahydrofolate in the methionine biosynthesis pathway
29	chr9	0	134	YIL177C	YIL177C	N/A	Putative protein of unknown function
30	chr15	968041	968168	YOR342C	YOR342C	OX	Putative protein of unknown function
31	chr8	98207	98267	STE20	YHL007C	OX	Cdc42p-activated signal transducing kinase of the PAK (p21-activated kinase) family
32	chr4	0	160	COS7	YDL248W	N/A	Protein of unknown function, member of the DUP380 subfamily of conserved, often subtelomerically-encoded proteins
33	chr12	29512	29658	YCT1	YLL055W	OX	High-affinity cysteine-specific transporter with similarity to the Dal5p family of transporters
34	chr5	141235	141263	YEL007W	YEL007W	N/A	Putative protein with sequence similarity to S. pombe gti1+ (gluconate transport inducer 1)
35	chr7	156340	156369	STR3	YGL184C	OX	Cystathionine beta-lyase, converts cystathionine into homocysteine
36	chr15	1043347	1043434	GDH1	YOR375C	OX	NADP(+)-dependent glutamate dehydrogenase, synthesizes glutamate from ammonia and alpha-ketoglutarate
37	chr2	392532	392583	SLM4	YBR077C	RC	Component of the EGO complex, which is involved in the regulation of microautophagy, and of the GSE complex, which is required for proper sorting of amino acid permease Gap1p
38	chr4	591761	591797	IPT1	YDR072C	RC	Inositolphosphotransferase, involved in synthesis of mannose-(inositol-P)2-ceramide (M(IP)2C), the most abundant sphingolipid
39	chr4	117447	117515	RPL35A	YDL191W	OX	Protein component of the large (60S) ribosomal subunit, identical to Rpl35Bp and has similarity to rat L35 ribosomal protein
40	chr12	809395	809506	FKS1	YLR342W	OX	Catalytic subunit of 1,3-beta-D-glucan synthase, functionally redundant with alternate catalytic subunit Gsc2p
41	chr3	0	349	YCL073C	YCL073C	N/A	Protein of unconfirmed function
42	chr13	306182	306229	SOK2	YMR016C	OX	Nuclear protein that plays a regulatory role in the cyclic AMP (cAMP)-dependent protein kinase (PKA) signal transduction pathway
43	chr15	254028	254112	RPP2A	YOL039W	OX	Ribosomal protein P2 alpha, a component of the ribosomal stalk, which is involved in the interaction between translational elongation factors and the ribosome
44	chr11	258456	258485	YKL096C-B	YKL096C-B	N/A	Putative protein of unknown function
45	chr7	323397	323484	SRM1	YGL097W	OX	Nucleotide exchange factor for Gsp1p, localizes to the nucleus, required for nucleocytoplasmic trafficking of macromolecules
46	chr7	609969	609997	ERG25	YGR060W	RC	C-4 methyl sterol oxidase, catalyzes the first of three steps required to remove two C-4 methyl groups from an intermediate in ergosterol biosynthesis
47	chr16	502775	502865	SKS1	YPL026C	OX	Putative serine/threonine protein kinase
48	chr16	76425	76454	RPL36B	YPL249C-A	OX	Protein component of the large (60S) ribosomal subunit, nearly identical to Rpl36Ap and has similarity to rat L36 ribosomal protein
49	chr12	84252	84347	TPO1	YLL028W	RC	Polyamine transporter that recognizes spermine, putrescine, and spermidine
50	chr9	439765	439879	YIR042C	YIR042C	RB	Putative protein of unknown function
51	chr13	226584	226612	RPS17A	YML024W	OX	Ribosomal protein 51 (rp51) of the small (40s) subunit
52	chr4	628787	628889	RLI1	YDR091C	OX	Essential iron-sulfur protein required for ribosome biogenesis and translation initiation and termination
53	chr15	27821	27916	YOL155W-A	YOL155W-A	N/A	Putative protein of unknown function
54	chr9	21786	21814	YIL172C	YIL172C	N/A	Alpha-glucosidase with broad substrate specificity for alpha-1,4- and alpha-1,6-glucosides
55	chr4	523168	523196	ARO3	YDR035W	RC	3-deoxy-D-arabino-heptulosonate-7-phosphate (DAHP) synthase, catalyzes the first step in aromatic amino acid biosynthesis and is feedback-inhibited by phenylalanine
56	chr13	924312	924474	PAU19	YMR325W	RC	Protein of unknown function, member of the seripauperin multigene family encoded mainly in subtelomeric regions
57	chr6	270128	270160	YFR057W	YFR057W	N/A	Putative protein of unknown function

58	chr12	449576	449644	RNH203	YLR154C	N/A	Ribonuclease H2 subunit, required for RNase H2 activity
59	chr15	978727	978800	TYE7	YOR344C	OX	Serine-rich protein that contains a basic-helix-loop-helix (bHLH) DNA binding motif
60	chr13	551677	551790	RPS16A	YMR143W	OX	Protein component of the small (40S) ribosomal subunit
61	chr7	310774	310864	RPL28	YGL103W	OX	Ribosomal protein of the large (60S) ribosomal subunit, has similarity to E. coli L15 and rat L27a ribosomal proteins
62	chr12	253446	253545	ERG3	YLR056W	OX	C-5 sterol desaturase, catalyzes the introduction of a C-5(6) double bond into episterol, a precursor in ergosterol biosynthesis
63	chr13	91204	91269	RPM2	YML091C	RB	Protein subunit of mitochondrial RNase P, has roles in nuclear transcription, cytoplasmic and mitochondrial RNA processing, and mitochondrial translation
64	chr13	408599	408660	MOT3	YMR070W	N/A	Nuclear transcription factor with two Cys2-His2 zinc fingers
65	chr11	518656	518791	UTH1	YKR042W	OX	Mitochondrial outer membrane and cell wall localized SUN family member involved in cell wall biogenesis and required for mitochondrial autophagy
66	chr8	36061	36158	RPL8A	YHL033C	OX	Ribosomal protein L4 of the large (60S) ribosomal subunit, nearly identical to Rpl8Bp and has similarity to rat L7a ribosomal protein
67	chr11	68350	68409	MNN4	YKL201C	RC	Putative positive regulator of mannosylphosphate transferase (Mnn6p), involved in mannosylphosphorylation of N-linked oligosaccharides
68	chr10	646925	646954	YJR120W	YJR120W	N/A	Protein of unknown function
69	chr3	78356	78431	AGP1	YCL025C	OX	Low-affinity amino acid permease with broad substrate range, involved in uptake of asparagine, glutamine, and other amino acids
70	chr15	520678	520745	RGS2	YOR107W	RC	Negative regulator of glucose-induced cAMP signaling
71	chr12	65531	65585	UBI4	YLL039C	RC	Ubiquitin, becomes conjugated to proteins, marking them for selective degradation via the ubiquitin-26S proteasome system
72	chr14	356739	357161	MEP2	YNL142W	OX	Ammonium permease involved in regulation of pseudohyphal growth
73	chr6	95666	95737	GAT1	YFL021W	OX	Transcriptional activator of genes involved in nitrogen catabolite repression
74	chr11	381766	381872	IXR1	YKL032C	RC	Protein that binds DNA containing intrastrand cross-links formed by cisplatin, contains two HMG (high mobility group box) domains, which confer the ability to bend cisplatin-modified DNA
75	chr14	217438	217467	PDR16	YNL231C	OX	Phosphatidylinositol transfer protein (PITP) controlled by the multiple drug resistance regulator Pdr1p, localizes to lipid particles and microsomes, controls levels of various lipids
76	chr16	641311	641733	GLN1	YPR035W	N/A	Glutamine synthetase (GS), synthesizes glutamine from glutamate and ammonia
77	chr4	366141	366530	KNH1	YDL049C	RC	Protein with similarity to Kre9p, which is involved in cell wall beta 1,6-glucan synthesis
78	chr2	415461	415489	RPL19A	YBR084C-A	OX	Protein component of the large (60S) ribosomal subunit, nearly identical to Rpl19Bp and has similarity to rat L19 ribosomal protein
79	chr8	18073	18135	YHL042W	YHL042W	N/A	Putative protein of unknown function
80	chr15	216493	216532	MAM3	YOL060C	RC	Protein required for normal mitochondrial morphology, has similarity to hemolysins
81	chr16	653994	654068	RPL43A	YPR043W	OX	Protein component of the large (60S) ribosomal subunit, identical to Rpl43Bp and has similarity to rat L37a ribosomal protein
82	chr4	1080593	1080621	GIC2	YDR309C	OX	Redundant rho-like GTPase Cdc42p effector
83	chr16	328954	329040	IDI1	YPL117C	RC	Isopentenyl diphosphate:dimethylallyl diphosphate isomerase (IPP isomerase), catalyzes an essential activation step in the isoprenoid biosynthetic pathway
84	chr16	302914	303035	RPL5	YPL131W	OX	Protein component of the large (60S) ribosomal subunit with similarity to E. coli L18 and rat L5 ribosomal proteins
85	chr14	661956	662283	ACC1	YNR016C	N/A	Acetyl-CoA carboxylase, biotin containing enzyme that catalyzes the carboxylation of acetyl-CoA to form malonyl-CoA
86	chr2	376112	376145	BAP2	YBR068C	RC	High-affinity leucine permease, functions as a branched-chain amino acid permease involved in the uptake of leucine, isoleucine and valine
87	chr13	774418	774446	HOR7	YMR251W-A	RC	Protein of unknown function
88	chr16	822270	822298	ASN1	YPR145W	OX	Asparagine synthetase, isozyme of Asn2p
89	chr3	163644	163762	PMP1	YCR024C-A	RC	Small single-membrane span proteolipid that functions as a regulatory subunit of the plasma membrane H(+)-ATPase Pma1p
90	chr1	68400	68429	CLN3	YAL040C	OX	G1 cyclin involved in cell cycle progression
91	chr4	386967	387061	BSC1	YDL037C	OX	Protein of unconfirmed function, similar to cell surface flocculin Muc1p
92	chr12	645989	646018	HAP1	YLR256W	RC	Zinc finger transcription factor involved in the complex regulation of gene expression in response to levels of heme and oxygen
93	chr9	187812	187870	LYS12	YIL094C	OX	Homo-isocitrate dehydrogenase, an NAD-linked mitochondrial enzyme required for the fourth step in the biosynthesis of lysine, in which homo-isocitrate is oxidatively decarboxylated to alpha-ketoadipate
94	chr16	576288	576381	SUT2	YPR009W	OX	Putative transcription factor
95	chr12	950341	950384	YLR412C-A	YLR412C-A	N/A	Putative protein of unknown function
96	chr15	94517	94562	RPL18A	YOL120C	OX	Protein component of the large (60S) ribosomal subunit, identical to Rpl18Bp and has similarity to rat L18 ribosomal protein
97	chr1	141755	141825	SSA1	YAL005C	RC	ATPase involved in protein folding and nuclear localization signal (NLS)-directed nuclear transport
98	chr11	99953	99985	FAS1	YKL182W	RC	Beta subunit of fatty acid synthetase, which catalyzes the synthesis of long-chain saturated fatty acids
99	chr5	140542	140610	GCN4	YEL009C	RC	Basic leucine zipper (bZIP) transcriptional activator of amino acid biosynthetic genes in response to amino acid starvation
100	chr12	187603	187765	IZH3	YLR023C	RB	Membrane protein involved in zinc ion homeostasis, member of the four-protein IZH family, expression induced by zinc deficiency

Table 2.4. The top 100 peaks in RC phase for SAGA/Input ranked by max|FC|, as called by CisGenome (Ji et al., 2008).

	Chr	start	end	Standard Name	Systematic Name	YMC phase	Description
1	chr16	644954	645925	YPR036W-A	YPR036W-A	N/A	Protein of unknown function
2	chr11	21592	21620	JEN1	YKL217W	RC	Lactate transporter, required for uptake of lactate and pyruvate
3	chr7	398038	398066	SDS23	YGL056C	RC	One of two S. cerevisiae homologs (Sds23p and Sds24p) of the S. pombe Sds23 protein, which is implicated in APC/cyclosome regulation
4	chr1	230027	230272	YAR075W	YAR075W	OX	Non-functional protein with homology IMP dehydrogenase
5	chr4	894075	894176	ADR1	YDR216W	RC	Carbon source-responsive zinc-finger transcription factor, required for transcription of the glucose-repressed gene ADH2, of peroxisomal protein genes
6	chr4	465328	465398	SNQ2	YDR011W	RC	Plasma membrane ATP-binding cassette (ABC) transporter, multidrug transporter involved in multidrug resistance and resistance to singlet oxygen species
7	chr7	772085	772218	BTN2	YGR142W	RC	v-SNARE binding protein that facilitates specific protein retrieval from a late endosome to the Golgi
8	chr4	1242506	1242535	ATO3	YDR384C	RC	Plasma membrane protein, regulation pattern suggests a possible role in export of ammonia from the cell
9	chr9	249235	249282	VHR1	YIL056W	RB	Transcriptional activator, required for the vitamin H-responsive element mediated induction of VHT1 and BIO5 in response to low biotin concentrations
10	chr4	368363	369552	STP4	YDL048C	OX	Protein containing a Kruppel-type zinc-finger domain
11	chr16	75105	75153	ICY2	YPL250C	RC	Protein of unknown function
12	chr12	875195	875261	FBP1	YLR377C	RC	Fructose-1,6-bisphosphatase, key regulatory enzyme in the gluconeogenesis pathway, required for glucose metabolism
13	chr11	231113	231213	HAP4	YKL109W	RB	Subunit of the heme-activated, glucose-repressed Hap2p/3p/4p/5p CCAAT-binding complex, a transcriptional activator and global regulator of respiratory gene expression
14	chr4	892528	892585	AHA1	YDR214W	RC	Co-chaperone that binds to Hsp82p and activates its ATPase activity
15	chr13	774387	774459	HOR7	YMR251W-A	RC	Protein of unknown function
16	chr4	806354	806457	HSP42	YDR171W	RC	Small heat shock protein (sHSP) with chaperone activity
17	chr15	1039529	1039634	ALD4	YOR374W	RC	Mitochondrial aldehyde dehydrogenase, required for growth on ethanol and conversion of acetaldehyde to acetate
18	chr12	783627	783710	TMA10	YLR327C	RC	Protein of unknown function that associates with ribosomes
19	chr5	264047	265114	GIP2	YER054C	RC	Putative regulatory subunit of the protein phosphatase Glc7p, involved in glycogen metabolism
20	chr5	545328	545383	BMH1	YER177W	N/A	14-3-3 protein, major isoform
21	chr7	994128	994219	YGR250C	YGR250C	RC	Putative RNA binding protein
22	chr2	372892	373039	TIP1	YBR067C	RC	Major cell wall mannoprotein with possible lipase activity
23	chr1	141644	141794	SSA1	YAL005C	RC	ATPase involved in protein folding and nuclear localization signal (NLS)-directed nuclear transport
24	chr7	809793	809848	RTS3	YGR161C	RC	Putative component of the protein phosphatase type 2A complex
25	chr7	625216	625330	YGR067C	YGR067C	RC	Putative protein of unknown function
26	chr4	76809	76904	PRR2	YDL214C	RC	Serine/threonine protein kinase that inhibits pheromone induced signalling downstream of MAPK, possibly at the level of the Ste12p transcription factor
27	chr16	432008	432077	ALD6	YPL061W	RC	Cytosolic aldehyde dehydrogenase, activated by Mg2+ and utilizes NADP+ as the preferred coenzyme
28	chr11	516854	516934	YKR041W	YKR041W	OX	Putative protein of unknown function
29	chr5	85180	85300	UTR5	YEL035C	RC	Protein of unknown function
30	chr15	968104	968149	YOR342C	YOR342C	OX	Putative protein of unknown function
31	chr5	141164	141273	YEL007W	YEL007W	N/A	Putative protein with sequence similarity to S. pombe gti1+ (gluconate transport inducer 1)
32	chr13	874601	874656	ADH2	YMR303C	RC	Glucose-repressible alcohol dehydrogenase II, catalyzes the conversion of ethanol to acetaldehyde
33	chr12	88310	88411	HSP104	YLL026W	RC	Heat shock protein that cooperates with Ydj1p (Hsp40) and Ssa1p (Hsp70) to refold and reactivate previously denatured, aggregated proteins
34	chr1	45189	45285	ACS1	YAL054C	RC	Acetyl-coA synthetase isoform which, along with Acs2p, is the nuclear source of acetyl-coA for histone acetlyation
35	chr12	65509	65598	UBI4	YLL039C	RC	Ubiquitin, becomes conjugated to proteins, marking them for selective degradation via the ubiquitin-26S proteasome system
36	chr3	137339	137400	PGK1	YCR012W	RC	3-phosphoglycerate kinase, catalyzes transfer of high-energy phosphoryl groups from the acyl phosphate of 1,3-bisphosphoglycerate to ADP to produce ATP
37	chr12	83747	84580	TPO1	YLL028W	RC	Polyamine transporter that recognizes spermine, putrescine, and spermidine
38	chr11	381820	381862	IXR1	YKL032C	RC	Protein that binds DNA containing intrastrand cross-links formed by cisplatin, contains two HMG (high mobility group box) domains, which confer the ability to bend cisplatin-modified DNA
39	chr10	608801	608908	SFC1	YJR095W	RC	Mitochondrial succinate-fumarate transporter, transports succinate into and fumarate out of the mitochondrion
40	chr15	109367	109395	SHR5	YOL110W	RC	Subunit of a palmitoyltransferase, composed of Shr5p and Erf2p, that adds a palmitoyl lipid moiety to heterolipidated substrates such as Ras1p and Ras2p through a thioester linkage
41	chr7	484044	484072	YGL007C-A	YGL007C-A	N/A	Putative protein of unknown function, identified by gene-trapping, microarray-based expression analysis, and genome-wide homology searching
42	chr11	68366	68440	MNN4	YKL201C	RC	Putative positive regulator of mannosylphosphate transferase (Mnn6p), involved in mannosylphosphorylation of N-linked oligosaccharides
43	chr4	636272	636317	GIS1	YDR096W	RC	JmjC domain-containing histone demethylase
44	chr7	977001	977042	FMP43	YGR243W	RC	Putative protein of unknown function
45	chr2	477389	477438	TEF2	YBR118W	N/A	Translational elongation factor EF-1 alpha
46	chr4	591690	591854	IPT1	YDR072C	RC	Inositolphosphotransferase, involved in synthesis of mannose-(inositol-P)2-ceramide (M(IP)2C), the most abundant sphingolipid
47	chr15	83202	83326	MDH2	YOL126C	RC	Cytoplasmic malate dehydrogenase, one of three isozymes that catalyze interconversion of malate and oxaloacetate
48	chr2	381633	381692	HSP26	YBR072W	RC	Small heat shock protein (sHSP) with chaperone activity
49	chr14	197988	198075	ZWF1	YNL241C	N/A	Glucose-6-phosphate dehydrogenase (G6PD), catalyzes the first step of the pentose phosphate pathway
50	chr7	914969	915069	ZPR1	YGR211W	OX	Essential protein with two zinc fingers, present in the nucleus of growing cells but relocates to the cytoplasm in starved cells via a process mediated by Cpr1p
51	chr7	323397	323536	SRM1	YGL097W	OX	Nucleotide exchange factor for Gsp1p, localizes to the nucleus, required for nucleocytoplasmic trafficking of macromolecules
52	chr12	449565	449640	RNH203	YLR154C	N/A	Ribonuclease H2 subunit, required for RNase H2 activity
53	chr7	883839	884427	TDH3	YGR192C	N/A	Glyceraldehyde-3-phosphate dehydrogenase, isozyme 3, involved in glycolysis and gluconeogenesis
54	chr5	461984	462015	FTR1	YER145C	RB	High affinity iron permease involved in the transport of iron across the plasma membrane
55	chr4	769210	769268	CPR1	YDR155C	RC	Cytoplasmic peptidyl-prolyl cis-trans isomerase (cyclophilin), catalyzes the cis-trans isomerization of peptide bonds N-terminal to proline residues
56	chr15	161774	161850	PHM7	YOL084W	RC	Protein of unknown function, expression is regulated by phosphate levels
57	chr13	557059	557088	NDE1	YMR145C	RB	Mitochondrial external NADH dehydrogenase, a type II NAD(P)H:quinone oxidoreductase that catalyzes the oxidation of cytosolic NADH

58	chr4	1490342	1490427	SNA2	YDR525W-A	RC	Protein of unknown function, has similarity to Pmp3p, which is involved in cation transport
59	chr9	382471	382541	YIR016W	YIR016W	RC	Putative protein of unknown function
60	chr15	978686	978749	TYE7	YOR344C	OX	Serine-rich protein that contains a basic-helix-loop-helix (bHLH) DNA binding motif
61	chr10	525675	525751	CYC1	YJR048W	RB	Cytochrome c, isoform 1
62	chr5	69080	69176	GLY1	YEL046C	OX	Threonine aldolase, catalyzes the cleavage of L-allo-threonine and L-threonine to glycine
63	chr15	877818	877903	MBF1	YOR298C-A	RC	Transcriptional coactivator that bridges the DNA-binding region of Gcn4p and TATA-binding protein Spt15p
64	chr2	444774	444823	FES1	YBR101C	RC	Hsp70 (Ssa1p) nucleotide exchange factor, cytosolic homolog of Sil1p, which is the nucleotide exchange factor for BiP (Kar2p) in the endoplasmic reticulum
65	chr7	428216	428279	PNC1	YGL037C	RC	Nicotinamidase that converts nicotinamide to nicotinic acid as part of the NAD(+) salvage pathway, required for life span extension by calorie restriction
66	chr10	348700	348798	YJL047C-A	YJL047C-A	N/A	Putative protein of unknown function
67	chr2	292026	292075	OLA1	YBR025C	OX	P-loop ATPase with similarity to human OLA1 and bacterial YchF
68	chr4	416941	417082	RPN4	YDL020C	RC	Transcription factor that stimulates expression of proteasome genes
69	chr7	650822	651008	PIL1	YGR086C	RC	Primary component of eisosomes, which are large immobile cell cortex structures associated with endocytosis
70	chr14	301385	301946	RPS3	YNL178W	OX	Protein component of the small (40S) ribosomal subunit, has apurinic/apyrimidinic (AP) endonuclease activity
71	chr14	405831	405938	DCP2	YNL118C	RC	Catalytic subunit of the Dcp1p-Dcp2p decapping enzyme complex, which removes the 5' cap structure from mRNAs prior to their degradation
72	chr6	106305	106394	MDJ1	YFL016C	N/A	Co-chaperone that stimulates the ATPase activity of the HSP70 protein Ssc1p
73	chr2	193686	193784	ACH1	YBL015W	RB	Protein with CoA transferase activity, particularly for CoASH transfer from succinyl-CoA to acetate
74	chr11	91983	92021	YKL187C	YKL187C	RC	Putative protein of unknown function
75	chr13	334939	335007	YMR031C	YMR031C	RC	Protein of unknown function with similarity to Ykl050cp and Uso1p
76	chr13	192492	192563	CAT2	YML042W	RC	Carnitine acetyl-CoA transferase present in both mitochondria and peroxisomes, transfers activated acetyl groups to carnitine to form acetylcarnitine which can be shuttled across membranes
77	chr16	17534	17593	YPL277C	YPL277C	RC	Putative protein of unknown function
78	chr4	599809	599852	SED1	YDR077W	RC	Major stress-induced structural GPI-cell wall glycoprotein in stationary-phase cells, associates with translating ribosomes, possible role in mitochondrial genome maintenance
79	chr16	843033	843069	YPR158W	YPR158W	RC	Protein of unknown function involved in destabilization of [URE3] prions
80	chr10	521510	521572	TAH11	YJR046W	OX	DNA replication licensing factor, required for pre-replication complex assembly
81	chr4	974408	974507	HSP78	YDR258C	RC	Oligomeric mitochondrial matrix chaperone that cooperates with Ssc1p in mitochondrial thermotolerance after heat shock
82	chr13	408593	408739	MOT3	YMR070W	N/A	Nuclear transcription factor with two Cys2-His2 zinc fingers
83	chr5	222448	222505	EDC2	YER035W	RC	RNA-binding protein, activates mRNA decapping directly by binding to the mRNA substrate and enhancing the activity of the decapping proteins Dcp1p and Dcp2p
84	chr16	832035	832136	SUE1	YPR151C	RC	Mitochondrial protein required for degradation of unstable forms of cytochrome c
85	chr11	630235	630291	PCK1	YKR097W	RB	Phosphoenolpyruvate carboxykinase, key enzyme in gluconeogenesis, catalyzes early reaction in carbohydrate biosynthesis, glucose represses transcription and accelerates mRNA degradation
86	chr2	809650	809860	DAN3	YBR301W	N/A	Cell wall mannoprotein with similarity to Tir1p, Tir2p, Tir3p, and Tir4p
87	chr6	180993	181021	YFR016C	YFR016C	RB	Putative protein of unknown function
88	chr13	91214	91338	RPM2	YML091C	RB	Protein subunit of mitochondrial RNase P, has roles in nuclear transcription, cytoplasmic and mitochondrial RNA processing, and mitochondrial translation
89	chr3	133225	133776	ADY2	YCR010C	RC	Acetate transporter required for normal sporulation
90	chr6	224939	225008	QCR6	YFR033C	RB	Subunit 6 of the ubiquinol cytochrome-c reductase complex, which is a component of the mitochondrial inner membrane electron transport chain
91	chr12	1012183	1012300	YLR437C	YLR437C	RC	Protein that regulates the nuclear localization of ribonucleotide reductase Rnr2p and Rnr4p subunits
92	chr7	384835	384970	PYC1	YGL062W	RB	Pyruvate carboxylase isoform, cytoplasmic enzyme that converts pyruvate to oxaloacetate
93	chr16	679123	679294	ROX1	YPR065W	OX	Heme-dependent repressor of hypoxic genes
94	chr11	258433	258462	YKL096C-B	YKL096C-B	N/A	Putative protein of unknown function
95	chr7	609975	610028	ERG25	YGR060W	RC	C-4 methyl sterol oxidase, catalyzes the first of three steps required to remove two C-4 methyl groups from an intermediate in ergosterol biosynthesis
96	chr10	646900	646990	YJR120W	YJR120W	N/A	Protein of unknown function
97	chr10	622827	622938	SOD1	YJR104C	RC	Cytosolic copper-zinc superoxide dismutase
98	chr4	1161701	1161812	HXT6	YDR343C	RC	High-affinity glucose transporter of the major facilitator superfamily, nearly identical to Hxt7p, expressed at high basal levels relative to other HXTs, repression of expression by high glucose requires SNF3
99	chr13	119388	119417	HMG1	YML075C	RC	One of two isozymes of HMG-CoA reductase that catalyzes the conversion of HMG-CoA to mevalonate, which is a rate-limiting step in sterol biosynthesis
100	chr14	662049	662172	ACC1	YNR016C	N/A	Acetyl-CoA carboxylase, biotin containing enzyme that catalyzes the carboxylation of acetyl-CoA to form malonyl-CoA

Timepoint	Relative collection time (min)
t1	0
t2	19
t3	26
t4	30.5
t5	40
t6	50
t7	60
t8	70
t9	80
t10	90
t11	100
t12	110.5
t13	120.75
t14	153
t15	185
t16	218

Table 2.5 Timepoint collection over theYMC for RNA-seq and H3K9ac ChIP-seq
t1 was setted as 0 and the relative collection time for the 16 timepoints were given in the table. Note that the interval between timepoints collected from OX and RB phases (t2-t13) is shorter than that from the RC phase.

CHAPTER THREE

Dynamic Modification of Ifh1p in Response to Nutrient Cues

Ifh1p is a Key Transcription Factor for Ribosome Biogenesis

Although ribosome biogenesis is known to be regulated by nutrient-sensing signal transduction pathways such as the TOR (Target of Rapamycin) and PKA (Protein Kinase A) pathways, the precise manner by which key nutritional cues are relayed to the ribosome biogenesis machinery has not been fully elucidated (Zaman et al., 2008). The transcription factor Ifh1p is an essential regulator of ribosomal protein (RP) genes. This coactivator can be dynamically recruited to RP gene promoters in response to nutrient availability and interacts with other transcription factors including Fhl1p and Rap1p (Martineau et al., 2004; Rudra et al., 2005; Schawalder et al., 2004; Wade et al., 2004). Ifh1p also forms a complex with rRNA processing factors Rrp7p, Utp22p, and casein kinases, which has been termed the CURI complex (Rudra et al., 2007). Hence, Ifh1p might also regulate rRNA processing.

Ifh1p Binds to Promoters of RP Genes and Non-RP Genes

As previously characterized in the YMC, RP gene expression is induced robustly in the OX growth phase (Tu et al., 2005). And we have confirmed this robust and transient induction of RP genes by RNA-seq across 16 timepoints of a YMC (Figure 3.1). The association of Ifh1p at the promoters of RP genes is sensitive to growth conditions in batch culture (Schawalder et al., 2004; Wade et al., 2004). We tested whether Ifh1p binding at RP gene promoters is dynamic as a function of changes in the metabolic state experienced by

cells during the YMC. Chromatin immunoprecipitation (ChIP) analysis confirmed that Ifh1p exhibited increased binding to a RP gene promoter (*RPS11B*) in the OX growth phase when massive RP gene transcription takes place (Figure 3.2A, 3.2B). To investigate how Ifh1p occupancy changes on a genome-wide scale, we conducted ChIP-Seq experiments with cells collected from the OX, growth phase and the RC, quiescent-like phase.

Peaks called by CisGenome from OX phase data are listed (Table 3.1). The majority of Ifh1p targets are RP genes, in agreement with previous findings (Wade et al., 2004). Moreover, Ifh1p binding to RP genes was more apparent in OX than RC phase (Figure 3.2C), consistent with the ChIP-PCR data (Figure 3.2B). We also manually inspected the ChIP-Seq data to identify putative targets that might have eluded peak-calling algorithms. Examination of all 137 RP genes revealed Ifh1p binding to proximal genomic regions of every RP gene except *RPS28A*, *RPL4A*, *RPL4B*, *RPL1A* and *RPL18B*. Interestingly, Ifh1p also displayed binding to several non-RP genes, including metabolic genes (Figure 3.3A), translation factors (Figure 3.3B) and others such as *GCN4*, a transcription factor regulating amino acid biosynthetic genes (Figure 3.3C). Some additional peaks with weak signals are shown (Figure 3.4). Unlike peaks at RP genes which are always at intergenic regions, some of the peaks at non-RP genes span the entire open reading frame. The gene expression pattern across YMC and H3K9ac occupancy were shown in Figure 3.5. Note that unlike RP genes, these non-RP targets of Ifh1p have different expression pattern and H3K9ac occupancy in the YMC. These data indicate that in addition to RP genes, Ifh1p regulates additional targets important for cell growth and metabolism.

Ifh1p is Dynamically Acetylated and Phosphorylated during Growth

In the previous chapter, we reported that acetyl-CoA, a central metabolite of carbon sources, drives the cellular transcriptional growth program by inducing the acetylation of histones present at growth genes (Cai et al., 2011). This regulatory mechanism was discovered through a proteomic screen that identified dynamically acetylated components of the acetyltransferase complex SAGA (Spt-Ada-Gcn-Acetyltransferase) (Cai et al., 2011). This finding then led to the observation that its substrate histone H3 was also dynamically acetylated in tune with acetyl-CoA levels. In subsequent validation of candidates, this screen also revealed Ifh1p to be a dynamically acetylated, non-histone protein. Ifh1p is acetylated precisely in tune with the increase in acetyl-CoA levels that accompanies entry into the OX growth phase (Figure 3.6A). This acetylation of Ifh1p mirrors that of SAGA and histones, occurring during the same temporal window of the YMC (Cai et al., 2011). Besides dynamic acetylation, we also observed a mobility shift of the full-length Ifh1-FLAG protein as well as its degradation products at a single time point in the midst of OX phase (Figure 3.6A). This single time point is precisely when RP genes are heavily induced (Figure 3.1). The upshifted band in OX phase was reduced to the same size as the band in RC phase after treatment with phosphatase, indicating the band shift was due to phosphorylation (Figure 3.6B). Since the TORC1 effector Sch9p and PKA have been linked to the ribosome biogenesis program (Zaman et al., 2008), we tested whether the phosphorylation of Ifh1p could be detected by a phospho-PKA substrate-specific antibody that recognizes the phosphorylate serine or threonine in RRXS/T motifs (Figure 3.6C). This antibody recognized the phosphorylated form of Ifh1p but not following phosphatase treatment, confirming that it is a likely substrate of this family of kinases. We then verified that Ifh1p is dynamically phosphorylated in the

YMC specifically during the OX growth phase when ribosomal genes are activated (Figure 3.6D). Thus, using the YMC, we observed that Ifh1p is subjected to both acetylation and phosphorylation modifications which occur during growth phase.

We then investigated these dynamic modifications on Ifh1p under typical batch culture conditions. In synthetic dextrose minimal medium (SD), as cells grew to a higher density and entered stationary phase, protein levels of Ifh1p decreased substantially (Figure 3.7A). However, the acetylation of Ifh1p began to decrease prior to the decrease in Ifh1p protein levels, consistent with the idea that this modification is sensitive to nutrient state (Figure 3.7A). Since TORC1 signaling has been shown to play key roles in nutrient sensing and ribosome biogenesis (Martineau et al., 2004; Zaman et al., 2008), we tested whether post-translational modifications of Ifh1p might be regulated by TORC1 (Target of Rapamycin Complex 1). To modulate TORC1 signaling, we used either rapamycin to inhibit TORC1 activity, or cycloheximide, a translation elongation inhibitor that has been reported to stimulate TORC1 signaling (Huber et al., 2009). We observed that both acetylation and phosphorylation of Ifh1p were strongly inhibited by rapamycin treatment. In contrast, these modifications were stimulated by cycloheximide (Figure 3.7B). The translation stress induced by cycloheximide treatment might signal the need for an increase in translational capacity and RP gene transcription. Taken together, these data indicate that TORC1 can regulate the dynamic acetylation and phosphorylation of Ifh1p.

Acetylation by Gcn5p and Deacetylation by Sirtuins Regulates Stability of Ifh1p

As we previously reported, only substrates of SAGA appear to be dynamically acetylated in tune with intracellular acetyl-CoA fluctuations (Cai et al., 2011). Therefore, we suspected that SAGA might also catalyze the acetylation of Ifh1p. We confirmed that Ifh1p was no longer acetylated in strains lacking Gcn5p, the acetyltransferase present within SAGA (Figure 3.8A). We then deleted several candidate deacetylases to determine which of them might regulate Ifh1p acetylation. Surprisingly, Rpd3p, the histone deacetylase known to regulate transcription of RP and ribi genes (Huber et al., 2011) and opening of rDNA repeats (Sandmeier et al., 2002), was not responsible for Ifh1p deacetylation. Instead, deletion of the NAD^+-dependent deacetylase *SIR2* resulted in significantly increased acetylation of Ifh1p (Figure 3.8A). Deletion of *HST1* (Homolog of SIR TWO), the closest *SIR2* homolog in combination with *sir2*Δ further increased Ifh1p acetylation, suggesting these deacetylases are primarily responsible for Ifh1p deacetylation (Figure 3.8A). To further clarify the contribution of *SIR2* as well as the *HST* genes, we compared single deletion mutants as well as double deletion mutants combining *SIR2* deletion with different *HST* gene deletions. These data indicate that Sir2p is the primary deacetylase for Ifh1p. However, in the absence of Sir2p, Hst1p and Hst2p can also contribute to the deacetylation of Ifh1p (Figure 3.8B, 3.8C). Thus, Ifh1p is a significant non-histone substrate of sirtuins in budding yeast.

Next, we mapped the acetylation sites on Ifh1p. The amino acid sequence composition of Ifh1p contains many clusters of basic and acidic residues which impose significant difficulty for proteomic analysis (Figure 3.9). Therefore, we sought an alternative approach by inducing peptide cleavage at cysteine residues following cyanylation (Tu and Wang, 1999). Fortuitously, Ifh1p contains only two endogenous cysteine residues (Figure

3.10A) and mutation of both these cysteines to serine did not affect cell growth (data not shown). We performed the mapping experiments using C-terminally FLAG-tagged Ifh1p immunoprecipitated from cells grown to log phase, conditions under which the protein is heavily acetylated. When the wild type protein was cleaved at C580 and C665, peptide fragments C-terminal to the cleavage sites were recognized by a FLAG antibody. However, they ran at different sizes compared to the peptides recognized by an acetyl-lysine (acK) antibody, suggesting the acetylated sites are N-terminal to C580 (Figure 3.10B) In a C580S/C665S Ifh1p mutant strain background, serine to cysteine mutations were introduced at various sites before residue 580 to induce peptide cleavage. The pattern of peptides recognized by FLAG antibody was compared with those recognized by acK antibody to deduce the acetylated region within Ifh1p. To map additional sites possibly acetylated upon cycloheximide treatment (Figure 3.10C), we also included a set of cycloheximide-treated cells in the experiment. The peptides generated by cleavage at aa 189 were the same size in both blots, whereas peptides generated by cleavage at aa 297 were different sizes. Thus, the acetylated sites were likely present between aa 189 and aa 297 (Figure 3.10). However, mutating the 18 lysines within this region to arginines decreased but did not abolish acetylation of Ifh1p, indicating there are additional lysines that can be modified (Figure 3.10D). Due to a limitation of the method, the light chain of the antibody used for immunoprecipitation was also detected by the acK antibody. It is possible that the cleavage fragment N-terminal to aa 189 was also acetylated, but masked by the light chain following SDSPAGE and Western analysis. We then mutated 21 additional lysine residues to arginine between aa 1-189. This new mutant exhibited no detectable acetylation signal with or without

cycloheximide treatment (Figure 3.10E). The K/Q acetylated mimic mutant was also made (Figure 3.10E). Although 39 lysines in this essential protein were mutated, no obvious growth phenotypes were observed when either the 39K/R or 39K/Q mutants were tested under a variety of conditions.

Surprisingly, we failed to observe any growth difference between WT and mutant IFH1 strains under various carbon sources (Figure 3.11). There is also no difference in chronological life span (Figure 3.12). Ifh1p in the mutants are localized the nucleus and the cytoplasm, same as in WT (Figure 3.13). Since Ifh1p can interact with Fhl1p and this interaction is essential for RP gene transcription activation, we also tested whether Ifh1p-Fhl1p interaction is affected in the mutants (Figure 3.14). Again, we did not detect any difference in the interaction. We also found that the mutants can still bind to the promoters of RP genes similar to the WT Ifh1p (Figure 3.15). And the mutants do not experience any delay when cells were switched from stationary phase to nutrient abundant environment for growth recovery (Figure 3.16). When we put these mutants into the chemostat, they all can undergo YMC and RP gene induction during a normal OX phase or acetate induced growth phase entry in the mutants were all similar to those of the WT (Figure 3.17).

We observed that the acetylation of Ifh1p decreased prior to a decrease in its protein levels as cells entered stationary phase (Figure 3.7A), suggesting that acetylation regulates its protein stability and half-life. To measure the stability of Ifh1p, we avoided using protein synthesis inhibitors such as cycloheximide because it can induce TORC1 signaling and acetylation of Ifh1p (Figure 3.7B), thereby confounding interpretation of the results. Instead, we measured Ifh1p levels in cells growing from a low to high density in SD media. Lower

levels of Ifh1p were detected in the acetylation defective 39K/R mutant, while higher levels of Ifh1p were detected in the acetylated mimic 39K/Q mutant, despite no differences in growth rate (Figure 3.18A). Consistent with these findings, sirtuin deletion mutants that harbor increased acetylated Ifh1p also exhibited increased protein levels of Ifh1p, supporting the idea that Ifh1p stability is regulated by nutrient responsive acetylation in its N-terminal region (Figure 3.18B).

PKA Phosphorylates Ifh1p and Regulates Replicative Lifespan

To map the phosphorylation sites on Ifh1p, we used the same set of cysteine substitution mutants to deduce the general region of phosphorylation following peptide cleavage. The pattern of peptides recognized by both the FLAG antibody and phospho-PKA substrate antibody matched very well, suggesting the phosphorylation site(s) lie C-terminal to C580 (Figure 3.19A). We then searched the C-terminal sequence of Ifh1p for PKA phosphorylation motifs (RRXS/T) and constructed single S/A or T/A mutants for each of the 5 sites that were identified. One single mutation at S969 was sufficient to eliminate the signal recognized by the phoshpo-PKA substrate antibody (Figure 3.19B). We next tested whether S969 was phosphorylated by PKA using a *tpk1*^{as} *tpk2*^{as} *tpk3*^{as} strain which expresses modified PKA alleles that are sensitive to the ATP analog 1NM-PP1 (Zaman et al., 2009). Upon treatment with 1NM-PP1, Ifh1p phosphorylation disappeared within 10 min, confirming that it is a PKA substrate (Figure 3.19C). Since Sch9p substrates share the same motif as PKA substrates, we also tested Ifh1p phosphorylation in a *sch9*Δ strain, however, no alteration of Ifh1p phosphorylation was observed (Figure 3.20). These data show that PKA

phosphorylates Ifh1p on S969 as cells enter growth. To test the functional role of Ifh1p phosphorylation, we constructed S969A and S969D mutants and observed that they did not exhibit any obvious growth defects under a variety of nutrient conditions (Figure 3.11). We also did not observe any significant phenotypes when subjecting these mutants to the same series of assays as the acetylation site mutants (Figure 3.11-3.17). Furthermore, mutation of acetylated sites in combination with the phosphorylated site also did not result in any substantial phenotype under the conditions tested. Interestingly, although both acetylation and phosphorylation of Ifh1p are correlated with the onset of RP gene transcription in the YMC, the modifications seem to be independent of each other (Figure 3.21).

Interestingly, the post-translational modifiers of Ifh1p – PKA, TORC1, and Sir2p, have each been implicated in the regulation of replicative lifespan (RLS) in budding yeast (Longo et al., 2012). Moreover, downstream targets of Ifh1p, such as RP subunits and *GCN4*, have also been linked to lifespan regulation (Steffen et al., 2008). We therefore tested whether mutations in the acetylated or phosphorylated sites of Ifh1p might also impact RLS. While the acetylation site mutants of Ifh1p exhibited a modestly shorter RLS compared to the WT control, notably the single S969A mutant that cannot be phosphorylated exhibited a significantly increased RLS (30- 40%) (Figure 2.22). However, the RLS of the S969D phosphomimetic mutant remained comparable to WT. Deletion of *GCN4*, which has been shown to be required for RLS extension triggered by 60S ribosomal subunit depletion (Steffen et al., 2008), did not affect RLS extension by the Ifh1p S/A mutant (Figure 2.22). This modification of Ifh1p also did not affect *GCN4* expression levels (Figure 2.23). Moreover, the S/A mutant was still able to extend RLS in a strain lacking TOR1 (Figure

2,22). However, the substantial RLS extension observed in the S/A mutant was entirely dependent on Sir2p (Figure 2.22). The dependency on Sir2p is not surprising as deletion of *SIR2* was observed to prevent lifespan extension in many long-lived yeast mutants (Delaney et al., 2011). Taken together, these data indicate that inhibiting the PKA-regulated phosphorylation of Ifh1p via mutation of a single site is sufficient to significantly increase RLS to an extent comparable to calorie-restriction mimetic mutants (Kaeberlein et al., 2005). As reducing PKA activity is often sufficient to increase RLS (Fabrizio et al., 2004; Kaeberlein et al., 2005; Lin et al., 2000), our results suggest these effects may be mediated in part through reducing phosphorylation of Ifh1p. Thus, this nutrient-responsive phosphorylation modification on Ifh1p is involved in the regulation of cellular replicative potential, as opposed to the regulation of rates of RP gene transcription.

Summary

Although ribosome biogenesis is recognized as a key component of the cellular growth program, much remains unclear regarding how this fundamental process is coordinated with nutrient availability and metabolic state. In this study, we sampled highly synchronized cells across different growth states in the YMC to discover that an essential transcription factor Ifh1p involved in ribosomal gene transcription is subject to regulation by multiple nutrient-responsive, post-translational modifications. Since ribosome biogenesis is such an energetically demanding task, such regulation may enable Ifh1p to integrate multiple nutrient signals to adjust rates of ribosomal gene transcription appropriately.

We also characterized the genome-wide occupancy of Ifh1p using the YMC. These ChIP-Seq experiments provide a higher resolution profile of Ifh1p occupancy in the genome and revealed additional important targets besides RP genes. Several translation elongation factors were bound by Ifh1p suggesting their transcription may be regulated by Ifh1p. Moreover, GCN4, a transcriptional activator of amino acid biosynthetic genes (Hinnebusch, 2005), is also a target, suggesting Ifh1p regulates the supply of amino acids for protein translation. Ifh1p is dynamically acetylated by the Gcn5p-containing SAGA complex specifically during growth. Gcn5p has the unique ability to acetylate its substrates in tune with acetyl-CoA levels (Cai et al., 2011). This property enables Gcn5p to coordinate the acetylation of its targets in tune with the metabolic state of a cell. Upon entry into growth, acetyl-CoA drives the acetylation of histones present at a set of over 1,000 growth genes which include virtually all RP and ribi genes (Cai et al., 2011). The dynamic acetylation of Ifh1p coincides with the acetylation of histones and subunits within SAGA, suggesting these substrates are all subjected to the same acetyl-CoA regulated acetylation mechanism used to coordinate cell growth with this important intermediate in energy metabolism that is also a key biosynthetic substrate.

Ifh1p is rapidly deacetylated as cells transition out of growth phase. Interestingly, the deacetylation of Ifh1p is catalyzed by NAD^+-dependent sirtuins instead of non-NAD^+-dependent deacetylases such as Rpd3p. When carbon sources become limiting, acetyl-CoA levels decrease along with Gcn5p activity, and the activity of NAD^+-dependent deacetylases may then predominate. Therefore, this transcriptional coactivator is subjected to a competition between acetyl-CoA-regulated acetylation and NAD^+-dependent deacetylation

that can be tipped in either direction by changes in metabolic state. Our studies further establish Ifh1p as a significant nonhistone substrate of Sir2p in yeast, with up to 39 lysine residues in its N-terminal region that can be deacetylated. As acetylation appears to stabilize Ifh1p, this may also help recruit sirtuins to the vicinity of RP genes and the rDNA, which may function to increase replicative potential. Ifh1p is also dynamically phosphorylated by PKA. Both the phosphorylation and acetylation of Ifh1p are inhibited by rapamycin, suggesting TORC1 is also a key regulator of Ifh1p. Previous studies implicated TORC1 and PKA signaling in the regulation of Crf1p, a repressor of RP gene transcription ((Martineau et al., 2004). TORC1 and PKA activation result in the dephosphorylation of Crf1p and its confinement to the cytosol. Upon inactivation of TORC1, Crf1p becomes phosphorylated and nuclear, leading to the repression of RP genes. Furthermore, TORC1 and PKA inactivate repressors of ribi genes such as Dot6p and Tod6p (Huber et al., 2011; Lippman and Broach, 2009). Stb3p, a repressor of rRNA processing genes, is also inactivated by TORC1 and glucose (Huber et al., 2011; Liko et al., 2010). We show that Ifh1p is yet another ribosomal transcription factor that is exposed to phosphorylation by TORC1 and PKA signaling.

The consequence of mutations in the acetylated or phosphorylated sites in Ifh1p appears extremely modest despite the fact that the protein is essential. We did not observe significant growth defects for the 39K/R, 39K/Q, S969A, S969D mutants, nor find any differences in their ability to bind RP gene promoters or activate RP genes. Although the 39K/R mutant decreased the overall Ifh1p levels in the cell, there is apparently still sufficient Ifh1p to achieve normal levels of RP gene transcription. Ifh1p has a very peculiar protein sequence that contains many clusters of acidic and basic residues while lacking any defined

domains. We predict it acts as a scaffold to bring together numerous other factors to enable activation of RP genes. The dynamic modifications within Ifh1p might also be a consequence of its proximity to other macromolecules that are subjected to nutrient-responsive regulation (e.g., the acetyl-CoA driven acetylation of histones at RP genes catalyzed by SAGA, and the phosphorylation-dependent regulation of Crf1p localization by TORC1/PKA). Nonetheless, we did observe significant RLS phenotypes in mutants of Ifh1p that disrupt these modifications, suggesting that the resulting consequences might only be manifested after many generations. Moreover, cycloheximide treatment significantly increased both phosphorylation and acetylation of Ifh1p, suggesting these modifications stimulate Ifh1p and possibly other RP transcription factors under conditions of translation stress that could be frequently encountered in the wild, in the face of unpredictable nutrient availability.

Finally, while the activation of RP and ribi genes can be induced by glucose, their repression is mediated by recruitment of histone deacetylase complexes (Huber et al., 2011; Liko et al., 2010; Zaman et al., 2009). We recently showed that the activation of these and other growth genes is induced by acetyl-CoA through its ability to promote histone acetylation. Acetate addition is sufficient to trigger activation of these genes and entry into growth (Cai et al., 2011). Since the glucose-induced PKA pathway activates carbohydrate mobilization and metabolism (Rolland et al., 2002), a key output of the PKA and TORC1 signaling pathways may be the upregulated production of acetyl-CoA. Upon stress or nutrient starvation, production of acetyl-CoA is compromised, resulting in deacetylation of histones and gene repression. Thus, despite numerous post-translational modifications of transcription

factors, the metabolite acetyl-CoA may represent the key trigger that sets in motion the cascade of events leading to activation of RP, ribi, and other growth genes.

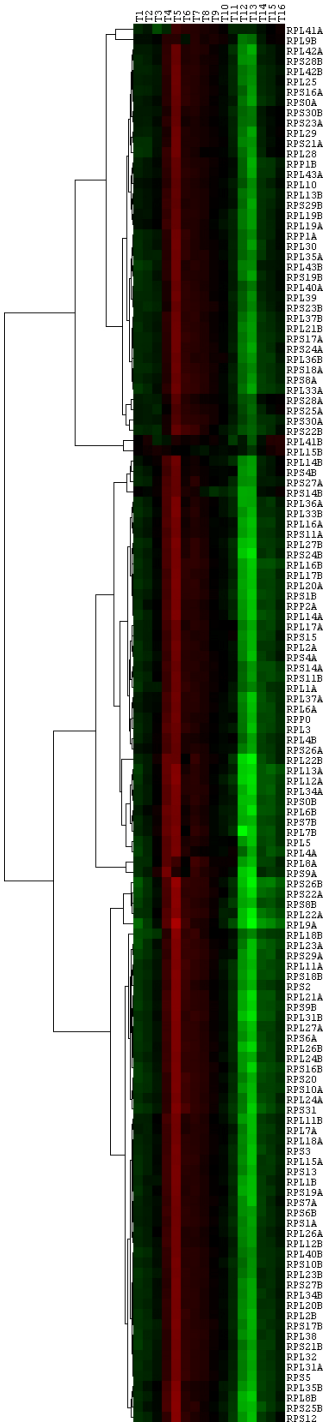

Figure 3.1 Heat map of RP gene expression levels across YMC
Normalized FPKM values of al the RP genes were used to generate this heat map following hierarchical clustering. Almost all the RP genes have the maximum expression at timepoint 5 in the OX growth phase of the YMC.

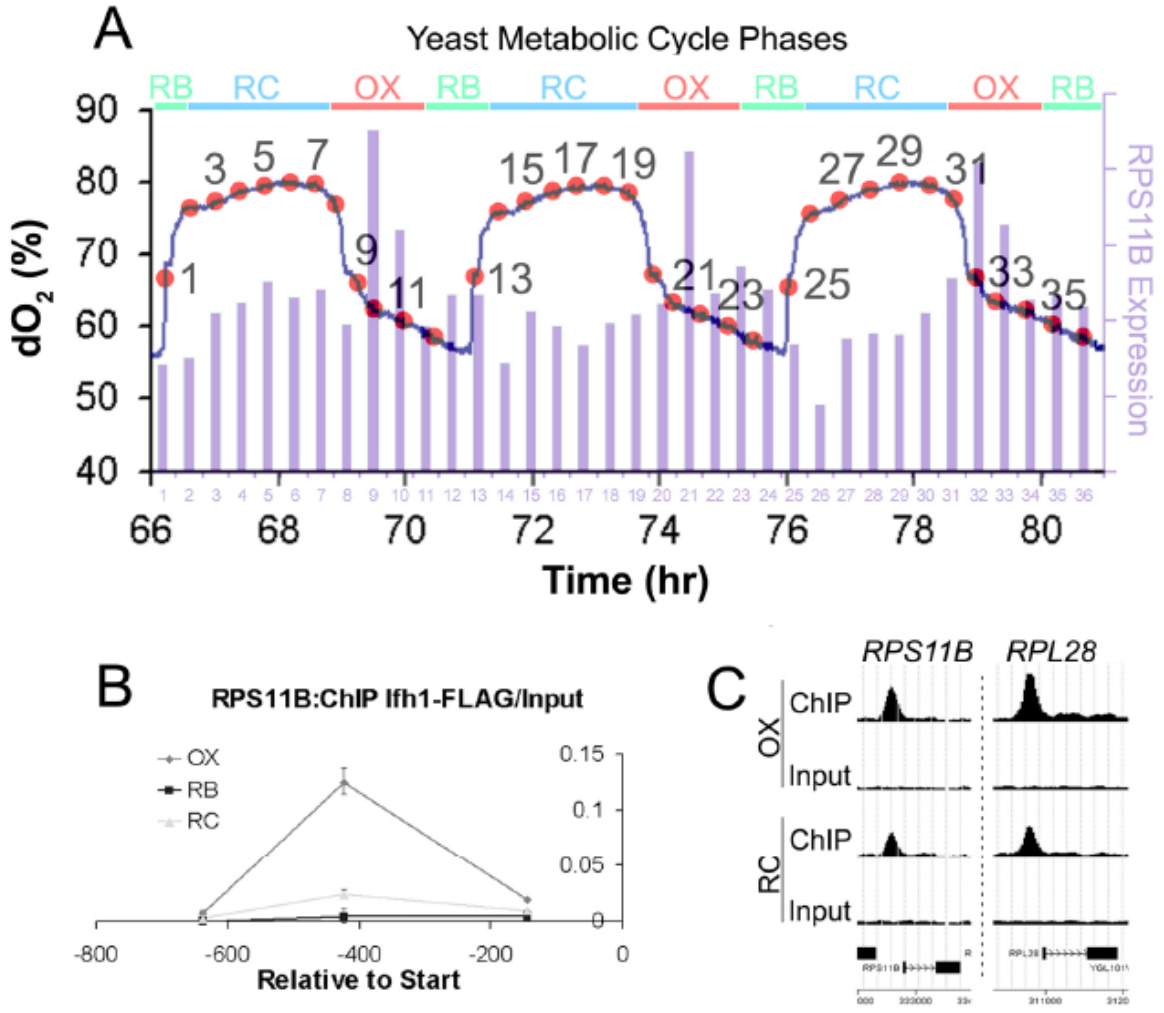

Figure 3.2 Ifh1p dynamically binds to ribosomal subunit genes during growth
(A) Ribosomal protein (RP) subunit genes are robustly induced during OX, growth phase of the YMC. Expression profile of a representative RP gene *RPS11B* over three consecutive metabolic cycles is shown (Tu et al., 2005).
(B) Ifh1p preferentially binds to RP genes during OX phase. Cells from representative time points at OX, RB and RC phases were collected and fixed for ChIP-PCR. Three primer sets spanning the promoter region of *RPS11B* were used in the analysis of Ifh1p binding.
(C) ChIP-Seq reveals increased binding of Ifh1p to RP genes during growth. Genome-wide occupancy profile of Ifh1-FLAG was obtained for cells collected from OX (growth) and RC (G0/quiescent-like) phase of the YMC. Ifh1p binds to regulatory regions of nearly all RP genes. Data visualized using the CisGenome browser for two representative RP genes are shown.

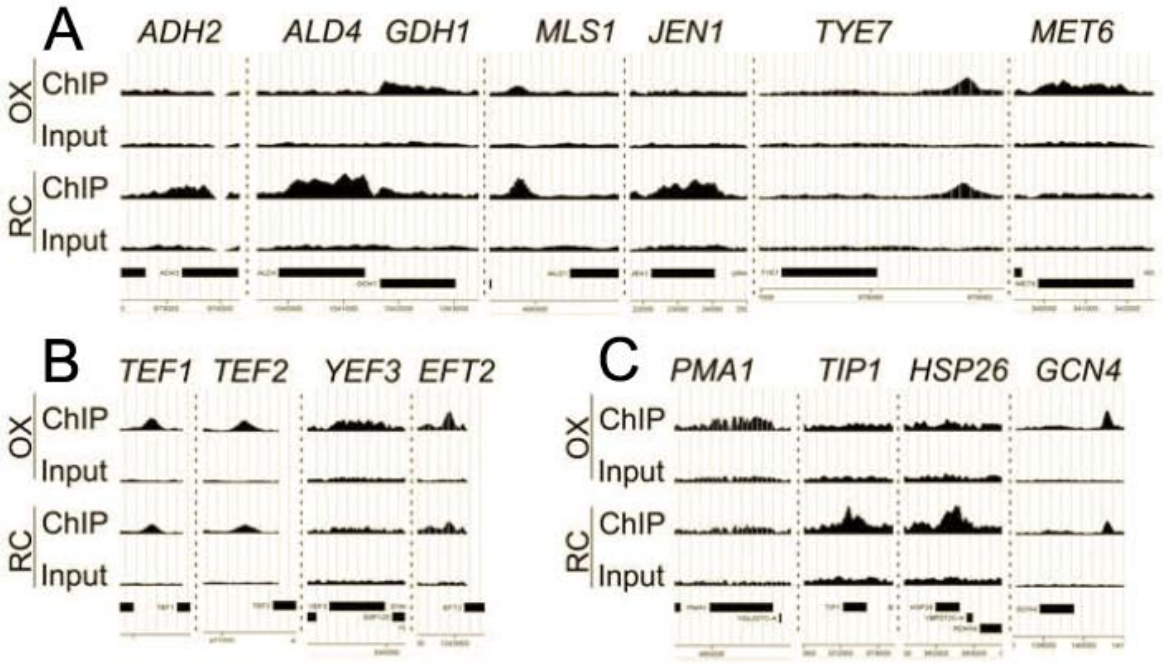

Figure 3.3 Ifh1p is Dynamically Acetylated by Gcn5p and Deacetylated by Sirtuins
(A) Ifh1p binds to non-RP genes including genes involved in metabolism. The ChIP-Seq data were scrutinized visually to identify all putative targets. Non-RP genes, including several involved in metabolism, are also targets of Ifh1p. Many of these genes have Ifh1p bound across the open reading frame instead of at the promoter. (B) Ifh1p binds to genes encoding translation elongation factors. (C) Ifh1p binds to other non-RP genes, including *GCN4*.

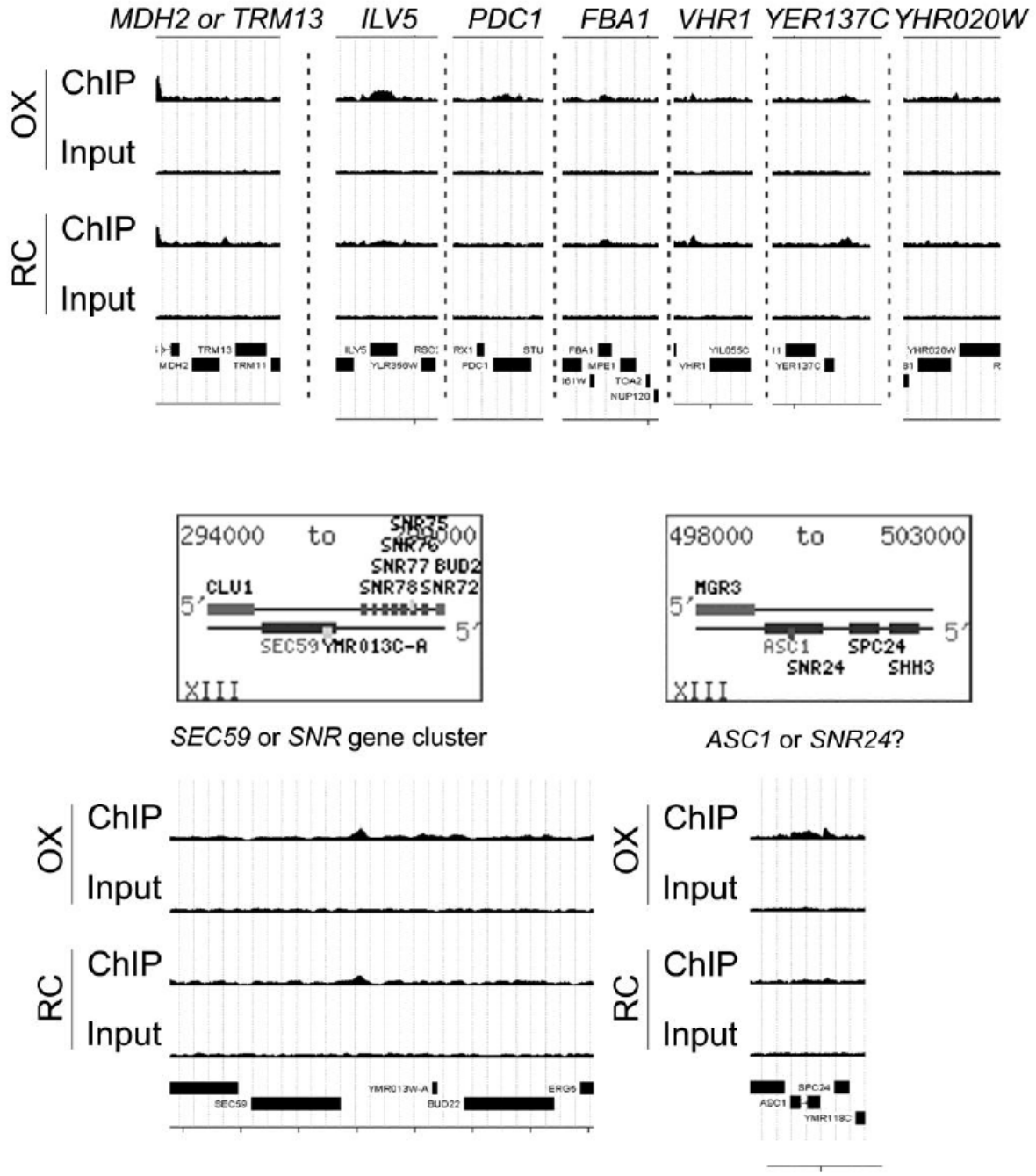

Figure 3.4 Potential additional targets of Ifh1p
Genomic regions bound by Ifh1p were visually identified from the ChIP-Seq data. Peaks with relatively weak signals are listed here. Genes whose promoters are closest to the peak are shown. Ifh1p binding occasionally spans the entire open reading frame. Note that Ifh1p binding near *SEC59* and *ASC1* might also function to regulate some small nucleolar (SNR) genes, as they are also very close to the peak.

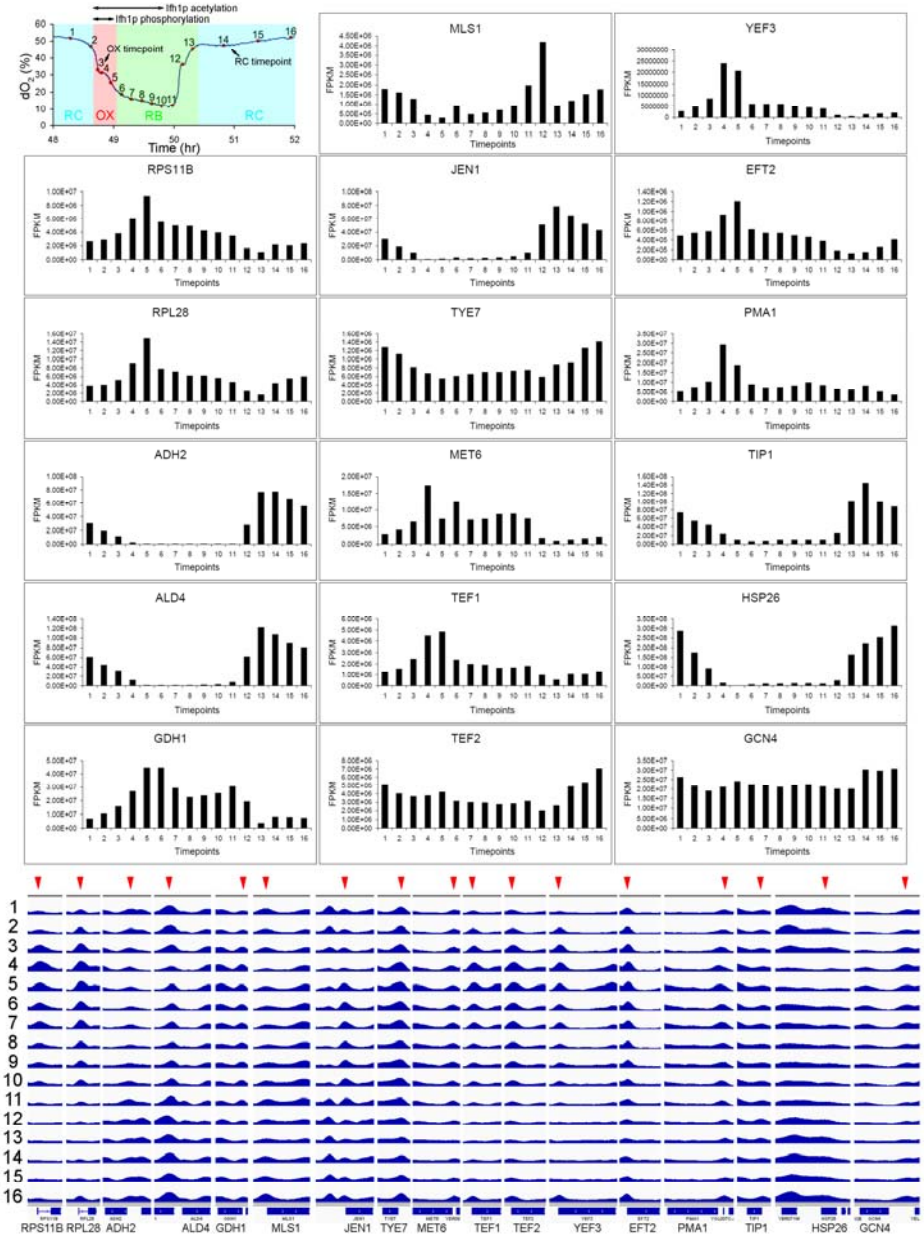

Figure 3.5 Expression and H3K9ac occupancy of Ifh1p non-RP target genes

The three phases OX, RB and RC are indicated. Representative time points collected for the experiments that use OX and RC YMC samples are marked on the cycle. The time windows of Ifh1p phosphorylation and acetylation have also been marked. Ifh1p phosphorylation peaks at around time point 3-4. RP gene transcription peaks at time point 5. Ifh1p acetylation occurs from time points 3-11. Expression data was retrieved from 16 timepoint RNA-seq from YMC while H3K9ac occupancy data was retrieved from 12 timepoint ChIP-seq from YMC. For non-RP genes, the expression profiles vary across the YMC. H3K9ac ChIP-seq peaks closest to the promoter of the selected genes have been pointed out by red arrows.

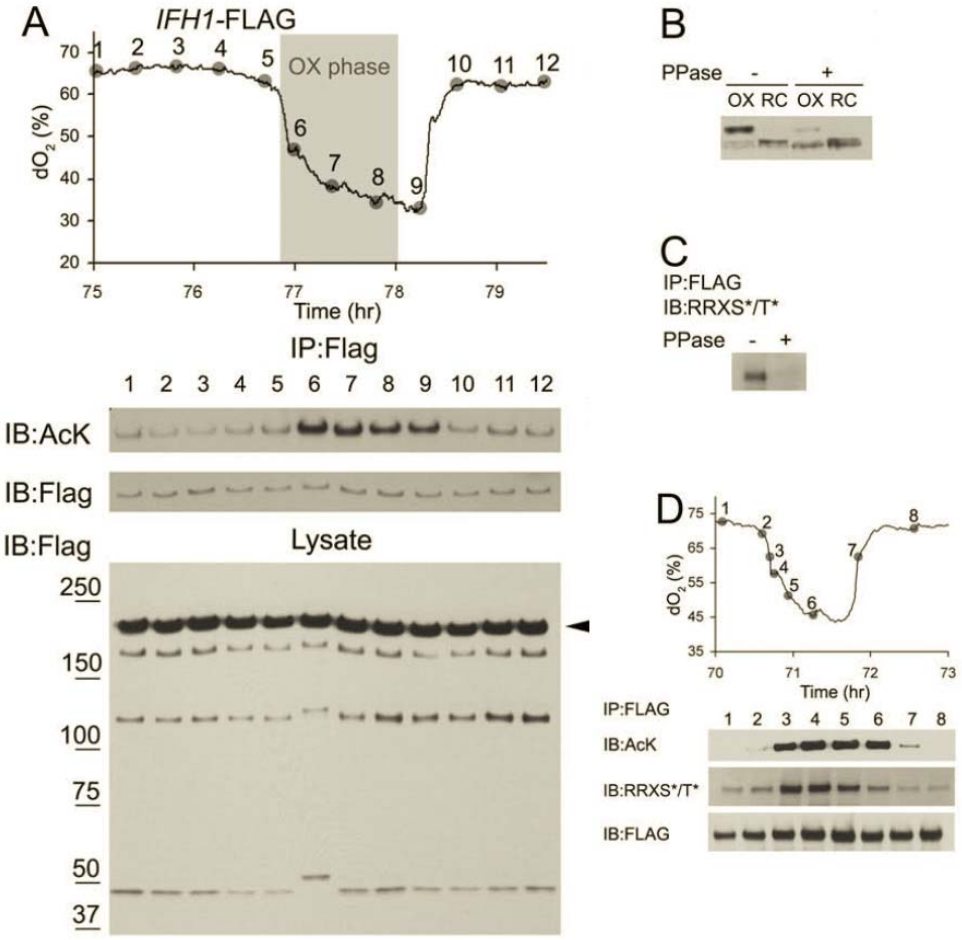

Figure 3.6 Ifh1p is dynamically acetylated and phosphorylated during growth
(A) Ifh1p is dynamically acetylated and possibly phosphorylated. Ifh1-FLAG was immunoprecipitated from cells collected across 12 time points of the YMC. Ifh1p is acetylated during the OX, growth phase precisely when acetyl-CoA levels increase. A mobility shift of both the full length Ifh1-FLAG protein (arrow) and its cleavage products was observed at time point 6, which is suggestive of phosphorylation.
(B) Ifh1p is phosphorylated. Lysates were prepared from OX and RC phase and treated with or without phosphatase (PPase). A cleavage product of Ifh1p at ~50 KDa is shown. The upshifted band in the OX phase sample was reduced after PPase treatment indicating the shift was due to phosphorylation.
(C) Phosphorylated Ifh1p is recognized by a PKA substrate-specific antibody. An antibody that recognizes the phospho-PKA substrate motif RRXS*/T* (* denotes phosphorylation) was used for immunoblotting against Ifh1p. The signal was eliminated after PPase treatment.
(D) Dynamic phosphorylation of Ifh1p. Ifh1-FLAG immunoprecipitated from indicated time points of YMC was blotted with acK and RRXS*/T* antibody. Both acetylation and phosphorylation of Ifh1p are upregulated during the OX, growth phase.

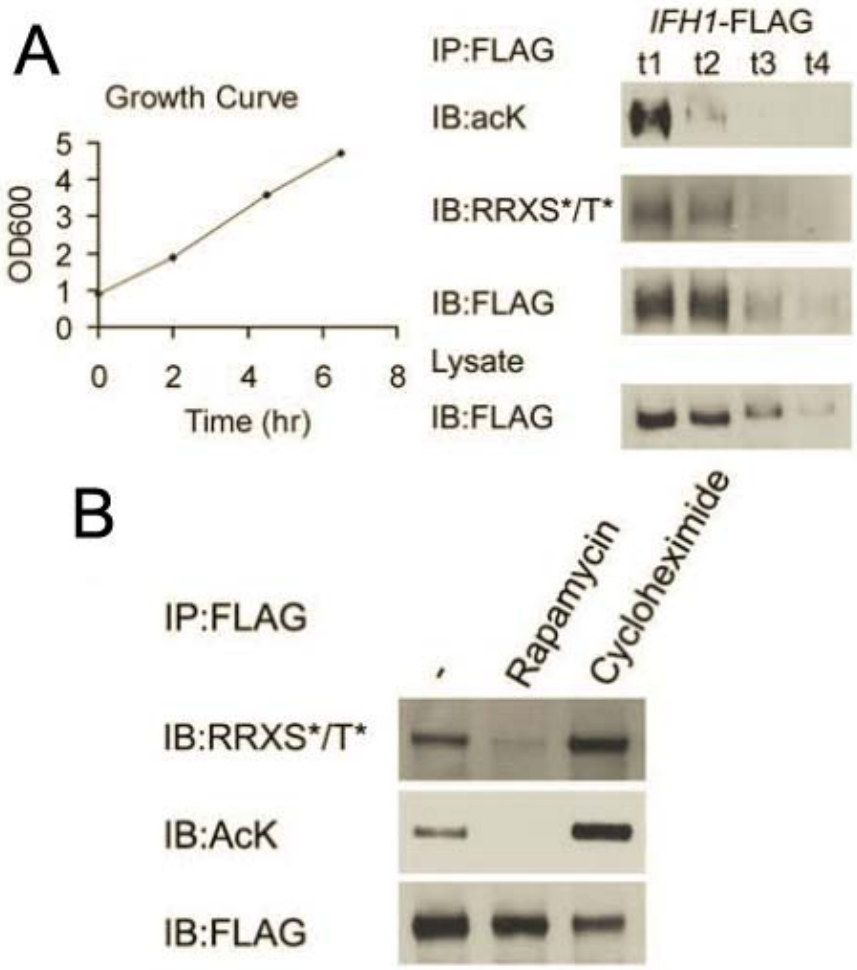

Figure 3.7 Post-Translational Modifications of Ifh1p are Sensitive to Nutrient Cues and Regulated by TORC1

(A) Acetylation of Ifh1p is sensitive to growth stage. IFH1-FLAG cells were cultured in SD medium to log phase and time points were collected as the cells were grown to a higher OD approaching stationary phase. Note Ifh1p becomes deacetylated prior to the decrease in its protein level.

(B) Acetylation and phosphorylation of Ifh1p are regulated by TORC1. Cells were grown in YPD to log phase and treated as indicated for 15min. Both phosphorylation and acetylation were inhibited by rapamycin and stimulated by cycloheximide.

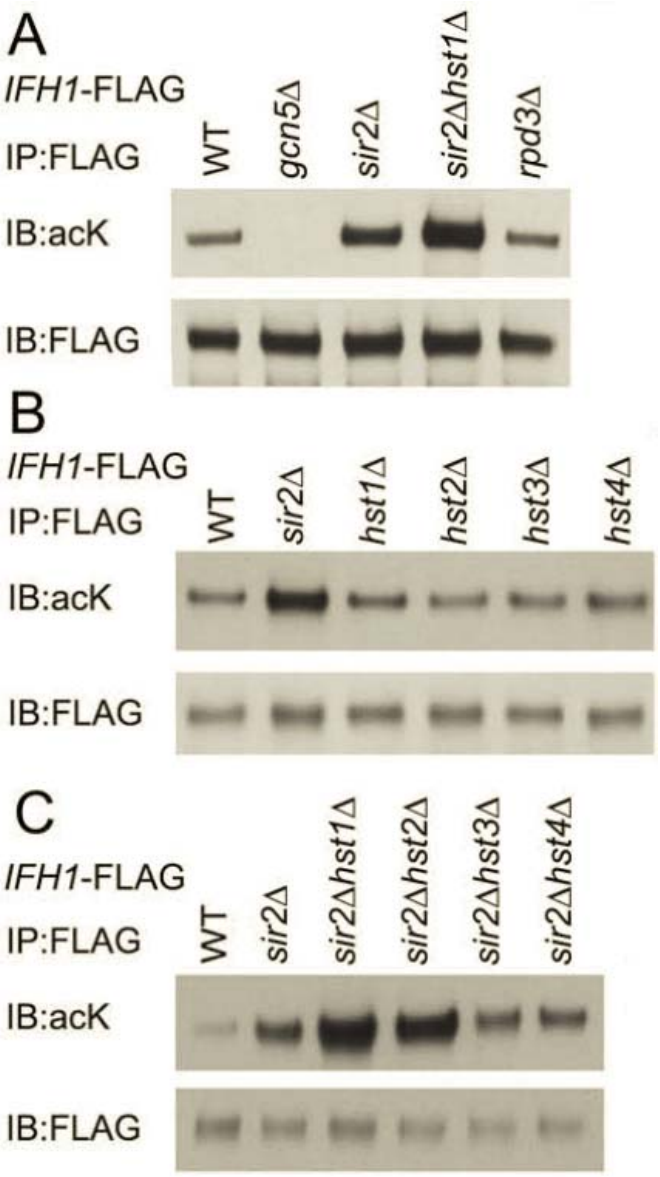

Figure 3.8 Ifh1p is acetylated by Gcn5p and deacetylated by sirtuins
(A) Ifh1-FLAG is acetylated by Gcn5p and deacetylated by Sir2p. Ifh1-FLAG was immunoprecipitated from YPD log phase cells from the indicated strains and probed with an acK antibody. Acetylation was abolished in a *gcn5*Δ strain and increased in *sir2*Δ but not rpd3Δ strains. Acetylation was further increased in a *sir2*Δ*hst1*Δ strain.
(B) Ifh1p is deacetylated primarily by Sir2p. Ifh1p acetylation was compared in single deletion mutants of the SIR2 family.
(C) Ifh1p is deacetylated by Hst1p and Hst2p in the absence of Sir2p. Ifh1p acetylation was compared in double deletion mutants combining *sir2*Δ with deletions in *HST* genes.

MAGKKSPRKSTINHSTHSGKLPANIKRLIKKGESDTKSRQSPPTLSTTRPRRFSLIYSSE
SSLSDVSDSDKNKSTNPHKIKRKAKNISNNSQGKKSKLIQRQIDNDDEGTESSDYQAVTD
GEESENEEEESEEEEEDDDEDDDDDDDDGSDSDSDSETSSDDENIDFVKLTAQRKKRAMK
ALSAMNTNSNTLYSSRENSNKNKSVKLSPKKENEEEQKEEKEKEKEEQQKQQESNKKEVN
GSGTTTTQQALSFKFKKEDDGISFGNGNEGYNEDIGEEVLDLKNKENNGNEEDKLDSKVM
LGNNDELRFPNISESDESEYDIDQDAYFDVINNEDSHGEIGTDLETGEDDLPILEEEEQN
IVSELQNDDELSFDGSIHEEGSDPVEDAENKFLQNEYNQENGYDEEDDEEDEIMSDFDMP
FYEDPKFANLYYYGDGSEPKLSLSTSLPLMLNDEKLSKLKKKEAKKREQEERKQRRKLYK
KTQKPSTRTTSNVDNDEYIFNVFFQSDDENSGHKSKKGRHKSGKSHIEHKNKGSNLIKSN
DDLEPSTHSTVLNSGKYDSSDDEYDNILLDVAHMPSDDECSESETSHDADTDEELRALDS
DSLDIGTELDDDYEDDDDDSSVTNVFIDIDDLDPDSFYFHYDSDGSSSLISSNSDKENSD
GSKDCKHDLLETVVYVDDESTDEDDNLPPPSSRSKNIGSKAKEIVSSNVVGLRPPKLGTW
ETDNKPFSIIDGLSTKSLYALIQEHQQLREQHQRAQTPDVKREGSSNGNNGDELTLNELL
NMSELEDDSPSHTDDMENNYNDAINSKSTNGHAADWYEVPKVPLSAFRNKGINAYEEDEY
MIPANSNRKVPIGYIGNERTRKKIDKMKELQRKKTEKKRQLKKKKKLLKIRKQRQKAIKE
QETMNLQLGINGHEIIGNNNSHSDINTGTDFTTNENTPMNELPSHAPEDASLIPHNSDLA
VDSNTRKNSTKSVGLDEIHEILGKDENDLLSVGDINGYDAQEGHVIEDTDADILASLTAP
VQFDNTLSHENSNSMWRRRQSMVEAAAENLRFTKNGLFSESALADIEGIMGNDVNHSFEF
NDVLQ*

Figure 3.9 Protein sequence of Ifh1p

The Ifh1p amino acid sequence (1,085 residues) was retrieved from the yeast genome database. The basic residues, lysine and arginine, are colored in blue and green. The acidic residue, aspartate and glutamate, are colored in red. Serines and threonines are colored in yellow. The 39 lysines in the N-terminal region that were mutated are underlined.

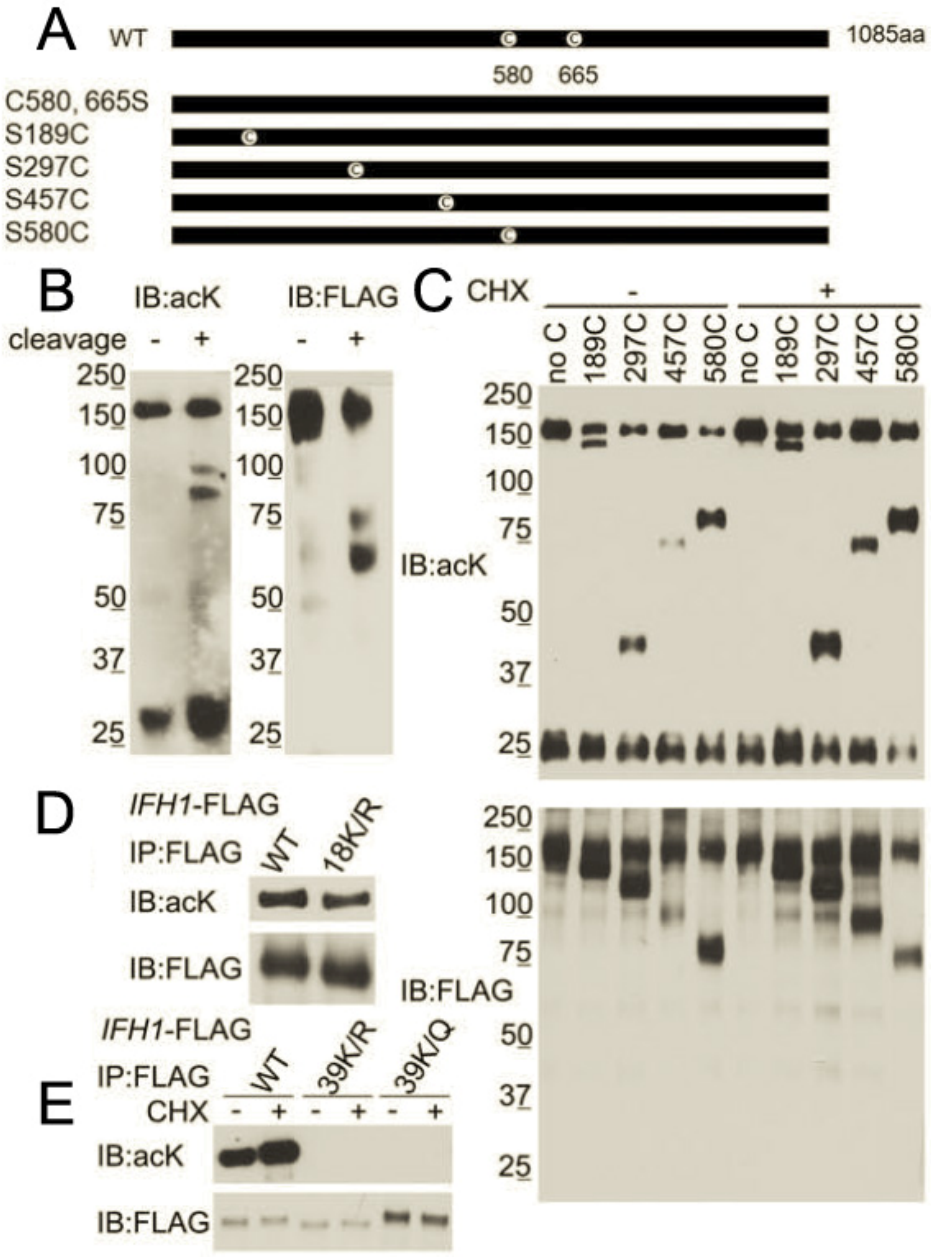

Figure 3.10 Mapping of Ifh1p acetylation sites

(A) Schematic diagram for cysteine substitution mutants of Ifh1p used for mapping modification sites. Wild type Ifh1p contains two cysteines. Mutations of C580 and C665 to serine were introduced. New serine to cysteine mutations were introduced at the indicated positions.

(B) Cleavage of the native form of Ifh1p suggests acetylation sites are N-terminal to C580. Wild type Ifh1p was immunoprecipitated from YPD log phase cultures and subjected to cleavage at cyanylated cysteines. The bands recognized by acK antibody and FLAG antibody

are different sizes, suggesting acetylation sites are not at fragments C-terminal to the cleavage sites, which are recognized by the FLAG antibody.

(C) The 189-297 region of Ifh1p contains acetylation sites. Based on a similar logic, it can be deduced that Ifh1p is acetylated between residues 189 - 297. Cycloheximide (CHX) which stimulates TORC1 signaling generates the same pattern as the non-treated group.

(D) Mutation of 18 lysines in the 189-297 region only slightly decreased acetylation of Ifh1p. K to R mutations were introduced to eliminate the lysines that can be acetylated in the above mapped region. Although acetylation was decreased, Ifh1p is still significantly acetylated.

(E) Mutation of 39 lysines in the 1-297 region eliminates acetylation of Ifh1p. An additional 21 lysines before S189 were mutated, eliminating the residual acetylation on Ifh1p. CHX treatment did not result in any observable acetylation of this Ifh1p 39K/R mutant.

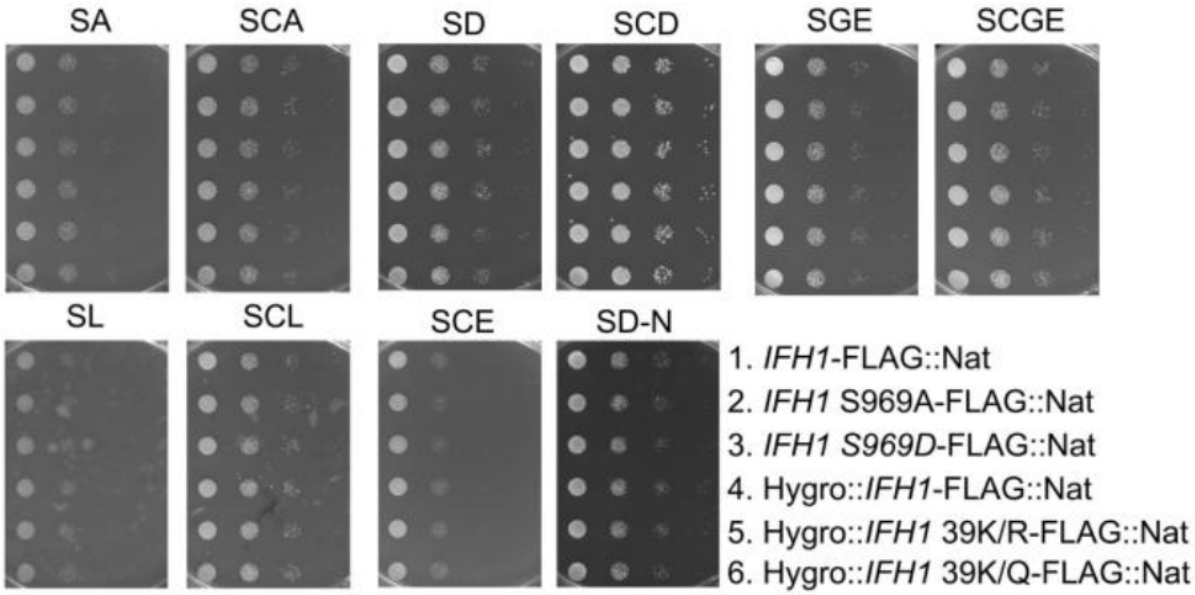

Figure 3.11 Growth on medium with different carbon sources.
WT and the indicated mutant strains in the CEN.PK background were tested for growth on different carbon sources. Synthetic minimal medium without or with amino acids (S or SC) were tested. Nitrogen starvation was also tested (SD-N). No significant growth difference for any mutant has been observed. Growth was also tested at 37°C. Mutant strains constructed in S288C background were also tested with SC based medium under 30°C or 37°C. Again, no differences in growth were observed (data not shown).

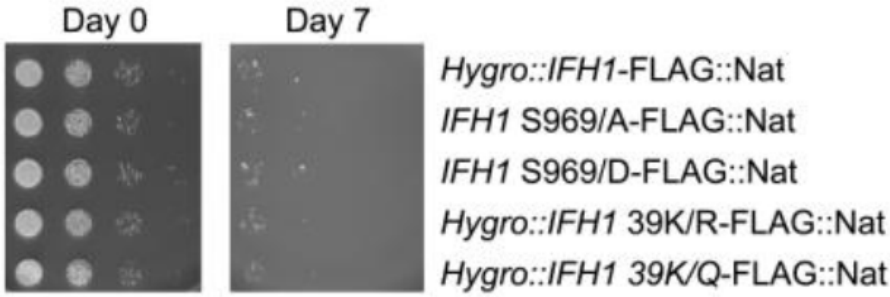

Figure 3.12 Chronological life span test
The indicated strains were grown to log phase in SD medium. Cells were pelleted, washed twice with H2O and resuspend in H2O to 1OD/ml. Cells were serial diluted and spotted onto YPD once a day for 7 days. No difference has been observed in the mutants.

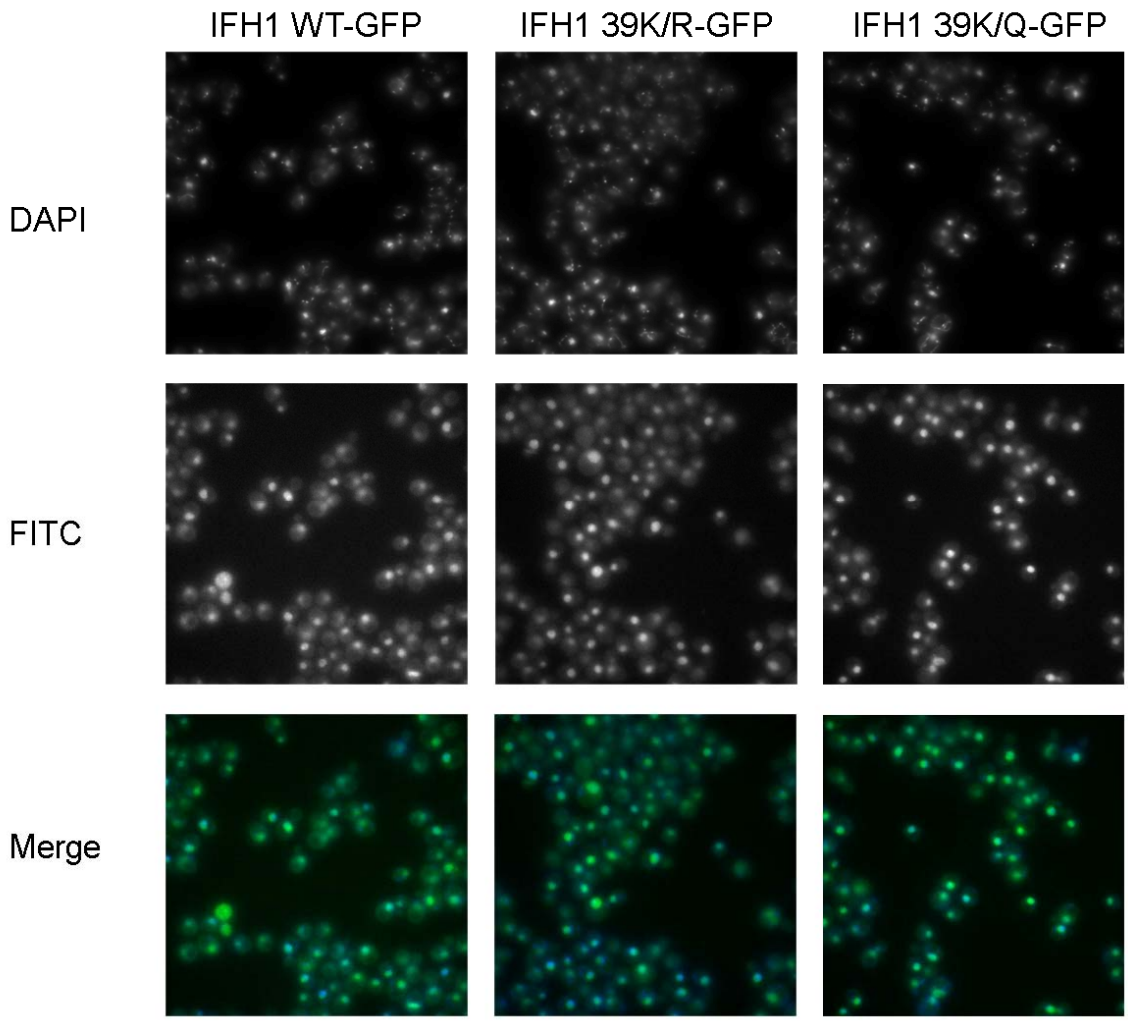

Figure 3.13 Localization of Ifh1p in WT and acetylation mutant strains
We have examined Ifh1p localization in IFH1 WT-GFP, IFH1 39K/R-GFP and IFH1 39K/Q-GFP strains as shown above. The majority of Ifh1p seems to be located in the nucleus and the localization of Ifh1p seems unaffected in the mutants.

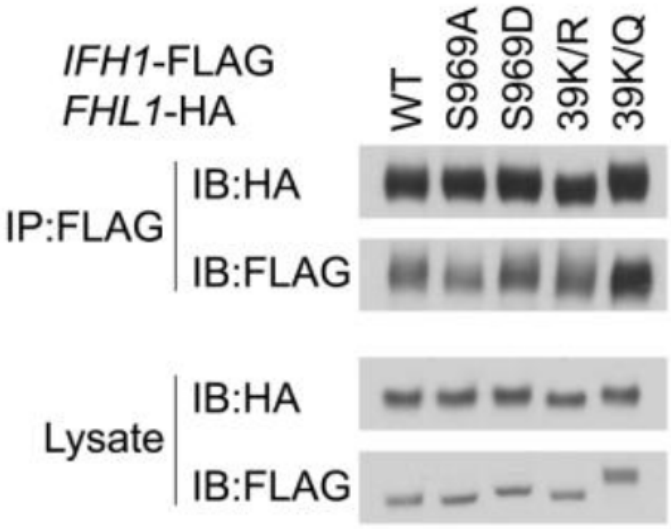

Figure 3.14 Interactions with Fhl1p
FHL1 was C-terminally tagged with HA in WT and different mutant strains. Cells from the indicated strains were collected during growth in YPD at log phase. Comparable amounts of Fhl1-HA were co-immunoprecipitated by Ifh1-FLAG in WT and mutant strains.

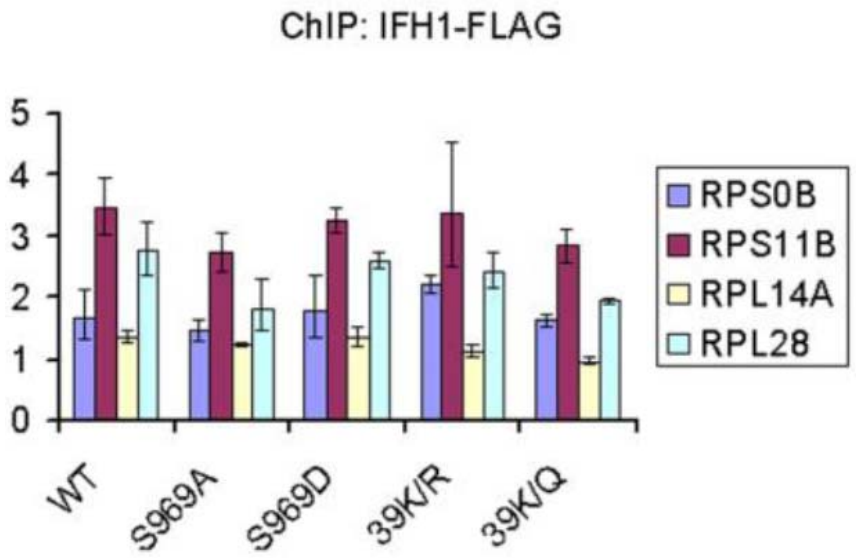

Figure 3.15 Binding to RP gene promoters.
Cells from the indicated strains were grown in SD medium to log phase and fixed. ChIP-PCR was performed. qPCR was performed using the ChIP DNA, results for RP gene promoters were normalized to *POX1* ORF qPCR, which is not bound by Ifh1p. No obvious difference has been observed in the mutants.

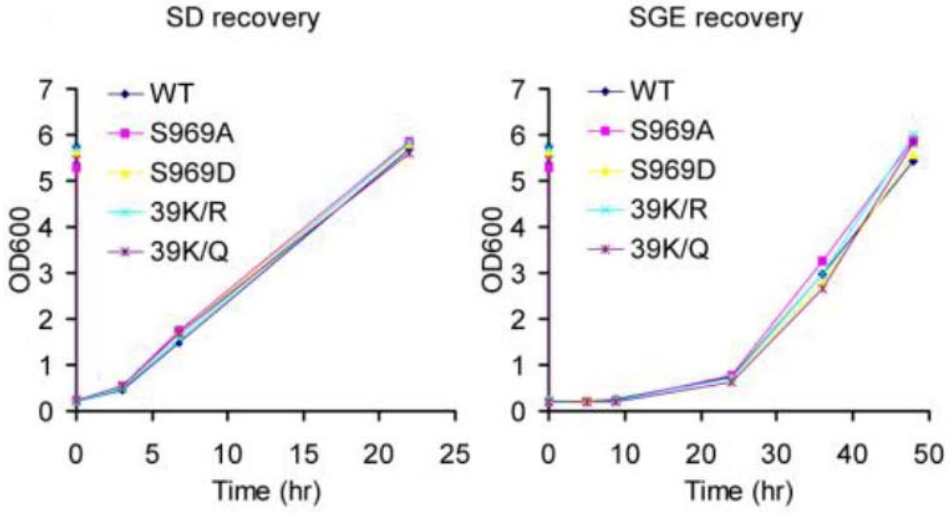

Figure 3.16 Recovery from stationary phase.
Cells were grown to stationary phase in SD. OD prior to dilution was indicated at time 0. Cells were then washed twice and resuspended in H_2O and diluted into either SD or SGE to OD 0.1. Their subsequent growth was plotted into growth curves. No difference has been observed between mutants and WT.

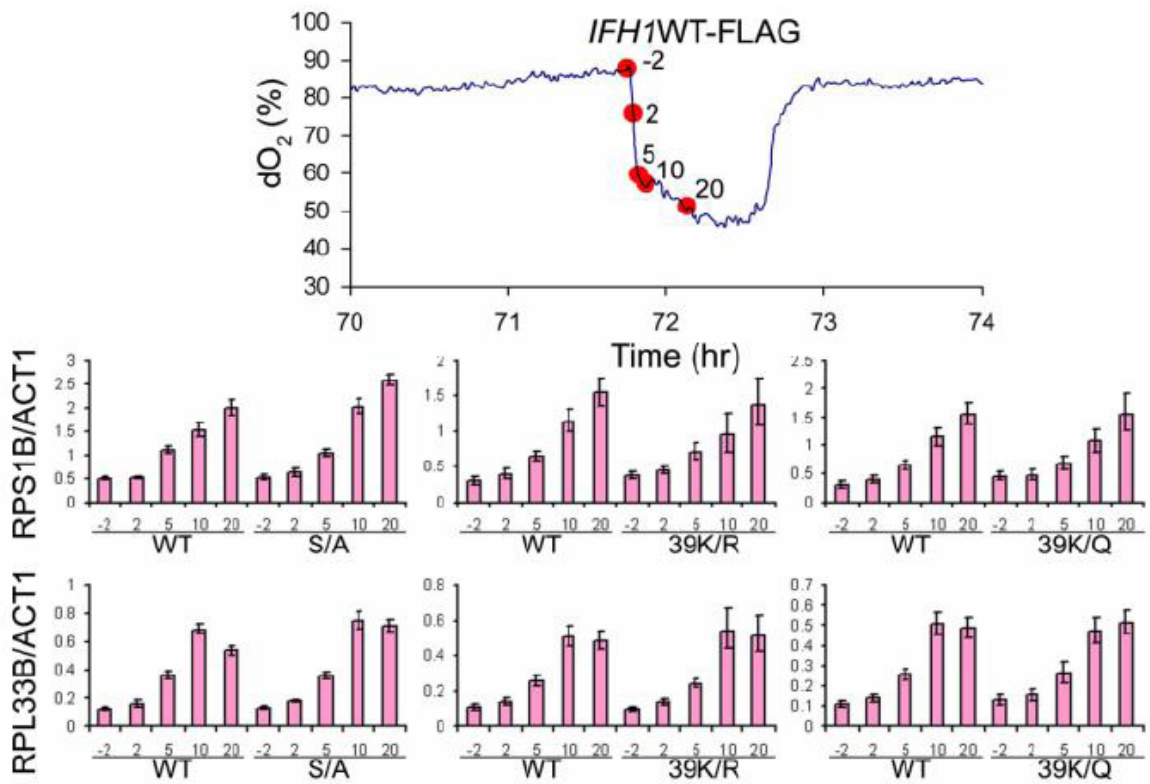

Figure 3.17 RP gene transcription during transition to growth in YMC.
During the YMC for WT, S/A, K/R and K/Q mutants, cells were collected during acetate-induced growth entry from RC phase. Time points were taken 2 min prior to addition of acetate, then 2, 5, 10 and 20min after acetate addition. RNA was extracted from these samples and cDNA was made. qPCR was performed for two representative RP genes. Both of them are induced robustly during entry into OX phase. These results suggest there is no difference in the downstream RP gene transcription activation response in the S/A, K/R and K/Q mutants compared to WT.

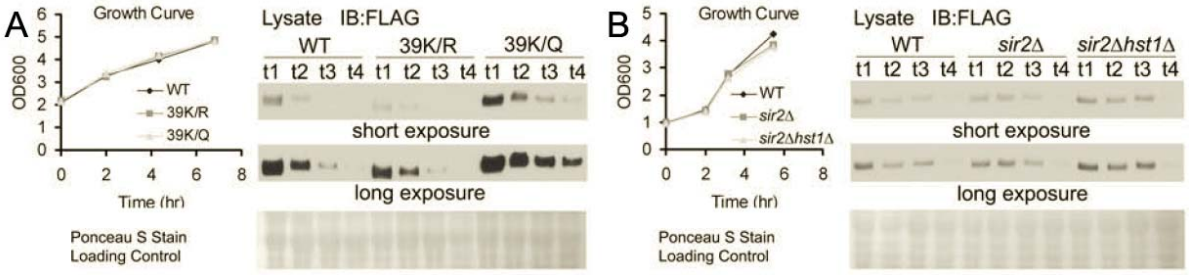

Figure 3.18 Acetylation regulates protein stability of Ifh1p

(A) The Ifh1p 39K/Q acetylated mimic mutant is more stable during nutrient depletion. Lysates were prepared from the indicated strains at the indicated time points on the growth curve. Ifh1p levels decrease as cells grow to a higher density approaching stationary phase. Levels of Ifh1p are lower in K/R mutant and higher in K/Q mutant. The membrane was stained by Ponceau S and shown as a loading control. Two different exposures of the same blot are shown.

(B) *sir2*Δ and *sir2*Δ*hst1*Δ mutants exhibit increased Ifh1p stability. Experiments were performed as described above with *sir2*Δ and *sir2*Δ*hst1*Δ strains. Ifh1p seems to be more stable in the mutants where it is highly acetylated. Two different exposures of the same blot are shown.

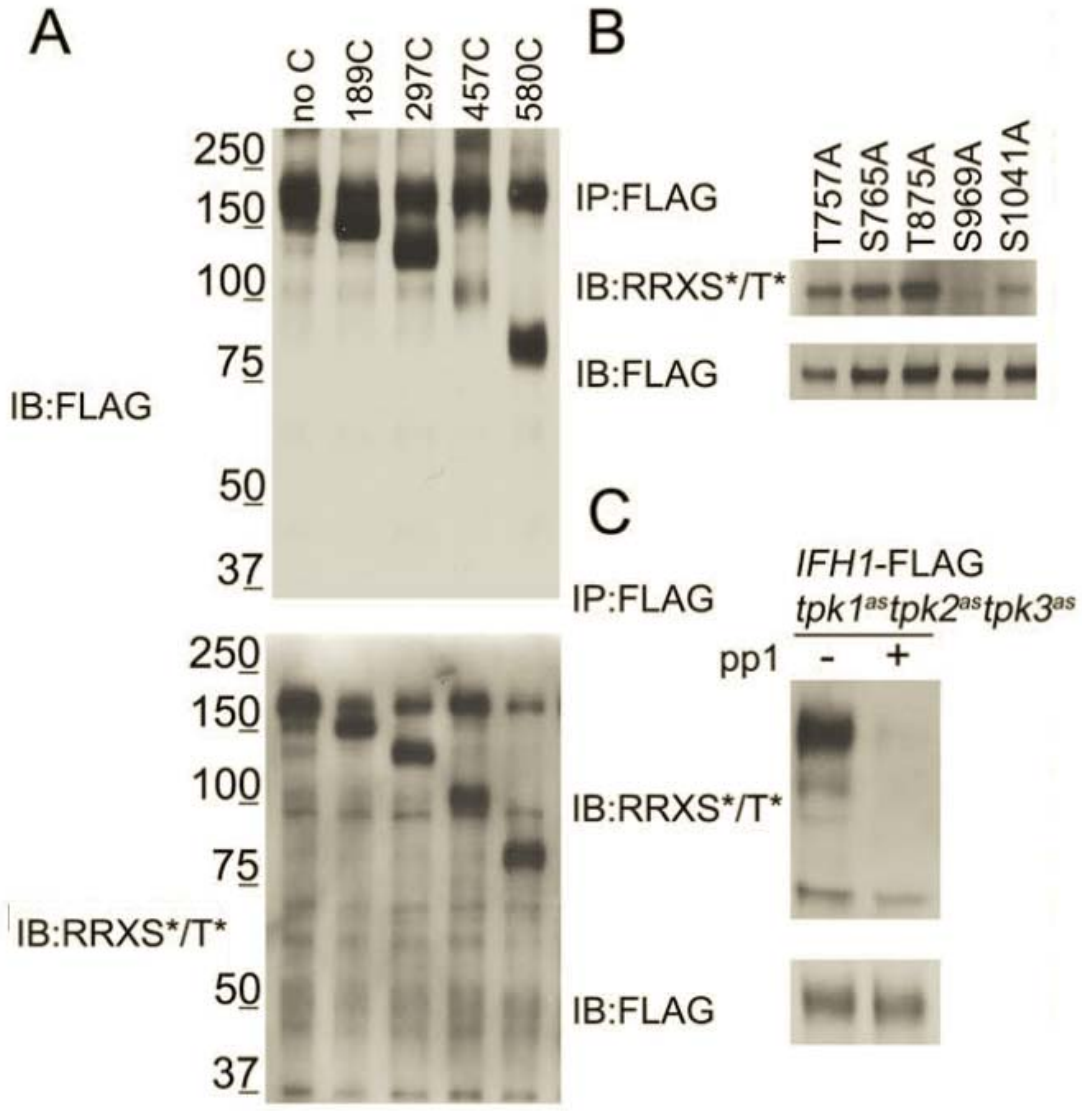

Figure 3.19 Ifh1p is phosphorylated at S969 by PKA and modifications of Ifh1p may regulate replicative lifespan

(A) Ifh1p is phosphorylated at site(s) C-terminal of C580. Based on the mapping method described above, the exact match of FLAG and RRXS*/T* blotting patterns indicates the phosphorylated sites are after residue 580.

(B) Ifh1p is phosphorylated at S969. Candidate sites that match the motif RXXS*/T* were mutated to alanine. Mutation at S969 eliminated the signal recognized by the phospho-specific antibody.

(C) Ifh1p is phosphorylated by PKA. In an engineered strain (*tpk1*^{as}*tpk2*^{as}*tpk3*^{as}) where PKA is rendered specifically sensitive to the inhibitor 1NM-PP1, phosphorylation of Ifh1p is eliminated within 10min treatment of 1NM-PP1.

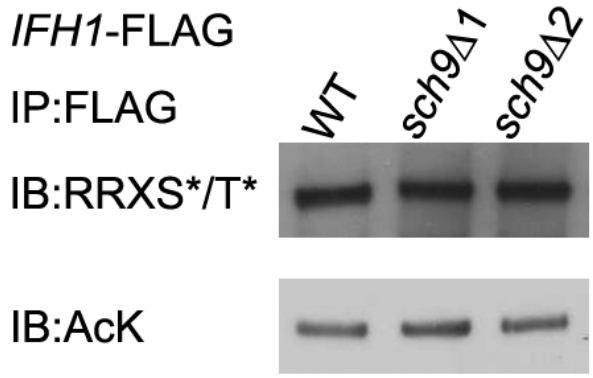

Figure 2.20. Ifh1p is not phosphorylated by Sch9p.
Ifh1p phosphorylation detected by an antibody specific to Sch9p and PKA phosphorylated substrates remained unchanged in *sch9*Δ cells. Two *sch9*Δ mutant clones were selected for analysis.

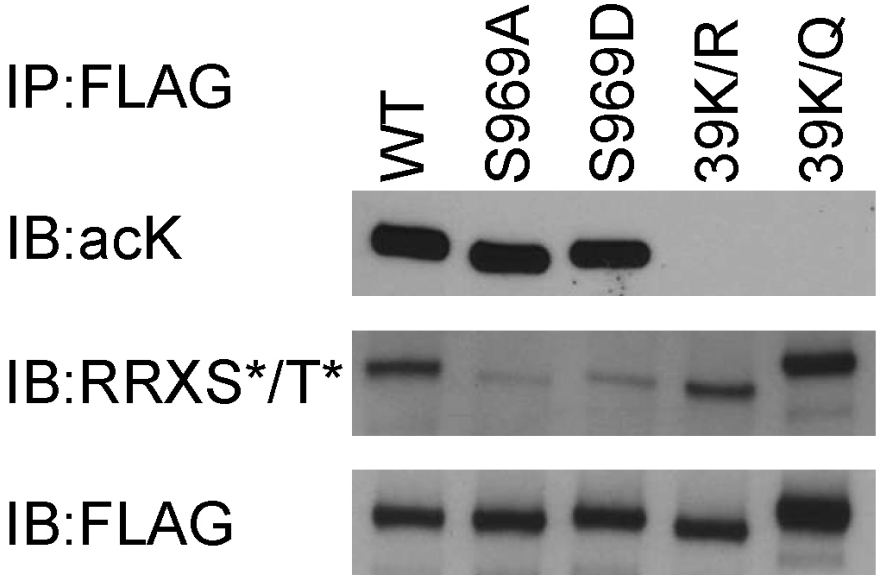

Figure 3.21 Ifh1p acetylation and phosphorylation are independent of each other
Levels of phosphorylation remain unchanged in the acetylation mutant while levels of acetylation remained unchanged in the phosphorylation mutant. Note that there is more Ifh1p from the K/Q mutant IP as seen in the IB:FLAG loading control. This is due to a more stable Ifh1p K/Q protein.

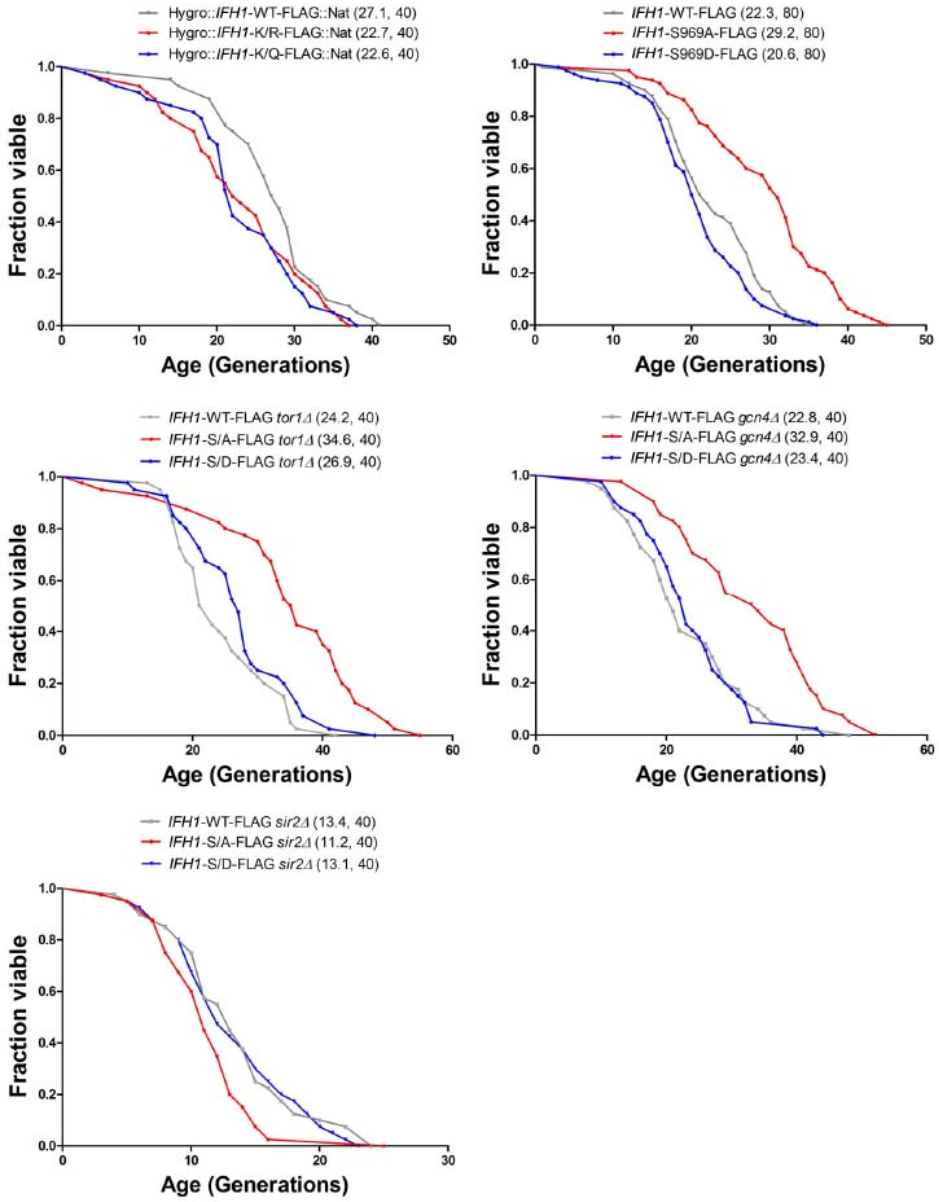

Figure 3.22. Nutrient-responsive post-translational modifications of Ifh1p may regulate replicative lifespan (RLS).

Nutrient-responsive phosphorylation of Ifh1p impacts replicative lifespan (RLS). Mutant strains were constructed in the BY4741 background. The ~30-40% increase in RLS of the S969A mutant was dependent on Sir2p, but not Gcn4p or Tor1p. Numbers in parentheses denote average lifespan, number of cells tested. Table 3.2 contains statistical analysis of the RLS data.

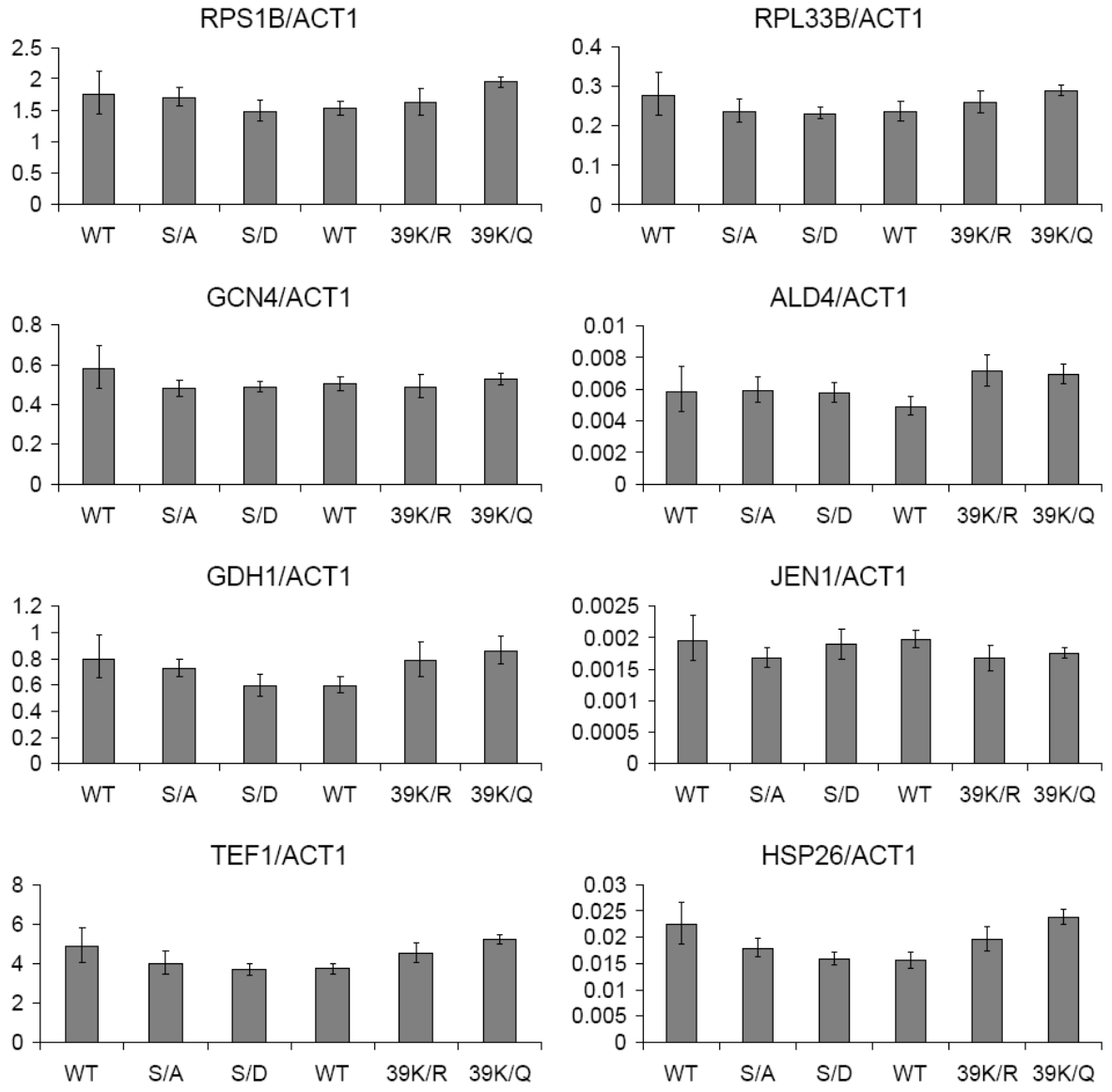

Figure 3.23 Transcription of Ifh1p target genes is unaffected in phosphorylation and acetylation mutants.

Strains (WT: *IFH1*-WT-FLAG::Nat, S/A: *IFH1*-S969A-FLAG::Nat, S/D: *IFH1*-S969D-FLAG:: Nat, WT: Hygro::*IFH1*-WT-FLAG::Nat, 39K/R: Hygro::*IFH1*-39K/R-FLAG::Nat, 39K/Q: Hygro::IFH1-39K/Q-FLAG::Nat) were grown in SD medium to log phase and expression profiles of selected Ifh1p targets including two representative RP genes and some of the non-RP gene targets were obtained by qPCR.

Table 3.1. Peaks from IFH1-FLAG ChIP-seq at OX phase annotated by CisGenome
The peaks were assigned to genes whose promoters were closest to the peak. Except for *GCN4* and *TEF2*, many of the non-RP genes are actually next to an RP gene and might be mis-annotated. The order is based on ascending false discovery rate (FDR).

#seq_id	Chromosome	Start	End	Standard Name	Systematic Name
1	chr16	76447	76491	*RPL36B*	*YPL249C-A*
2	chr10	75676	75705	*RPL39*	*YJL189W*
3	chr4	221983	222074	*RPL41B*	*YDL133C-A*
4	chr12	932090	932216	*YLR406C-A*	*YLR406C-A*
5	chr6	223917	223973	*YFR032C-B*	*YFR032C-B*
6	chr15	254037	254126	*RPP2A*	*YOL039W*
7	chr13	551681	551769	*RPS16A*	*YMR143W*
8	chr4	1359659	1359715	*RPS18A*	*YDR450W*
9	chr15	94517	94545	*RPL18A*	*YOL120C*
10	chr4	117457	117518	*RPL35A*	*YDL191W*
11	chr16	794711	794767	*RPS23B*	*YPR132W*
12	chr16	378706	378773	*RPS6A*	*YPL090C*
13	chr7	228484	228530	*RPL9A*	*YGL147C*
14	chr7	310777	310816	*RPL28*	*YGL103W*
15	chr16	731959	732031	*RPL11A*	*YPR102C*
16	chr4	321855	322045	*RPL31A*	*YDL075W*
17	chr15	80078	80106	*RPL25*	*YOL127W*
18	chr16	654021	654091	*RPL43A*	*YPR043W*
19	chr12	241907	241975	*RPS0B*	*YLR048W*
20	chr12	1028474	1028572	*RPL6B*	*YLR448W*
21	chr7	788415	788480	*YGR149W*	*YGR149W*
22	chr7	726669	726709	*YGR117C*	*YGR117C*
23	chr10	157150	157222	*RPS21B*	*YJL136C*
24	chr12	1019014	1019081	*RPS1A*	*YLR441C*
25	chr14	444480	444548	*RPS7B*	*YNL096C*
26	chr2	605960	606057	*RPL21A*	*YBR191W*
27	chr14	63109	63137	*RPS19B*	*YNL302C*
28	chr7	555588	555635	*RPL26B*	*YGR034W*
29	chr14	331007	331235	*RPL42A*	*YNL162W*
30	chr13	146138	146344	*RPS1B*	*YML063W*
31	chr13	754459	754488	*YMR242W-A*	*YMR242W-A*
32	chr8	382957	383060	*RPL42B*	*YHR141C*
33	chr12	522394	522424	*RPL37A*	*YLR185W*
34	chr3	178356	178421	*RPS14A*	*YCR031C*
35	chr2	415351	415635	*RPL19A*	*YBR084C-A*
36	chr7	149148	149229	*YGL188C-A*	*YGL188C-A*
37	chr12	897936	898008	*REH1*	*YLR387C*
38	chr14	302479	302556	*RPS3*	*YNL178W*
39	chr5	306060	306110	*RPS24A*	*YER074W*
40	chr7	254444	254498	*RPL1B*	*YGL135W*
41	chr6	221779	221872	*RPL2A*	*YFR031C-A*
42	chr11	431320	431359	*RPL14A*	*YKL006W*
43	chr2	332587	332648	*RPS11B*	*YBR048W*
44	chr10	651282	651310	*RPS5*	*YJR123W*
45	chr13	551376	551489	*RPL13B*	*YMR142C*
46	chr4	307926	307974	*RPS16B*	*YDL083C*
47	chr5	53468	53496	*RPL12A*	*YEL054C*
48	chr14	495215	495380	*RPL16B*	*YNL069C*
49	chr15	678913	679038	*RPS30B*	*YOR182C*

50	chr5	270340	270426	*RPL34A*	*YER056C-A*
51	chr10	703030	703091	*RPS4A*	*YJR145C*
52	chr4	1355692	1355792	*RPS17B*	*YDR447C*
53	chr7	920200	920289	*RPS0A*	*YGR214W*
54	chr15	866861	866991	*RPS10A*	*YOR293W*
55	chr16	406479	406507	*RPL21B*	*YPL079W*
56	chr13	225650	225678	*RPS17A*	*YML024W*
57	chr13	124352	124403	*RPL6A*	*YML073C*
58	chr7	366137	366181	*RPL7A*	*YGL076C*
59	chr16	302917	302946	*RPL5*	*YPL131W*
60	chr8	36123	36191	*RPL8A*	*YHL033C*
61	chr5	423346	423415	*RPS26B*	*YER131W*
62	chr7	438568	438625	*RPL30*	*YGL030W*
63	chr5	362449	362629	*RPS8B*	*YER102W*
64	chr2	604290	604345	*RPS9B*	*YBR189W*
65	chr2	592882	592985	*RPS6B*	*YBR181C*
66	chr2	45281	45350	*ROX3*	*YBL093C*
67	chr12	796495	796530	*RPS25B*	*YLR333C*
68	chr15	779697	779749	*RPL33B*	*YOR234C*
69	chr2	168106	168145	*RPL19B*	*YBL027W*
70	chr8	505908	505937	*MNL1*	*YHR204W*
71	chr9	257319	257489	*RPL34B*	*YIL052C*
72	chr5	140548	140637	*GCN4*	*YEL009C*
73	chr12	263032	263063	*RPL22A*	*YLR061W*
74	chr2	89648	89685	*YBL071C-B*	*YBL071C-B*
75	chr8	75233	75262	*RPS20*	*YHL015W*
76	chr7	649006	649065	*RPL11B*	*YGR085C*
77	chr9	232620	232686	*RPS24B*	*YIL069C*
78	chr2	477238	477267	*TEF2*	*YBR118W*
79	chr4	491181	491333	*RPS11A*	*YDR025W*
80	chr9	99743	99771	*RPL16A*	*YIL133C*
81	chr15	901379	901492	*RPL20B*	*YOR312C*
82	chr5	396516	396549	*RPL23B*	*YER117W*
83	chr8	148897	148925	*RPS27B*	*YHR021C*
84	chr7	277294	277322	*RPS2*	*YGL123W*
85	chr13	224057	224098	*RPS18B*	*YML026C*
86	chr9	68456	68484	*RPL40A*	*YIL148W*

Table 3.2 Replicative lifespan analysis of mutant strains

Pairwise Comparison	Mutant mean	Mutant N	WT mean	WT N	% Effect	Chi square	P value
Hygro::*IFH1* WT-FLAG::Nat vs. Hygro::*IFH1*-K/R-FLAG::Nat	22.7	40	27.1	40	-16.24%	4.049	0.0442
Hygro::*IFH1* WT-FLAG::Nat vs. Hygro::*IFH1*-K/Q-FLAG::Nat	22.6	40	27.1	40	-16.61%	5.162	0.0231
IFH1-WT-FLAG vs. *IFH1*-S969A-FLAG	29.2	80	22.3	80	30.94%	40.37	< 0.0001
IFH1-WT-FLAG vs. *IFH1*-S969D-FLAG	20.6	80	22.3	80	-7.62%	2.018	0.1555
IFH1-WT-FLAG *sir2*Δ::Hygro vs. *IFH1*-S969A-FLAG *sir2*Δ::Hygro	11.2	40	13.4	40	-16.42%	4.917	0.0266
IFH1-WT-FLAG *sir2*Δ::Hygro vs. *IFH1*-S969D-FLAG *sir2*Δ::Hygro	13.1	40	13.4	40	-2.24%	0.3221	0.5703
IFH1-WT-FLAG *gcn4*Δ::Hygro vs. *IFH1*-S969A-FLAG *gcn4*Δ::Hygro	32.9	40	22.8	40	44.30%	17.78	< 0.0001
IFH1-WT-FLAG *gcn4*Δ:: Hygro vs. *IFH1*-S969D-FLAG *gcn4*Δ:: Hygro	23.4	40	22.8	40	2.63%	0.001233	0.972
IFH1-WT-FLAG *tor1*Δ:: Hygro vs. *IFH1*-S969A-FLAG *tor1*Δ:: Hygro	34.6	40	24.2	40	42.98%	26.55	< 0.0001
IFH1-WT-FLAG *tor1*Δ:: Hygro vs. *IFH1*-S969D-FLAG *tor1*Δ:: Hygro	26.9	40	24.2	40	11.16%	2.727	0.0987

CHAPTER FOUR

Acetyl-CoA Synthetases in Yeast Metabolism

ACS1 and *ACS2* are Differentially Regulated

In yeast metabolism, the last step of glycolysis produces pyruvate and pyruvate can enter the mitochondria to be further metabolized through the TCA cycle or get converted into fermentation product such as acetate and ethanol (Figure 2.1B). When pyruvate is metabolized in the mitochondria, it is first converted to acetyl-CoA through the action of pyruvate dehydrogenase. This acetyl-CoA then joins the oxaloacetate to start the TCA cycle which generates energy through oxidative phosphorylation. However, acetyl-CoA cannot freely diffuse through membrane and the mitochondrial and nucleocytosolic acetyl-CoA pools are biochemically isolated. Therefore yeast cells require a substantial source of nucleocytosolic acetyl-CoA for lipid biosynthesis and protein acetylation, especially histone acetylation.

The main source of nucleocytosolic pool of acetyl-CoA in yeast comes from acetate. In *Saccharomyces cerevisiae,* there are two isoforms of acetyl-CoA synthetase (ACS), namely *ACS1* and *ACS2*. ACS catalyzes the reaction that converts acetate and CoA to acetyl-CoA using energy from ATP hydrolysis to pyrophosphate and AMP. This is crucial to the production of nuclear cytosolic pool of acetyl-CoA in yeast and deletion of both *ACS1* and *ACS2* results in inviability.

Despite the high similarity between Acs1p and Acs2p (Figure 4.1), the two enzymes are differentially regulated under different nutrient conditions. In the YMC, *ACS1* is

expressed in the RC quiescent like phase along with the other stress gene and glucose repressed genes such as *ADH2* for ethanol utilization. While *ACS2* is expressed in the RB phase during which cells start to divide (Figure 4.2). It has been previous determined that fermentation products ethanol and acetate peaks at the end of OX phase and beginning of RB phase (Tu 2005). Therefore the timing of *ACS2* expression at RB and *ACS1* expression at RC might indicate different utilization of acetate and ethanol after OX phase. In the batch culture condition, *ACS2* is abundantly expressed in glucose medium, while *ACS1*, having Adr1p and Cat8p binding site at its promoter, is repressed by glucose and only expressed after cells have gone through the diauxic shift.

Different Roles of Acs1p and Acs2p in Yeast Metabolism

The other evidence that ACS1 and ACS2 have different roles in yeast metabolism comes from the phenotype of the deletion mutants *acs1*Δ and *acs2*Δ.. Since *ACS1* is not expressed in glucose medium, deletion of *ACS2* renders the cell unable to grow on glucose medium. Although both Acs1p and Acs2p can convert acetate to acetyl-CoA, *acs1*Δ grows slower in ethanol containing medium while *acs2*Δ grows slower in acetate containing medium (Figure 4.3). The more surprising phenotype comes from culture in chemostat, while *acs2*Δ is still capable of undergoing YMC, *acs1*Δ is unable to enter YMC, indicating Acs1p has an important role in establishing YMC (Figure 4.4).

The localization of Acs1p and Acs2p are also quite differentially regulated. Acs2p is predominantly localized to the nucleus (Figure 4.5). Since histone acetylation relies on the nuclear cytosolic pool of acetyl-CoA which comes from acetate (Takahashi et al., 2006).

Nuclear localization of Acs2p could serve to provide a local supply of acetyl-CoA for histone acetylation.

Acs1p Can Form Foci Under Hypoxia

While the localization of Acs1-GFP looks less nuclear, we found Acs1-GFP can translocate into foci. This observation was first made when Acs1-GFP cells were put on a slide under the coverslip and imaged while being alive. The foci formation took place within a few minutes. We also found that cells near a bubble form foci later than those that are further away from the bubble (Figure 4.6). To find out what caused the translocation, we tested various conditions and determined that hypoxia was the trigger. We grew *ACS1*-GFP *ACS2*-Cherry cells to saturation and bubbled with nitrogen. Cells were fixed immediately when they were collected and foci formation was examined by fluorescent microscopy. We started to see foci forming cells at around 165min after switching from air to nitrogen, and by 225min, the majority of the cells have Acs1-GFP translocated into foci. Upon switching back to air, Acs1-GFP foci quickly dissipated within a few minutes (Figure 4.7).

To find out where these foci are localized, we constructed strains with different organelle markers tagged with red fluorescent protein. We confirmed that Acs1-GFP foci do not localize to the Golgi or peroxisome (Figure 4.8). We also tried to test whether Acs1-GFP foci are close to the lipid droplets since Acs1p might be important for supplying acetyl-CoA for lipid biogenesis. However, lipid droplets marked by Erg6-Cherry are only formed when cells were grown in glucose medium in which *ACS1* is repressed, Erg6-Cherry localize to ER instead when cells were grown in YPGE (Figure 4.9). We also checked Acs1-GFP foci in a

strain that has ER marked by Sec62-Cherry. However, it is not clear from the figure whether Acs1-GFP foci are close to the ER or not (Figure 4.10). We also examined the Acs1-GFP foci in a mitochondria marker strain (mitoRFP) in which RFP is fused to a mitochondrial targeting sequence. Although Acs1-GFP foci are not colocalized with the mitoRFP signal, they seem to be quite close to each other (Figure 4.11). It has been reported that N-terminally GFP tagged acetyl-CoA carboxylase Acc1p can form foci under hypoxia and nutrient limiting conditions and these foci localize to close vicinity of mitochondria (Figure 4.12). Acc1p is the enzyme that catalyzes the first step in fatty acid synthesis using acetyl-CoA and bicarbonate to generate malonyl-CoA. It is possible that Acs1p and Acc1p work closely together to generate acetyl-CoA and use it for lipid biogenesis. To see whether Acs1 and Acc1 foci colocalize, we generated a diploid strain Acs1-Cherry GFP-Acc1. However, in this strain, the cherry tagged Acs1 exhibited a different localization pattern under hypoxia. It adopts a filamentous rather than dot-like structure (Figure 4.13). Nevertheless, it can still change from cytosolic localization to filamentous structure under hypoxia and dissipate 1 minute upon switching back to air. In contrast, although GFP-Acc1 forms foci, it is not responsive to the switch back to air (Figure 4.13).

To find out what is contained in the foci, we tried to immunoprecipitate Acs1-GFP and identify the proteins that coimmunoprecipitated. However, since Acs1-GFP foci dissipate quickly once oxygen is available, we decided to crosslink to preserve the hypoxia specific protein-proteins interaction before the immunoprecipitation. We tested several crosslinkers and found that paraformaldehyde seems to work best in both preserving the foci and protein detection by western blot (Figure 4.14). We also looked into interaction data from SGD for

Acs1p. Finally we found that Yat1p colocalizes with Acs1p under hypoxia (Figure 4.15). Although Yat1-Cherry forms foci later than Acs1-GFP, it is not dependent on Acs1p as Yat1-Cherry can still form foci in *acs1Δ* cells (Figure 4.16). Yat1p is the one of the outer mitochondrial carnitine acetyltransferases that are responsible for transporting acetyl-CoA across the mitochondria. It transfers the acetyl group from acetyl-CoA to carnitine to form acetyl-carnitine and acetyl-carnitine can be transported into mitochondria through carnitine transporter Crc1p localized at the inner mitochondrial membrane. Once acetyl-carnitine gets into mitochondria, it can be converted back to acetyl-CoA and carnitine by the mitochondrial carnitine acetyl-CoA transferase Cat2p. And carnitine can go back to the cytosol to reinitiate another transport cycle (Figure 4.17). Besides Yat1p, Yat2p is the other outer mitochondrial carnitine acetyltransferases and is highly similar to Yat1p. We have shown that both Yat1p and Yat2p have increased interaction with Acs1p under hypoxia (Figure 4.18).

Acs1p foci formation can also be triggered by blocking electron transport chain

What might be the function of the Acs1p and Yat1p containing foci under hypoxia? It has been suggested that Yat1p and Yat2p are important for transportation of acetyl-CoA into mitochondria when mitochondria are dysfunctional. Such observation was first made from cells depleted of mitochondrial DNA (cells) (Liu and Butow, 2006). Mitochondrial DNA is mainly responsible for making electron transport complex. ρ0 cells lacking functional electron transport chain cannot undergo oxidative phosphorylation to convert NADH back to NAD^+. Therefore to keep the NAD^+/NADH ratio balanced, the full TCA cycle can no longer be carried out. However, cells still relies on part of the TCA cycle to generate glutamate and

glutamine from α-ketoglutarate. Glutamine and glutamate are essential nitrogen donors for anabolic processes such as synthesis of amino acids, purines and pyrimdines (Cai and Tu, 2012). In TCA cycle, mitochondrial acetyl-CoA is produced from pyruvate using pyruvate dehydrogenase which generates NADH from NAD^+. In these ρ0 cells, an alternative route is used. That is to generate oxaloacetate from pyruvate using pyruvate carboxylase, and acetyl-CoA from acetate. Having cytosolic acetyl-CoA transported into the mitochondria through carnitine shuttle, it can then join oxaloacetate to produce citrate. After citrate is isomerized to isocitrate, isocitrate is converted to α-ketoglutarate by isocitrate dehydrogenase. Although this reaction generates NADH, it can be consumed in the next step when α-ketoglutarate is converted to glutamate by the reverse reaction of glutamate dehydrogenase. This way there is no net changes in NAD^+/NADH (Figure 4.19).

There is some similarity between ρ0 cells and cells under hypoxia. In both cases the mitochondrial electron transport chain is not active. However, there are also important differences. As pointed out in Figure 4.19, ρ0 cells have another alternative way to generate glutamate and glutamine besides using acetyl-CoA from acetate as described above. They can use acetyl-CoA generated in the peroxisome from fatty acid oxidation. The peroxisomal acetyl-CoA can be converted to citrate through citrate synthase encoded by *CIT2*. And the peroxisomal citrate can be transported into the mitochondria (Figure 4.19). In fact, increased peroxisome proliferation and increased expression of genes involved in β-oxidation have been observed in ρ0 cells (Epstein et al., 2001). However, this route would not be possible under hypoxia because β-oxidation requires the participation of molecular oxygen. Hence,

the first route that involves acetyl-CoA into mitochondria might be the key to glutamate biosynthesis for cells grown under hypoxia.

To see whether the acetyl-carnitine transporter Crc1p and mitochondrial acetyl-carnitine transferase that releases carnitine and acetyl-CoA also form foci under hypoxia, we constructed *CRC1-Cherry ACS1-GFP* and *CAT2-Cherry ACS1-GFP* strains. However, we found that Crc1-Cherry and Cat2-Cherry do not form foci as Acs1-GFP does (Figure 4.20).

To test whether Acs1-GFP foci can also form in ρ0 cells with deficient mitochondria, we generated ρ0 cells from *ACS1-GFP* strain. We indeed observed foci using fluorescent microscopy under GFP channel. However, it turned out to be an artifact due to auto-fluorescence, since such foci were also observed in WT cells and *acs1*Δ cells (Figure 4.21). We then tested whether Acs1-GFP can form foci in cells treated with electron transport chain inhibitor antimycin (inhibitor of mitochondrial electron transport by blocking the reoxidation of reduced cytochrome b) and CCCP (uncoupler of ATP synthesis by dissipating the proton gradient across the inner mitochondrial membrane). To also compare the antimycin or CCCP treated cells with cells under hypoxia or normoxia, we grew cells under hypoxia overnight and collected the hypoxia sample, then switched to normoxia for 30 minutes before adding antimycin or CCCP. After another 30min, the antimycin or CCCP treated samples as well as untreated samples (normoxia) were collected. Cells were fixed and imaged or lysed for immunoprecipitation and western blot. Upon antimycin and CCCP treatment, Acs1-GFP relocalized to foci just as in hypoxia (Figure 4.22) and immunoprecipitation of crosslinked Acs1-GFP have pulled down more associated proteins with a similar pattern to samples from

hypoxia (Figure 4.23) suggesting these inactivating electron transport chain by depriving oxygen or using specific inhibitor treatment can both trigger Acs1-GFP foci formation.

Summary

The two acetyl-CoA synthetase enzymes Acs1p and Acs2p in yeast play distinct roles in metabolism and are differentially regulated by nutrient availability. While Acs2p is the key for growth in glucose rich medium, Asc1p is important for growth on ethanol and establishing yeast metabolic cycle. Intriguingly, Acs1p and acetyl-carnitine transferase Yat1p can localize to foci structure under hypoxia. Such foci are in the proximity of mitochondria. Asc1p foci can also form when electron transport chain is blocked by inhibitors, suggesting it is triggered by inactive mitochondria electron transport chain. Previous studies have revealed that acetyl-CoA generated from acetate could be imported into mitochondria through carnitine shuttling and serve as an alternative source for glutamate synthesis in cells with deficient mitochondria. It remains to be tested whether Acs1p foci is important for glutamate synthesis under hypoxia.

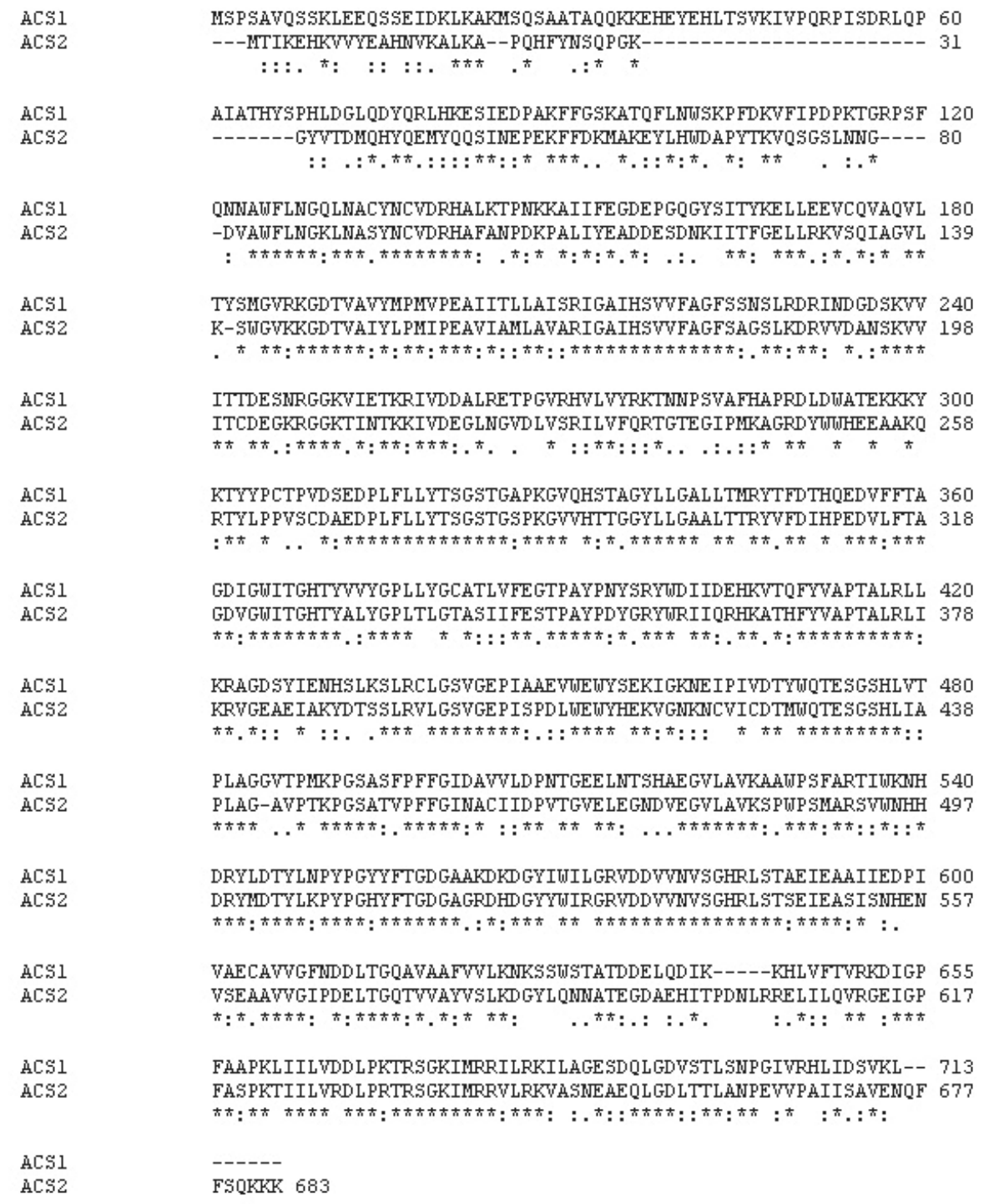

Figure 4.1 Alignment of *ACS1* and *ACS2* protein sequence
ACS1 and ACS2 are highly similar but with major difference in the N-terminus and last few residues in the C-terminus.

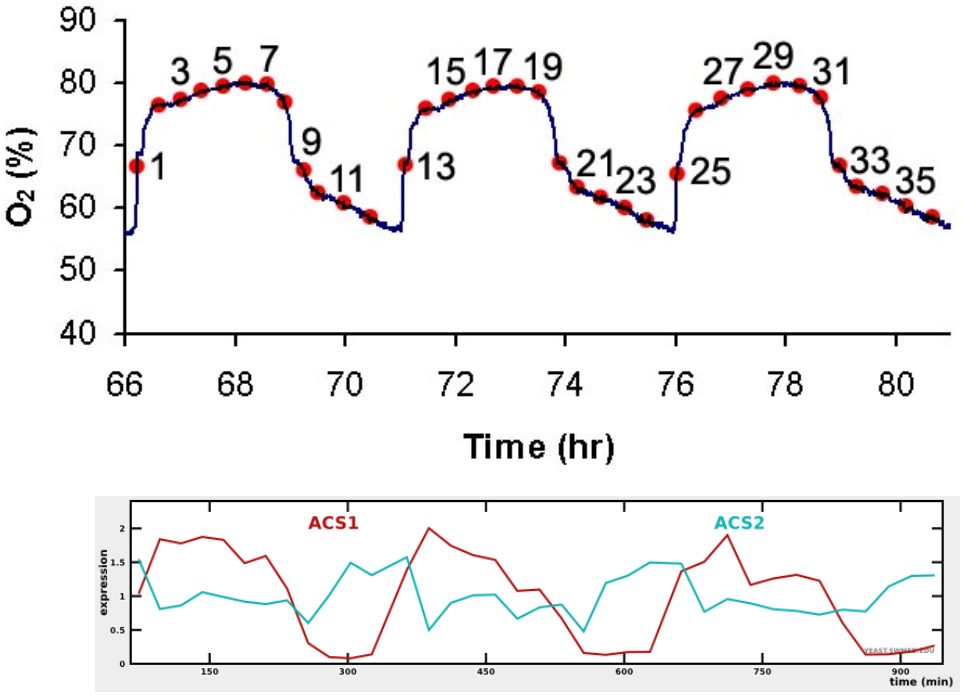

Figure 4.2 Different expression pattern of *ACS1* and *ACS2* across YMC
ACS1 and ACS2 expression was retrieved from previous microarray data from cells collected from three consecutive cycles (Tu 2005). ACS1 has the highest expression level during the RC quiescent phase while ACS2 has the highest expression level during RB phase when cells start to divide.

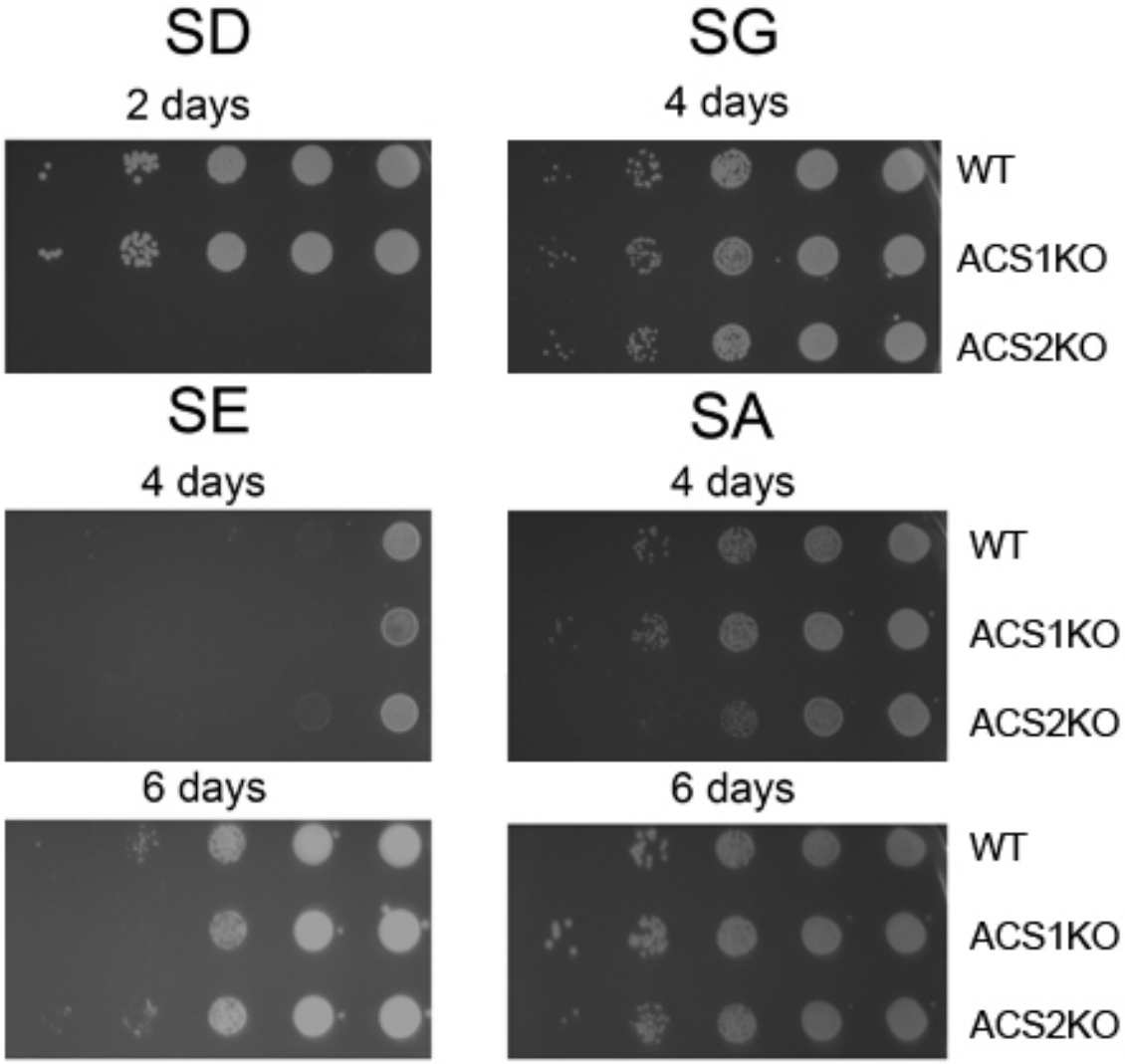

Figure 4.3 *acs1*Δ has slow growth on ethanol while *acs2*Δ has slow growth on acetate
After 10 fold serial dilution, yeast cells with indicated genotype were spotted onto synthetic medium plates with indicated carbon sources. *acs2*Δ is inviable on SD and has slower growth on SA, *acs1*Δ has slower growth on SE. SD (synthetic medium with D-glucose), SG (synthetic medium with glycerol), SE (synthetic medium with ethanol), SA (synthetic medium with acetate).

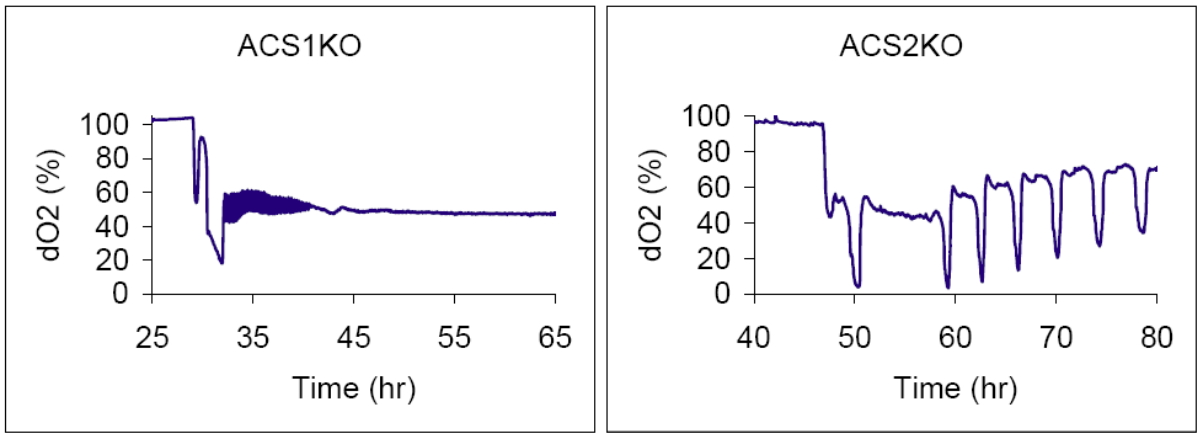

Figure 4.4 YMC phenotype of *acs1*Δ and *acs2*Δ
*acs1*Δ is unable to undergo YMC while *acs2*Δ have close to normal YMC. Since *acs2*Δ is inviable in glucose medium, ethanol and glycerol was used instead of glucose for the batch culture phase after cells were inoculated into the chemostat. After cells have reached saturation and starved, the original 1% glucose medium was used for continuous feeding mode.

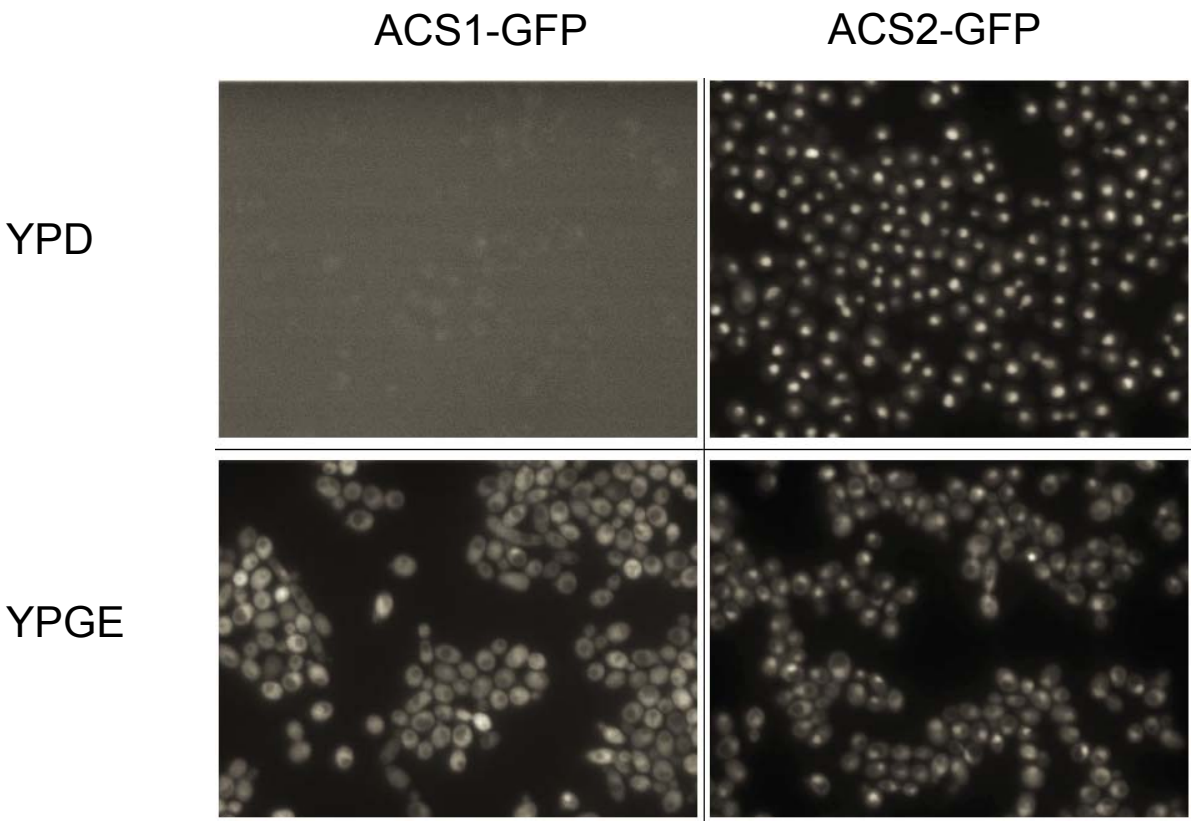

Figure 4.5 Expression and Localization of Acs1-GFP and Acs2-GFP in YPD and YPGE
Acs1-GFP and Acs2-GFP cells were grown to log phase in YPD or YPGE medium and fixed. *ACS1* is repressed in the glucose medium while Acs2-GFP is the only ACS enzyme expressed in glucose and it is localized exclusively to the nucleus. In YPGE, both *ACS1* and *ACS2* are expressed and are localized to the nucleus and cytosol.

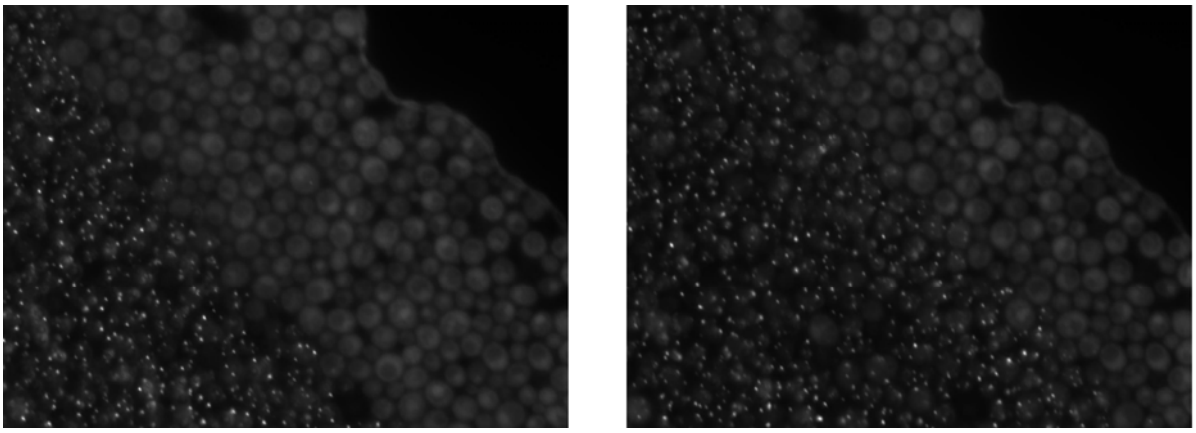

Figure 4.6 Acs1-GFP translocation into foci
Acs1-GFP live cells were put on a slide under the coverslip and imaged. A bubble was found at the upper right corner of the field. Translocation of Acs1-GFP into foci took place within a few minutes and spread from cells distant from the bubble to cells near the bubble.

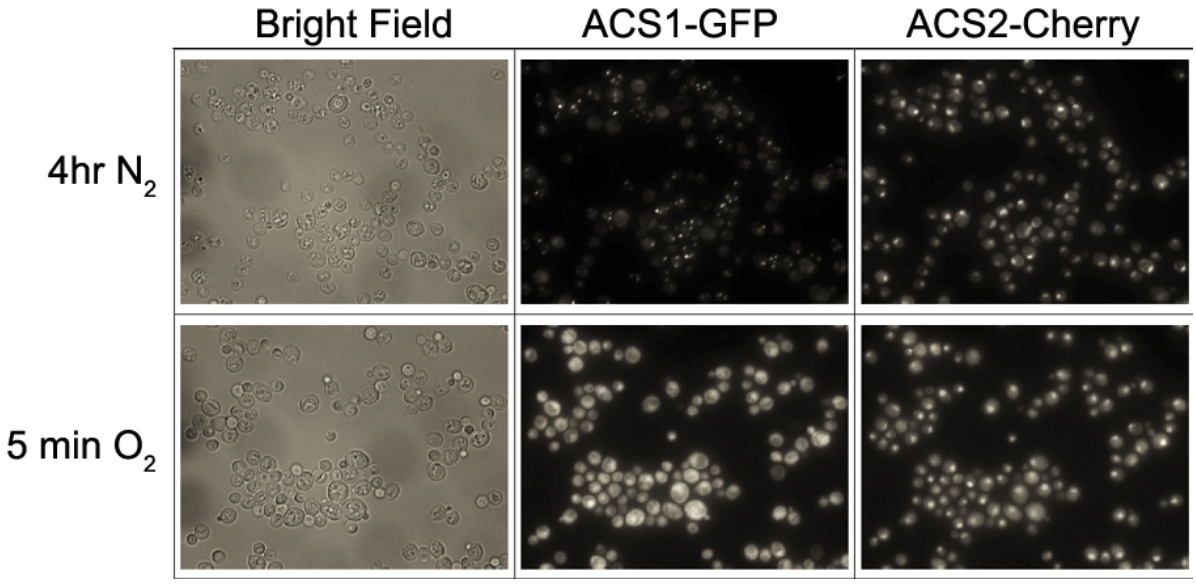

Figure 4.7 Acs1-GFP foci forms under hypoxia and dissipates under normoxia.
ACS1-GFP ACS2-Cherry cells were grown in the chemostat and bubbled with nitrogen for 4 hours, cells were fixed immediately at collection. ACS1-GFP already forms foci but ACS2-Cherry remained nuclear. After switching from nitrogen to oxygen for just 5 minutes, cells were collected and fixed immediately. ACS1-GFP has already dissipated back to the nucleus and cytosol.

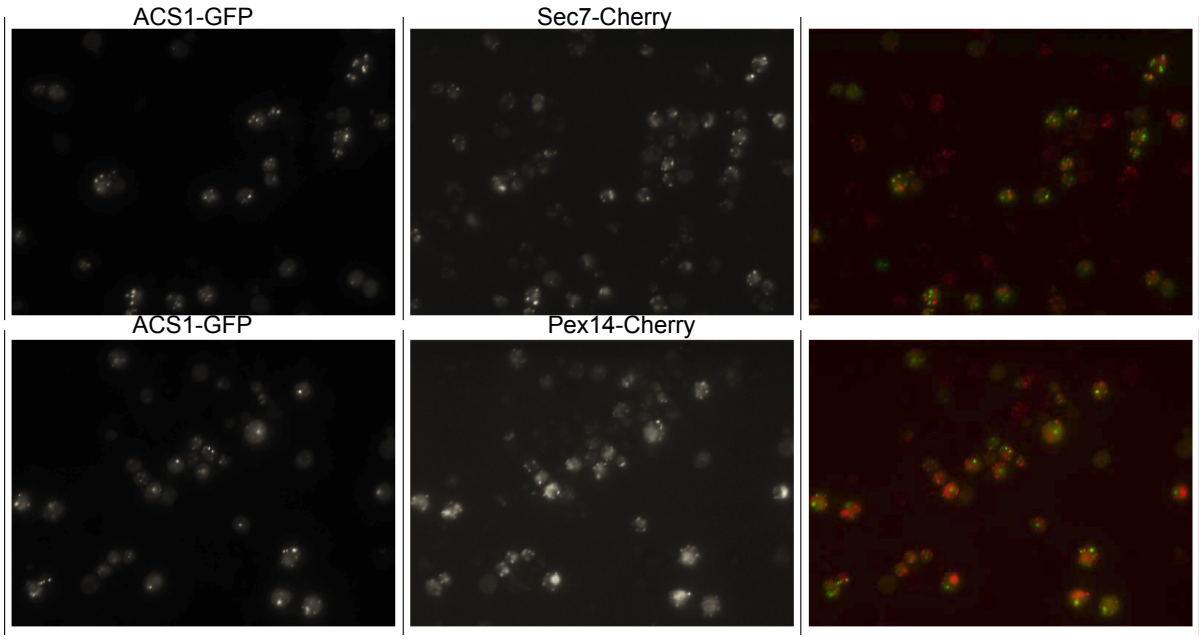

Figure 4.8 ACS1-GFP foci do not localize to Golgi or peroxisome
ACS1-GFP foci were studied in different organelle marker strains. Cells were grown in YPGE medium and checked alive on a glass slide under a coverslip. Sec7-Cherry marks the Golgi and Pex14-Cherry marks the peroxisome. ACS1-GFP foci do not overlap with these structure indicating ACS1-GFP foci are outside the Golgi or peroxisome.

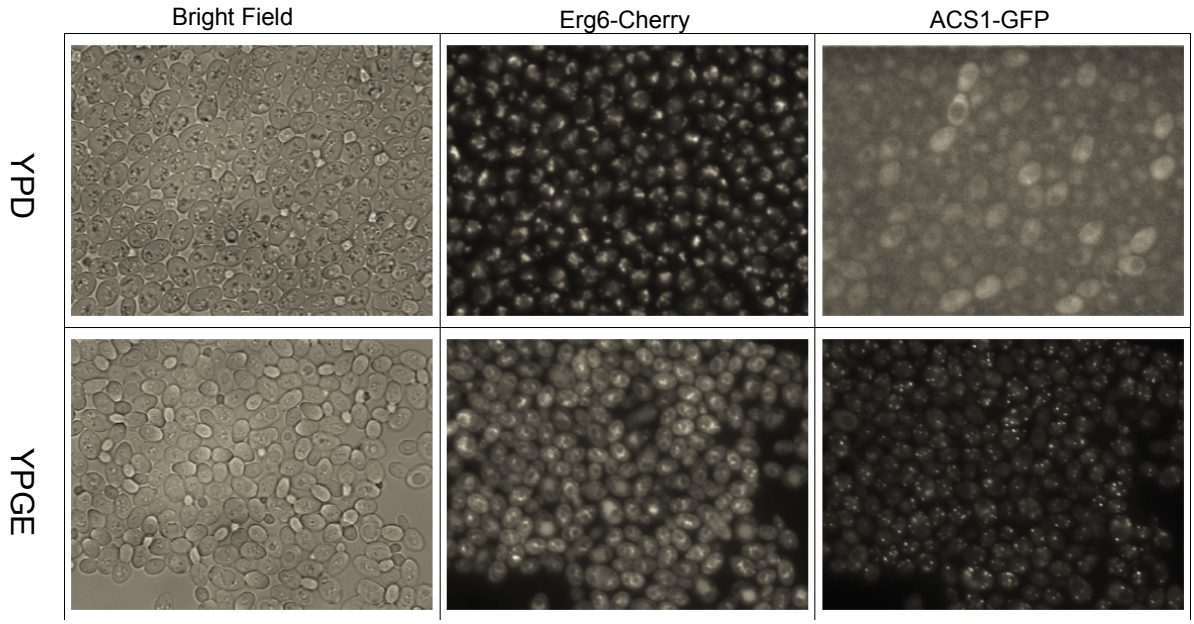

Figure 4.9 Acs1-GFP does no localize to lipid droplets
Lipid droplet marked by Erg6-Cherry is only found when cells were cultured in YPD, in YPGE culture, Erg6 localizes to the ER.

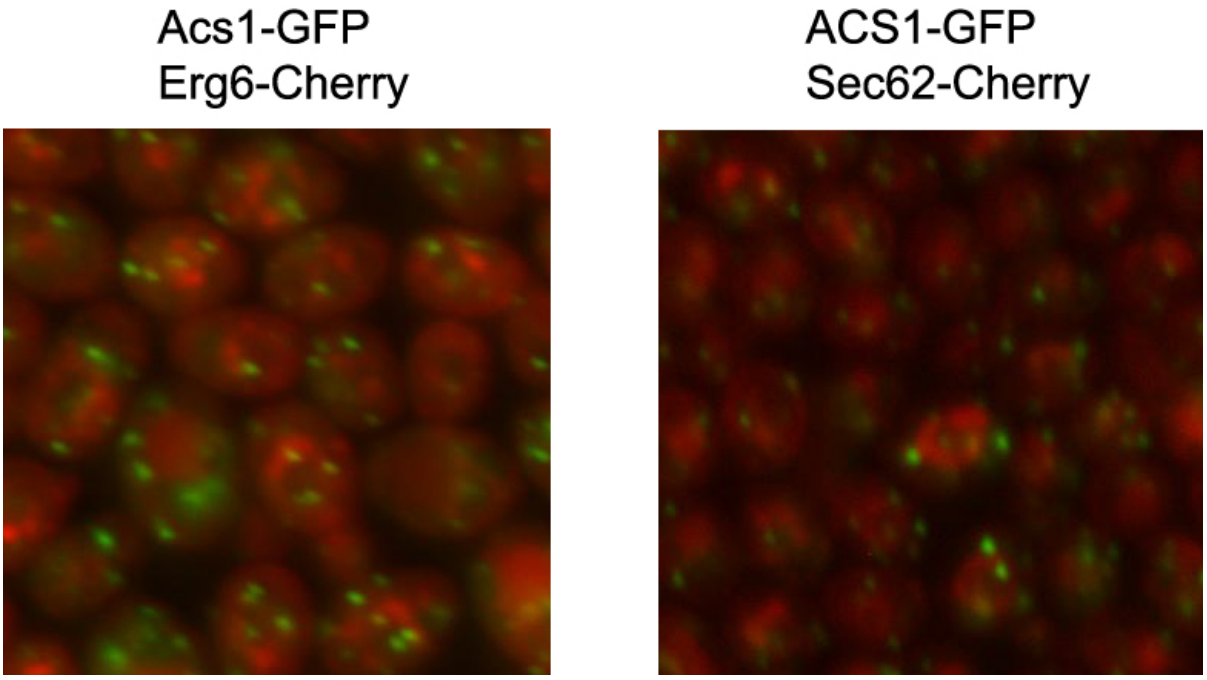

Figure 4.10 Acs1-GFP foci and ER markers
Erg6-Cherry and Sec62-Cherry marks the endosplasmic reticulum (ER) when grown in YPGE medium. Although Acs1-GFP foci do no colocalize to these ER markers, it is not clear how close they are.

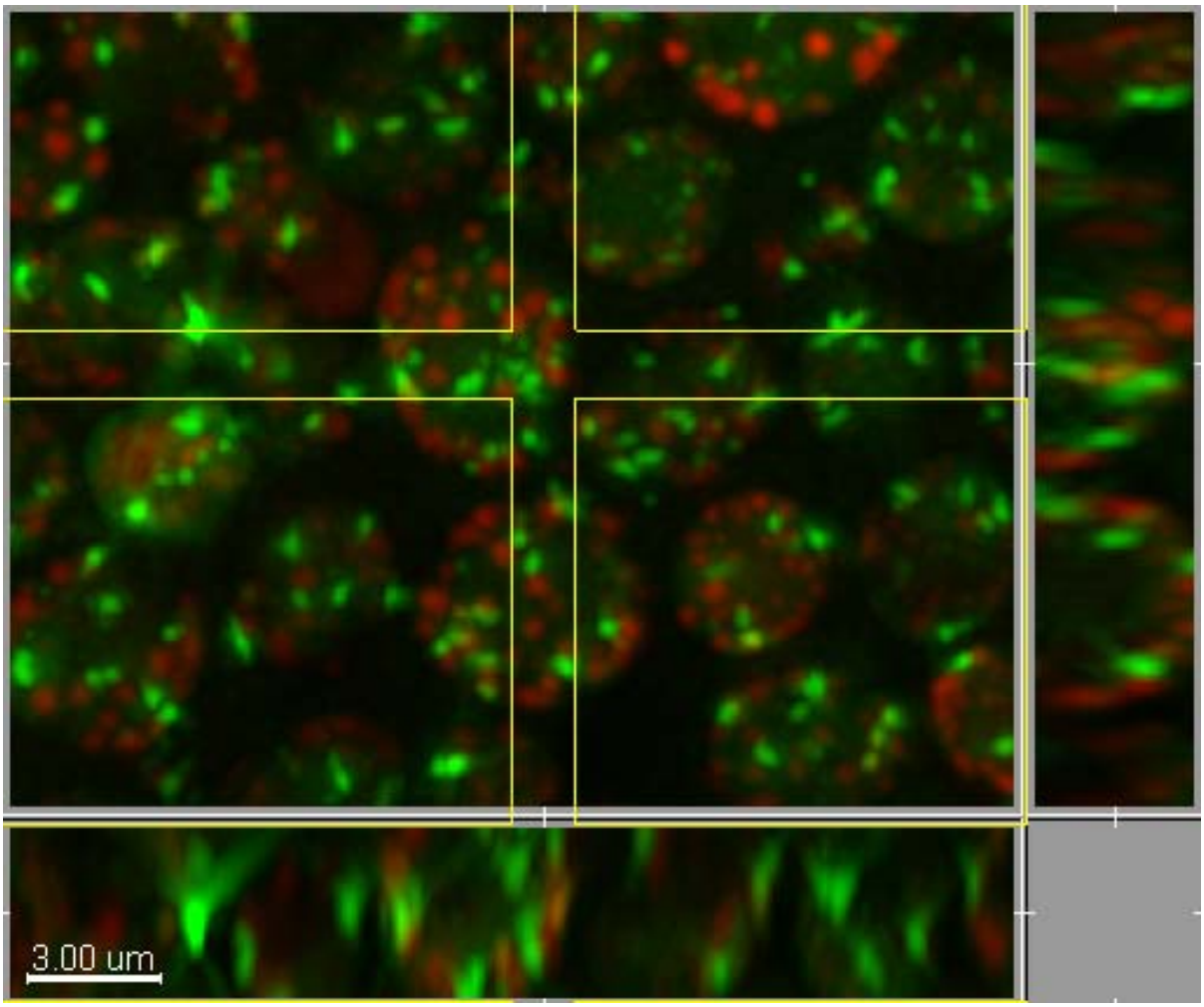

Figure 4.11 Acs1-GFP foci and mitochonrdia
Mitochondria are marked by mitoRFP which is RFP protein fused with a mitochondria targeting sequence. Acs1-GFP foci do not colocalize with mitochondria but they may be very close to each other.

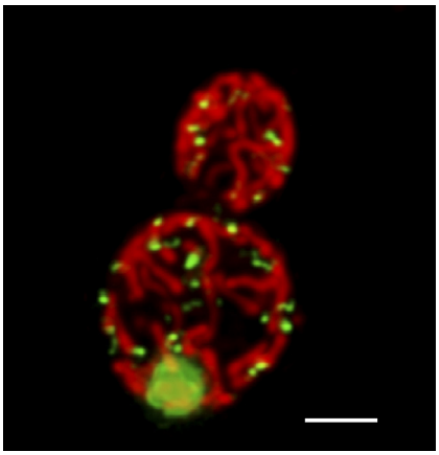

Figure 4.12 GFP-Acc1 foci
Figure was adapted from 16950653, Confocal micrograph of a live yeast cell stained for mitochondria (MitoTracker® Red CMXRos (Molecular Probes™, Invitrogen), in red) and acetyl-CoA carboxylase (GFP-fusion, in green). Note the pronounced aggregate formation of (cytosolic) Acc1, and the appearance of Acc1-foci in close vicinity to the mitochondria. Scale bar = 2 μm.

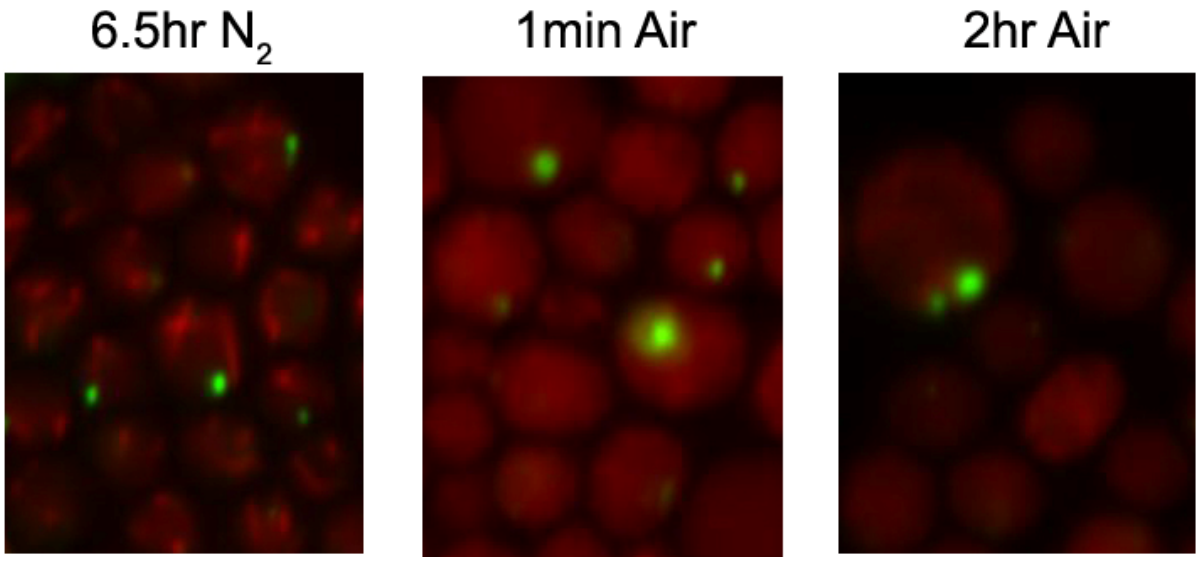

Figure 4.13 Acs1-Cherry GFP-Acc1 diploid
Acs1-Cherry forms filamentous structure rather than foci formed by Acs1-GFP. It does not colocalize with GFP-Acc1 foci. Acs1-Cherry filamentous structure dissipates back to cytosol upon switching back to air. However GFP-Acc1 remains in foci.

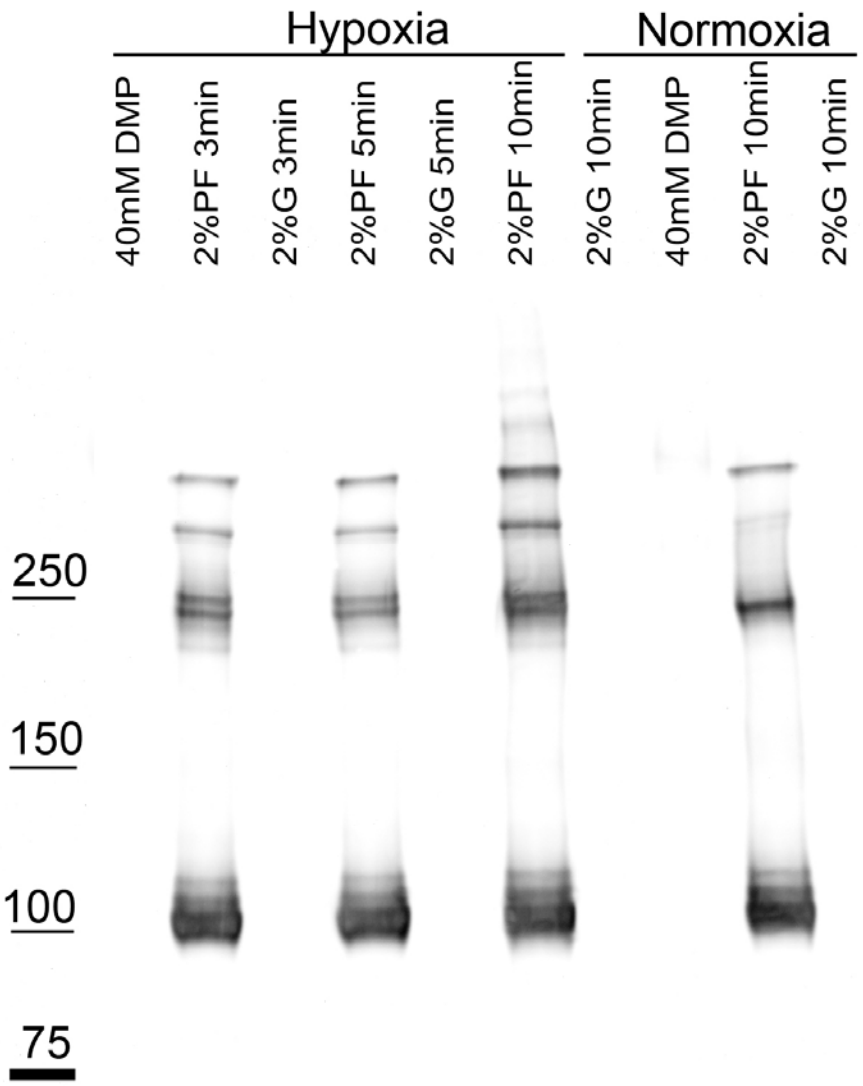

Figure 4.14 Immunoprecipitation of Acs1-GFP crosslinked by different crosslinkers
Different crosslinkers were tested and Acs1-GFP could only be detected in sample immunoprecipitated from paraformaldehyde crosslinked cells. Note that under the same fixing condition, several more bands are detected in the hypoxia versus normoxia sample.

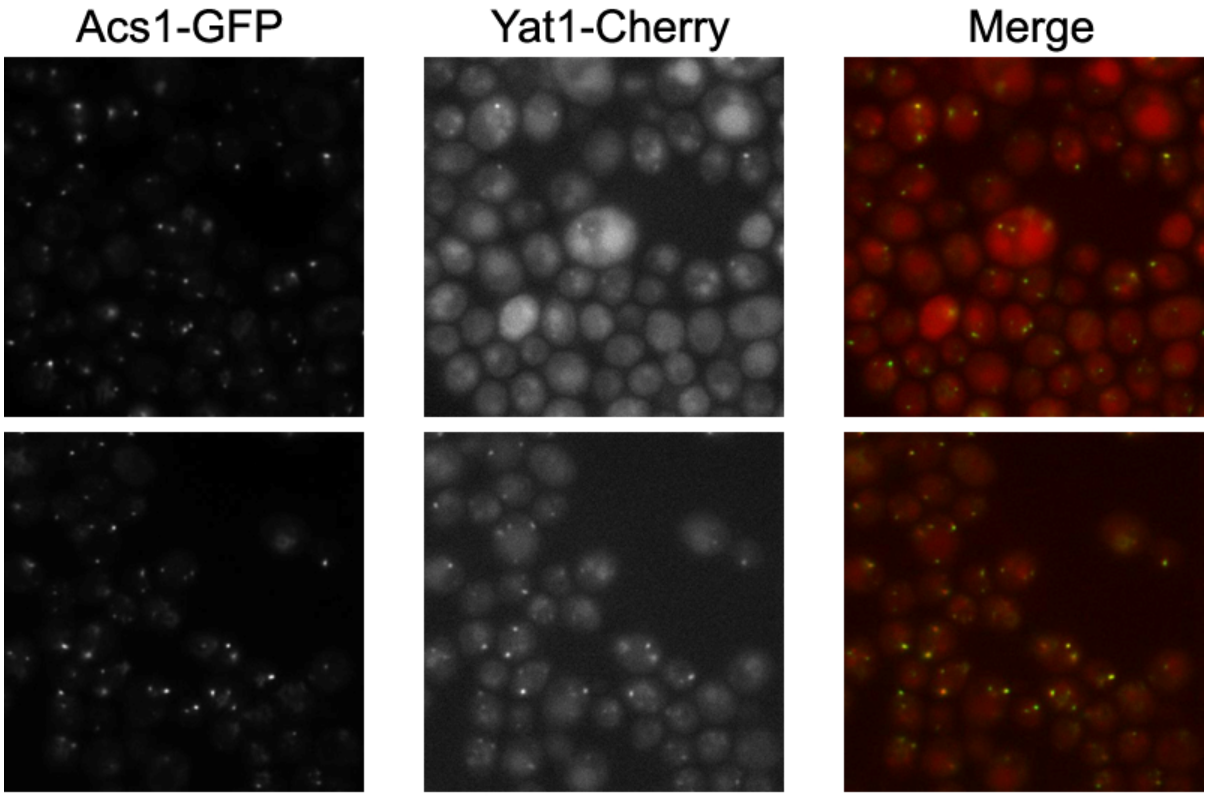

Figure 4.15 Colocalization of Acs1-GFP and Yat1-Cherry
Cells were imaged alive on a glass slide. Acs1-GFP foci formed quickly. In the upper panel, Yat1-Cherry also started forming foci in some but not all the cells. The lower panel were images taken at a later time, Yat1-Cherry foci have formed in all the cells and colocalize nicely with Acs1-GFP foci

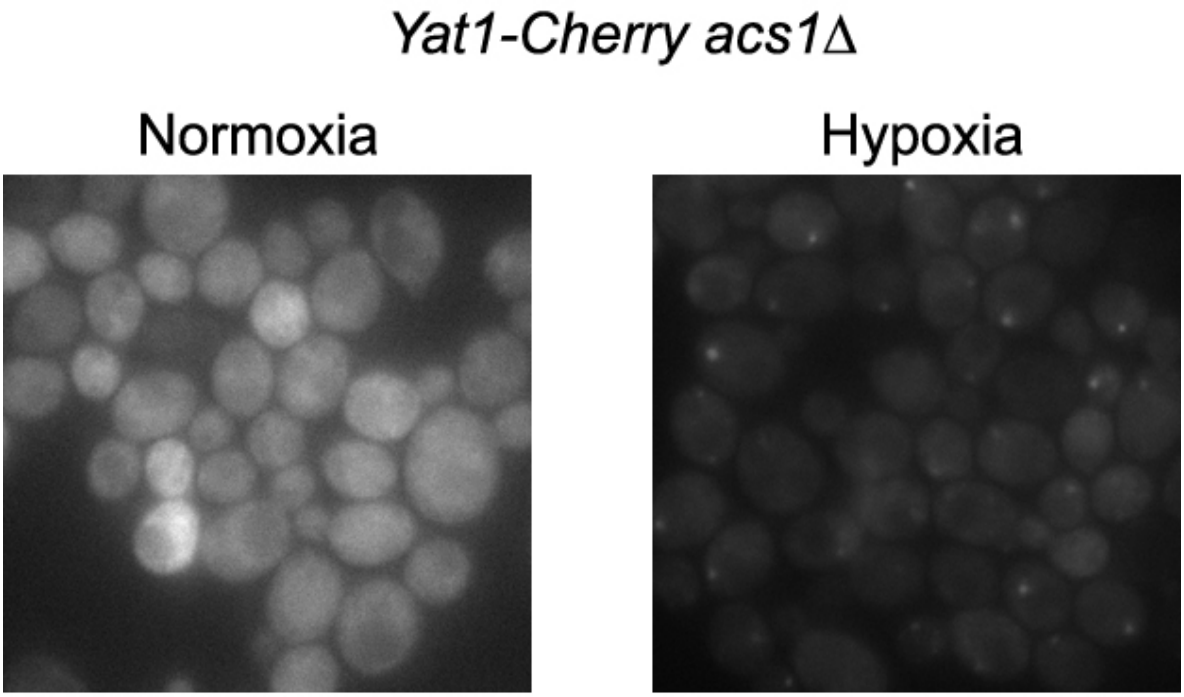

Figure 4.16 Yat1-Cherry can localize to foci under hypoxia in the absence of Acs1p
Images were taken for *Yat1-Cherry acs1*Δ cells, despite the absence of Acs1p, Yat1-Cherry can still localize to foci under hypoxia.

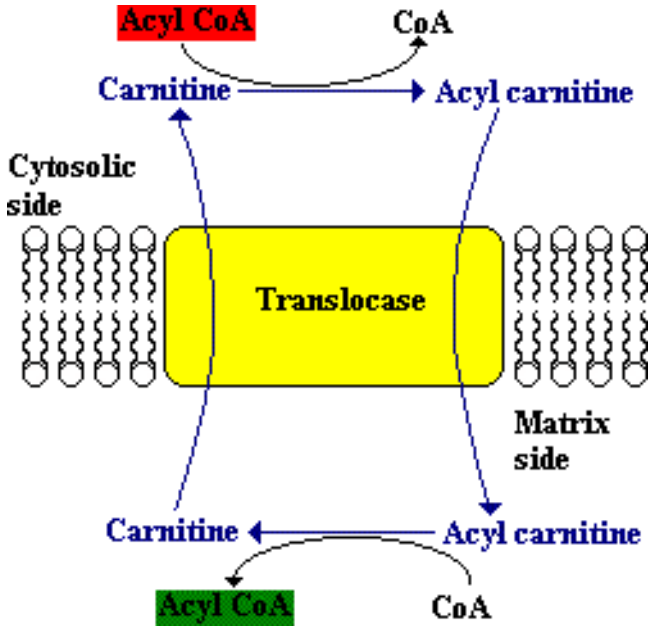

Figure 4.17 Schematic diagram showing carnitine-dependent acetyl-CoA transport from cytosol to mitochondria

Acetyl-CoA can not freely diffuse through membrane structure. Transportation of acetyl-CoA between cytosol and mitochondira is carnitine-dependent. Carnitine acetyl-transferase Yat1p and Yat2p on the mitochondrial outer membrane generates acetyl-carnitine from acetyl-CoA and carnitine, acetyl-carnitine can be transported into the mitochondria through the translocase Crc1p. Once in the mitochondria, acetyl-carnitine can be converted back to acetyl-CoA and carnitine by the mitochondrial acetyl-carnitine transferase Cat2p.

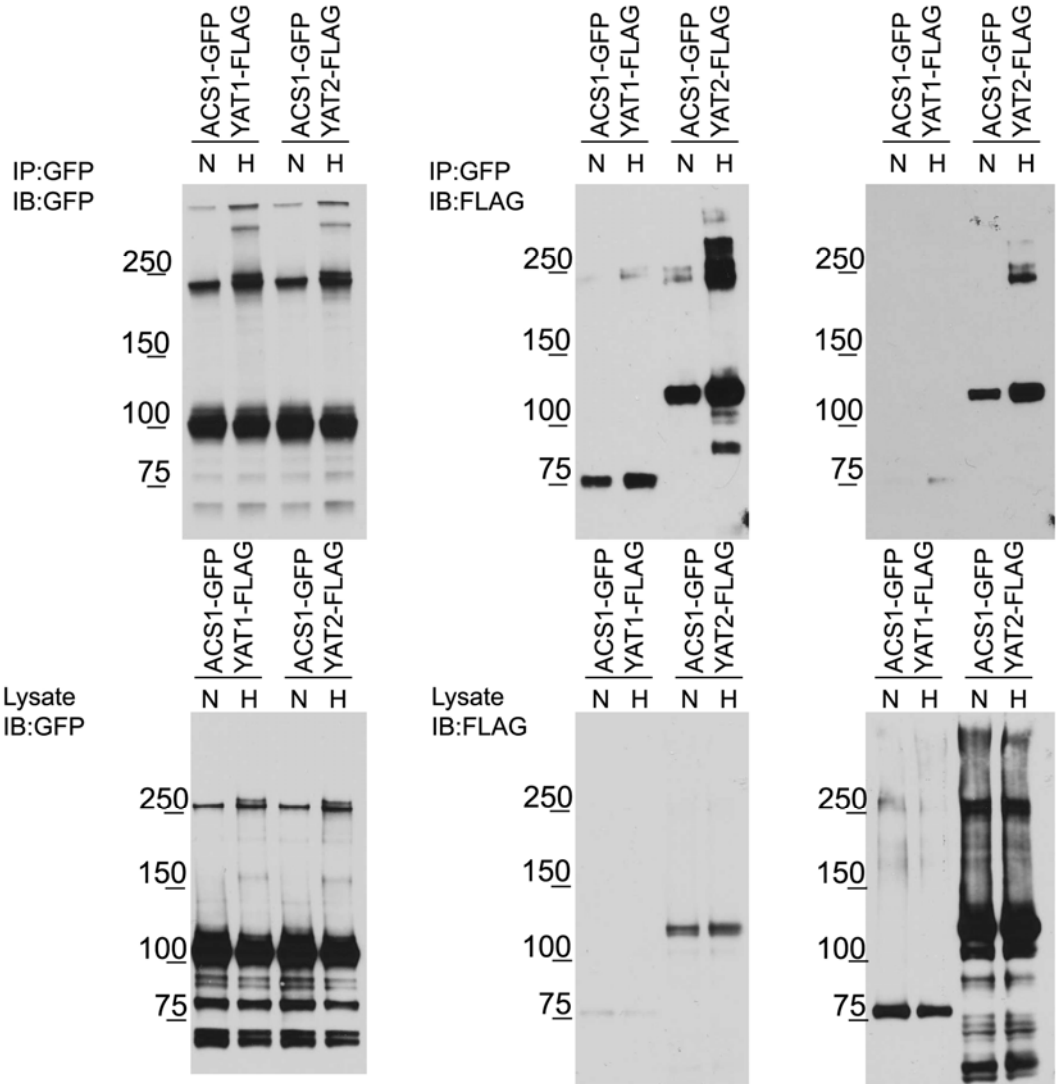

Figure 4.18 Increased interactions between Yat1p, Yat2p and Acs1p.
Cells from indicated strains under normoxia or hypoxia were fixed by paraformaldehyde and lysed for immunoprecipitation. The upper panel shows the immunoprecipitated Acs1-GFP as well as the co-immunoprecipitated Yat1-FLAG or Yat2-FLAG. Two different exposures were shown for the FLAG western blot. More Yat1-FLAG and Yat2-FLAG associate with Acs1-GFP under hypoxia than normoxia. The lower panel shows there are similar amount of protein in the lysate.

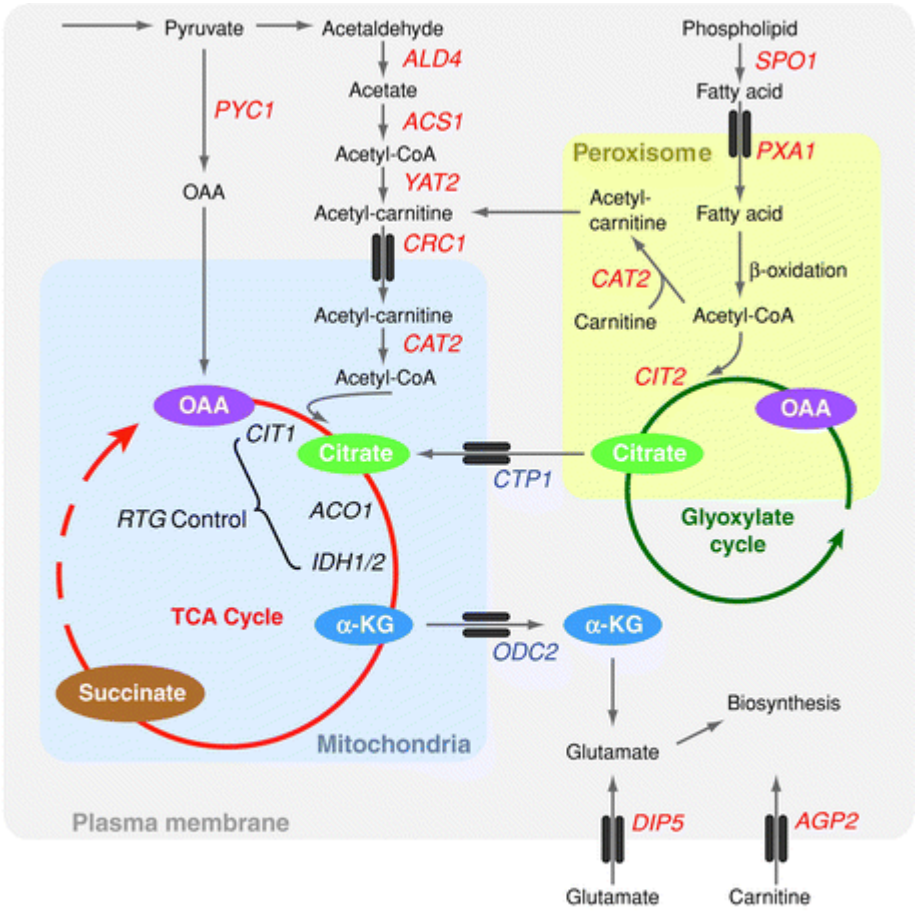

Liu Z, Butow RA. 2006.
Annu. Rev. Genet. 40:159–85

Figure 4.19 Metabolic reconfiguration in respiration-deficient cells

Only genes involved in glutamate biosynthesis and anaplerotic pathways are shown. The broken line in the TCA cycle indicates the block from succinate to oxaloacetic acid (OAA) in respiration-deficient cells. Genes whose expression is elevated in ρ0 cells are indicated in red. A metabolic reconfiguration of the retrograde pathway ensures a sufficient level of α-ketoglutarate for glutamate synthesis to meet the demand of nitrogen supply for biosynthetic reactions (Adapted from Liu Z, Butow RA. 2006).

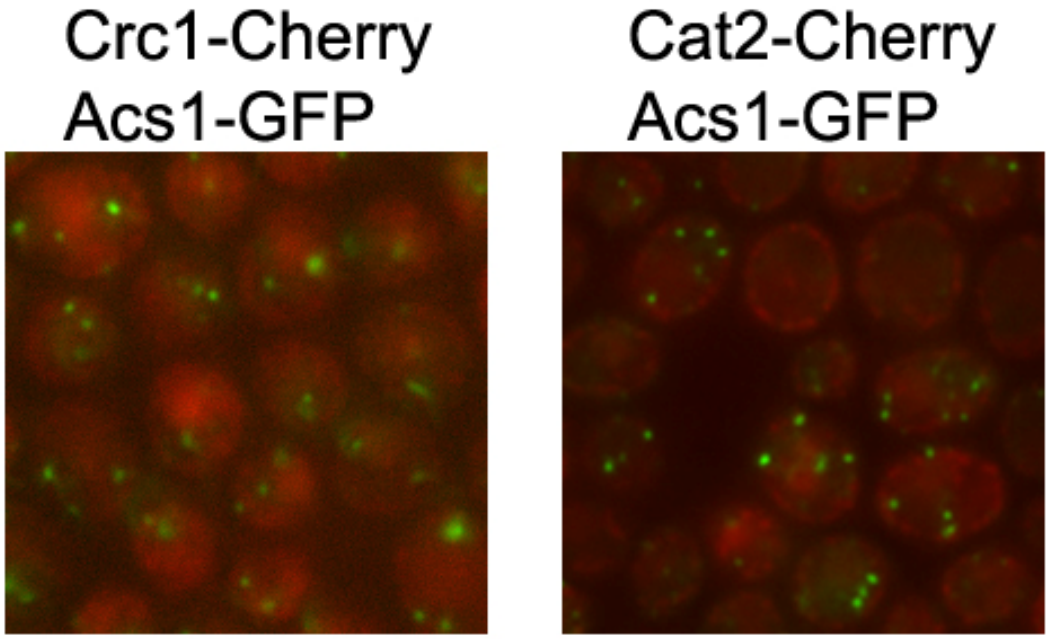

Figure 4.20 Crc1p and Cat2p do not localize to Acs1-GFP foci
Acs1-GFP foci were examined in Crc1-Cherry and Cat2-Cherry strains to check for potential colocalization. However, Crc1-Cherry and Cat2-Cherry do not form foci under the same condition.

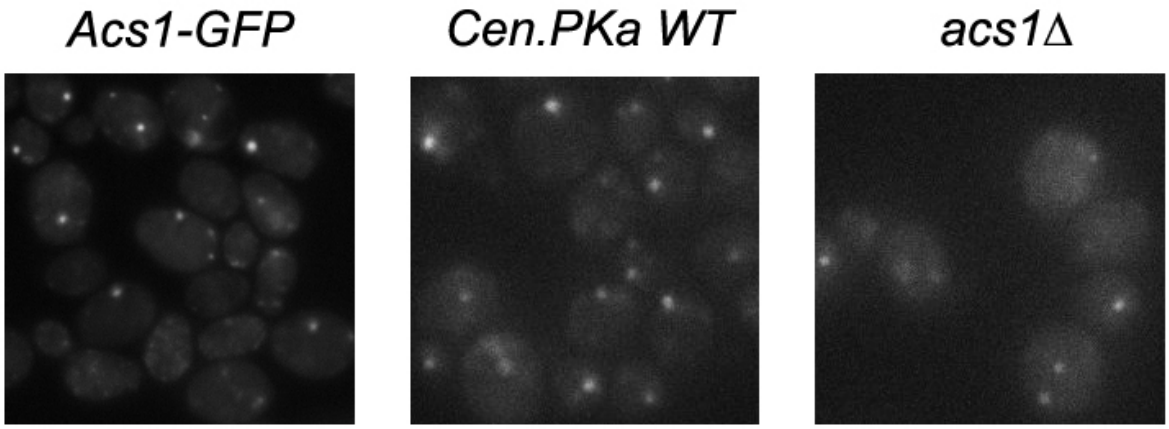

Figure 4.21 ρ0 cells have autofluoresence, foci at GFP channel is an artifact
Mitochondria deficient ρ0 cells were made for *Acs1-GFP, Cen.PKa WT* and *acs1*Δ strains. Foci could be detected in all these cells under FITC channel, but not other channels (DAPI, RFP, etc). Since *Cen.PKa WT* and *acs1*Δ cells still have foci, they are considered as autofluoresence artifact that is different from the Acs1-GFP foci seen previously. We have also found that Acs1p is no longer present in these ρ0 cells by western blot (data not shown).

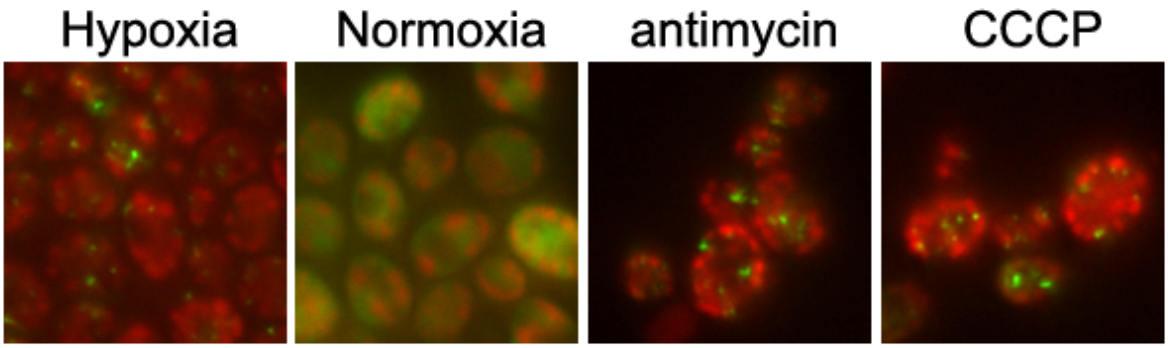

Figure 4.22 Electron transport chain inhibitor can also induce Acs1-GFP foci formation Mitochondria were marked by mito-RFP in red and Acs1-GFP is in green. Cells were grown to saturation in a chemostat and bubbled with nitrogen overnight and the hypoxia sample was cross-linked and collected. At the same time, hypoxic culture was drawn out from the chemostat and placed into three flasks and continued culture in a shaker. After 30 minutes, 10μM antimycin or 10μg/ml CCCP was added to two of the three cultures. Another 30 minutes later, cells from all three flasks were fixed and collected as normoxia, and antimycin or CCCP treated cells. While Acs1-GFP dissipated to cytosol in the normoxia sample, antimycin and CCCP triggered Acs1-GFP foci formation again.

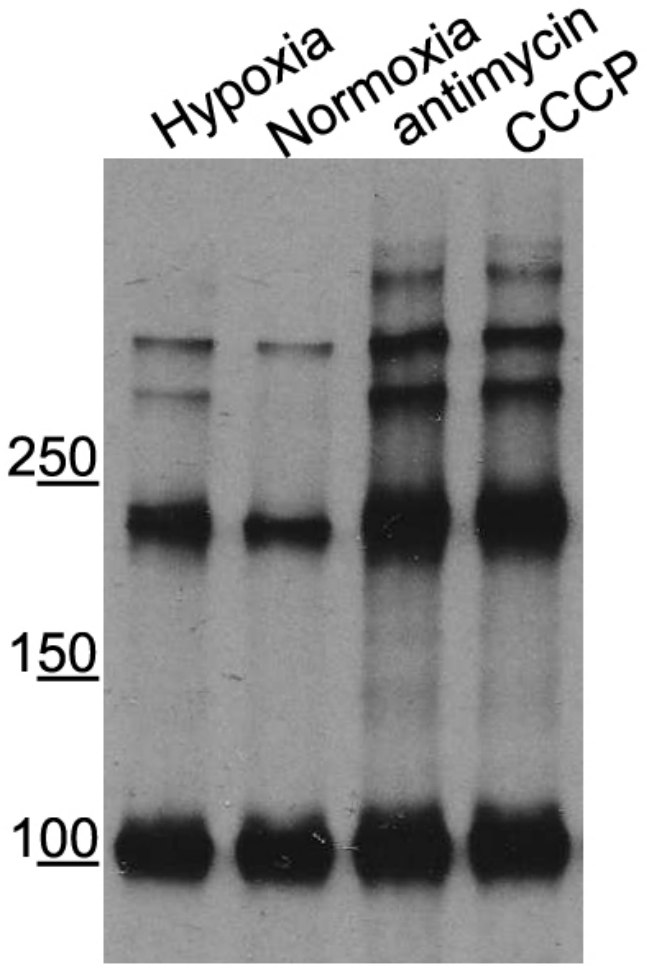

Figure 4.23 Acs1-GFP interacts with additional proteins under hypoxia as well as with antimycin or CCCP treatment

The same samples described in Figure 4.19 were used for immunoprecipitation experiments. Acs1-GFP was immunoprecipiated by anti-GFP antibody and western blot by anti-GFP was shown. The paraformaldehyde crosslinking resulted in multiple extra bands above 100KD (where Acs1-GFP is).

Note that antimycin and CCCP treatment resulted in an increased intensity of the multiple bands, especially those found only under hypoxia.

CHAPTER FIVE
Material and Methods

Antibodies

FLAG(M2): 200472-21 (Sigma)

HA(12CA5): 11583816001 (Roche)

GFP: 11814460001(Roche)

Acetyl-lysine: 9681S(Cell Signaling), ICP0380(ImmuneChem), ST1027(Calbiochem)

RXXS*/T*(100G7E): 9624S(Cell Signaling)

H3: 05-928 (Millipore)

H3K9ac: 06-942 (Millipore)

H3K14ac: 07-353 (Millipore)

H3K18ac: 07-354 (Millipore)

H3K23ac: 07-355 (Millipore)

H3K27ac: 07-360 (Millipore)

H3K56ac: 07-677 (Millipore)

H3K4triMe: ab8580 (Abcam)

H4K5ac: 07-327 (Millipore)

H4K8ac: 07-328 (Millipore)

H4K12ac: 07-595 (Millipore)

H4K16ac: 07-329 (Millipore)

Yeast Strains and Methods

All yeast strains were constructed in the CEN.PK background (van Dijken et al., 2000). Gene deletion strains were constructed by replacing the target gene with a drug cassette by homologous recombination (Longtine et al., 1998). C-terminal tagging of genes was also performed by homologous recombination followed by drug selection. Site-directed mutagenesis was performed by PCR in which primers containing the mutation were used to generate two PCR fragments that contain ~45 bp overlapping regions containing the mutation. Fusion PCR or isothermal assembly (Gibson et al., 2009) was then performed to fuse the fragments together and the product was used for transformation. The introduced mutations and the full-length gene sequences were verified by DNA sequencing.

Yeast Cell Lysis and Immunoprecipitation

Typically ~100 OD yeast cells were lysed in 1 ml lysis buffer (100 mM Tris-Cl pH 7.5, 100 mM NaCl, 50 mM NaF, 1 mM EDTA, 1 mM EGTA, 0.1% Tween-20, 10% glycerol, 50 mM sodium butyrate, 50 mM nicotinamide, 5 μM trichostatin A, 1 mM PMSF, 10 μM leupeptin, 5 μM pepstatin A, Roche protease inhibitor cocktail, 14 mM β-mercaptoethanol) by bead beating and immunoprecipitation was performed by incubating the lysate with 15 μl magnetic beads (Invitrogen) conjugated to 2 μg antibody for 3 hours. After washing 3 times in the same buffer, the beads were boiled. Alternatively, for FLAG IP, proteins could be eluted off the beads by 3xFLAG peptide.

Screening for newly acetylated protein in YMC

Identification of acetylated proteins by affinity purification of the acetylated peptides was performed largely according to a previously published protocol (Kim et al., 2006). Briefly, cycling cells were harvested at both 1 and 3.5 minutes following acetate addition. Lysates were prepared as described previously and ~10 mg total protein was precipitated and washed with acetone. The pellet was sonicated and then resuspended in NH4HCO3 buffer. Trypsin (Promega) was added at a ratio of 1:50 (w/w) to digest the peptides overnight at 37°C with gentle shaking. Reduction and alkylation of digested peptides was performed followed by an additional trypsin digestion for 3 hours. Antibodies against acetyl-lysine (Cell Signaling #9681 and Immunechem #ICP0380) were added to the peptide mixture and incubated overnight at 4°C. Beads were added to harvest the antibody-bound acetylated peptides. After five washes, peptides were eluted using 0.1% TFA and filtered through a Microcon YM-10 column and the eluate was dried down. The digests were then dissolved in a 5% formic acid aqueous solution. Two independent LC-MS/MS runs were performed to identify putative acetylated peptides. The LC-MS/MS data of two runs were combined and searched against NCBI nr-Saccharomyces cerevisiae database. Modifications included in the database searching were: Acetyl (K), Acetyl (+44) (K), Carbamidomethyl (C), Deamidation (NQ), Oxidation (M). To verify acetylated targets, candidate genes were FLAG-tagged at the C-terminus. Immunoprecipitation of the tagged protein from cells grown to log phase in YPGE (YP + glycerol, ethanol) culture was performed followed by Western blot using an antibody against acetyl-lysine (Immunechem #ICP0380) to confirm acetylation of the candidate protein. To determine whether the candidate protein was dynamically acetylated, cells were collected over 12 time points of the YMC and analyzed similarly.

Histone Western Blots

Western blots to detect histone modifications at the bulk level were performed using a protocol adapted from previously published studies (Keogh et al., 2006). Briefly, 1 ml of cycling cells were quickly spun down, washed with 20% TCA, and then flash frozen. The frozen pellet was resuspended in 20% TCA and lysed by bead beating. Lysate and precipitate/debris was mixed with 1 ml 5% TCA and pelleted. The pellet was washed with 0.75 ml 100% cold ethanol and resuspended in 150 µl loading buffer (50 µl 1 M Tris-Cl pH 8.0, 92.5 µl 3X SDS sample buffer and 7.5 µl 100% β-mercaptoethanol) and boiled for 5 min. The supernatant was collected and then proteins were separated using 15% SDS-PAGE. Western blots were performed using the following commercially available antibodies that are highly specific for the indicated modifications (Suka et al., 2001).

Silverstaining

Silverstaining was performed using SilverQuest from Invitrogen.

Chromatin Immunoprecipitation (ChIP)

Chromatin immunoprecipitation was performed according to a well-established protocol with minor modifications (Ezhkova and Tansey, 2006). Briefly, ~50 OD cycling cells collected from the appropriate time point were rapidly fixed in 1% formaldehyde for 15 min in 50 ml total volume and then quenched using 3 ml 2.5 M glycine for 10 min. The fixed cells were pelleted and washed twice with buffer containing 100 mM NaCl, 10 mM Tris-Cl pH 8.0, 1

mM EDTA, 1 mM PMSF, 1 mM benzamidine•HCl before freezing. The frozen pellet was resuspended in 0.45 ml ChIP lysis buffer (50 mM HEPES•KOH pH 7.5, 500 mM NaCl, 1 mM EDTA, 1% Triton X-100, 0.1% deoxycholate (DOC), 0.1% SDS, 1 mM PMSF, 10 µM leupeptin, 5 µM pepstatin A, Roche protease inhibitor cocktail) and lysed by bead beating. Lysate from 50 OD cells were split into two tubes each containing 280 µl lysate and sonicated for 16 cycles (30 sec on, 1 min off, high output) using a Bioruptor (Diagenode). The supernatant of the sonicated lysate was pre-cleared. 50 µl lysate was saved as input. For ChIP with histone antibodies, 50 µl whole cell extract (WCE) was diluted 1:10 and used for each ChIP. For SAGA ChIP, 500 µl WCE and 2 µg Flag M2 antibody was used. After incubation overnight, 20 µl magnetic beads resuspended in ChIP lysis buffer was added and incubated for 1.5 h. Beads were washed twice with ChIP lysis buffer, once with DOC buffer (10 mM Tris•Cl pH 8.0, 0.25 M LiCl, 0.5% DOC, 1 mM EDTA) and once with TE. 60 µl of TES buffer (50 mM Tris-Cl pH 8.0, 10 mM EDTA, 1% SDS) was added to resuspend the beads. Supernatant was collected after incubation at 65°C for 10 min. A second round of elution was performed and the eluates were combined. 150 µl TES was added to the input sample. Reverse crosslinking was performed for the ChIP and input sample by incubating for 6 hours at 65°C. An equal volume of TE containing 1.25 mg/ml proteinase K was added to the samples after reverse crosslinking and samples were incubated for 2 hours at 37°C. DNA was then purified with a QIAquick PCR purification kit. Real-time PCR was performed in triplicate using SYBR green reagents from Applied Biosystems. PCR primers were designed by Primer Express software from Applied Biosystems to target every ~250 bp region from -750 bp before to 750 bp after the start codon of the selected gene.

ChIP-Seq

Library construction was performed using a protocol from the following website:http://bioinfo.mbb.yale.edu/array/Solexa_LibraryPrep_20080229ge.pdf

ChIP-Seq libraries of H3K9ac and H3 were constructed using barcoded adaptors and four samples were multiplexed to run in a single lane. Libraries of SAGA and input were not multiplexed and each was run in a single lane. End repair was performed followed by adding 'A' base to 3' ends. Adaptors were ligated to DNA fragments. Barcoded adaptors were used to generate samples for multiplexing while non-barcode adaptors were used for samples run on single lanes. After ligation, DNA fragments about 200 bp were excised from the agarose gel and used for PCR. PCR products ~250 bp in size were gel-extracted and quantified using PicoGreen (Invitrogen). Samples were run on an Agilent Bioanalyzer to obtain precise size information for appropriate dilution of the DNA. Sequencing was performed on an Illumina GA IIX supervised by the UTSW Microarray Core Facility. More than 5 million mapped reads were obtained for each of the multiplexed samples and more than 20 million for the samples run on a single lane. H3K9ac/H3 data was analyzed using CLC Genomics Workbench software. Peaks were called with a maximum FDR = 1% and maximum p-value for Wilcoxon test = 1.0E-4. SAGA/Input data was assembled to the reference genome by Bowtie and analyzed by CisGenome as described in its online tutorial (Ji et al., 2008). Peaks with a fold-enrichment value max|FC| above 2 (>4-fold change) were selected. Peaks were annotated with the gene whose transcription start site (TSS) is closest to the peak region. The CisGenome browser was used to visualize ChIP-Seq peaks (Ji et al., 2008).

In vitro HAT Assay

SAGA was immunoprecipitated from OX and RC phase of the YMC as described above. Beads were washed twice with HAT buffer (50 mM Tris•Cl pH 8.0, 1 mM DTT, 5% glycerol, 1 mM PMSF, 0.03% NP-40) and incubated with HeLa core histones or long oligonucleosomes in the presence of 3H-acetyl-CoA in HAT buffer at 30°C for 1 hr. The reaction was spotted onto phosphocellulose filter paper, dried and washed twice with 50 mM NaHCO3-Na2CO3 buffer (pH 9.2), and rinsed with acetone. The dried filter paper was placed into vials for liquid scintillation counting to quantitate 3H signal.

Metabolic Cycles and Metabolite Analysis

Chemostat growth, metabolite extraction, and LC-MS/MS analysis of cellular metabolites were performed as described previously (Tu et al., 2005; Tu et al., 2007).

Real-Time PCR Analysis of mRNA Expression

RNA preparation was performed as described previously (Tu et al., 2005). 1 μg RNA was reverse transcribed into cDNA in 50 □l volume using Superscript II from Invitrogen and the final product was diluted 1:25. Real-time PCR was performed in triplicate. Transcript levels of selected genes were normalized against actin (ACT1).

Mapping by Cleavage at Cyanylated Cysteines

Immunoprecipitated Ifh1p bound to magnetic beads was resuspended in reaction buffer (0.1M Tris Acetate, pH 8.0 and 8M GnCl). 2-nitro-5-thiocyanobenzoic acid (NTCB) was

added to 1mM and the reaction was incubated at room temperature for 30min. NaOH was added to adjust pH to 9.0 and the reaction was incubated at 37°C overnight. The reaction was boiled and run on a 3-8% Tris-Acetate precast gel.

Lifespan assays

Replicative lifespan (RLS) assays were carried out as described previously (Steffen et al., 2009). Unless otherwise noted, all lifespan experiments were performed on YPD plates with 2% glucose. The BY strain background was used for RLS assays.

Crosslinking

16% freshly opened paraformaldehyde was added to culture to a final concentration of 2%. Cells were incubated for 10 minutes and spinned down. Supernatant was discarded. The cell pellet was washed with potassium phosphate buffer (0.1M pH 6.6) and pelleted again. For imaging, the pellet was resuspended in the same potassium phosphate buffer and kept in 4°C till used. For immunoprecipitation, the pellet was flash frozen and kept at -80°C till used.

Generation of ρ0 cells

Cells were cultured in YPD to log phase and ethidium bromide was added to a final concentration of 25μg/ml. After overnight incubation, cells were streaked on to a new YPD plate. A single colony was inoculated into YPD and after overnight growth, cells were pelleted and washed and resuspended in YPGE medium. After 5-6 hours, cells were fixed for imaging.

BIBLIOGRAPHY

Balasubramanian, R., Pray-Grant, M.G., Selleck, W., Grant, P.A., and Tan, S. (2002). Role of the Ada2 and Ada3 transcriptional coactivators in histone acetylation. J Biol Chem *277*, 7989-7995.

Berndsen, C.E., and Denu, J.M. (2008). Catalysis and substrate selection by histone/protein lysine acetyltransferases. Curr Opin Struct Biol *18*, 682-689.

Brownell, J.E., Zhou, J., Ranalli, T., Kobayashi, R., Edmondson, D.G., Roth, S.Y., and Allis, C.D. (1996). Tetrahymena histone acetyltransferase A: a homolog to yeast Gcn5p linking histone acetylation to gene activation. Cell *84*, 843-851.

Cai, L., Sutter, B.M., Li, B., and Tu, B.P. (2011). Acetyl-CoA induces cell growth and proliferation by promoting the acetylation of histones at growth genes. Mol Cell *42*, 426-437.

Cai, L., and Tu, B.P. (2012). Driving the cell cycle through metabolism. Annu Rev Cell Dev Biol *28*, 59-87.

Chen, Z., Odstrcil, E.A., Tu, B.P., and McKnight, S.L. (2007). Restriction of DNA replication to the reductive phase of the metabolic cycle protects genome integrity. Science *316*, 1916-1919.

Choudhary, C., Kumar, C., Gnad, F., Nielsen, M.L., Rehman, M., Walther, T.C., Olsen, J.V., and Mann, M. (2009). Lysine acetylation targets protein complexes and co-regulates major cellular functions. Science *325*, 834-840.

DeBerardinis, R.J., Lum, J.J., Hatzivassiliou, G., and Thompson, C.B. (2008). The biology of cancer: metabolic reprogramming fuels cell growth and proliferation. Cell metabolism *7*, 11-20.

Delaney, J.R., Sutphin, G.L., Dulken, B., Sim, S., Kim, J.R., Robison, B., Schleit, J., Murakami, C.J., Carr, D., An, E.H.*, et al.* (2011). Sir2 deletion prevents lifespan extension in 32 long-lived mutants. Aging Cell *10*, 1089-1091.

Epstein, C.B., Waddle, J.A., Hale, W.t., Dave, V., Thornton, J., Macatee, T.L., Garner, H.R., and Butow, R.A. (2001). Genome-wide responses to mitochondrial dysfunction. Mol Biol Cell *12*, 297-308.

Fabrizio, P., Pletcher, S.D., Minois, N., Vaupel, J.W., and Longo, V.D. (2004). Chronological aging-independent replicative life span regulation by Msn2/Msn4 and Sod2 in Saccharomyces cerevisiae. FEBS Lett *557*, 136-142.

Friis, R.M., Wu, B.P., Reinke, S.N., Hockman, D.J., Sykes, B.D., and Schultz, M.C. (2009). A glycolytic burst drives glucose induction of global histone acetylation by picNuA4 and SAGA. Nucleic Acids Res *37*, 3969-3980.

Gamper, A.M., Kim, J., and Roeder, R.G. (2009). The STAGA subunit ADA2b is an important regulator of human GCN5 catalysis. Mol Cell Biol *29*, 266-280.

Grant, P.A., Duggan, L., Cote, J., Roberts, S.M., Brownell, J.E., Candau, R., Ohba, R., Owen-Hughes, T., Allis, C.D., Winston, F.*, et al.* (1997). Yeast Gcn5 functions in two multisubunit complexes to acetylate nucleosomal histones: characterization of an Ada complex and the SAGA (Spt/Ada) complex. Genes Dev *11*, 1640-1650.

Grant, P.A., Eberharter, A., John, S., Cook, R.G., Turner, B.M., and Workman, J.L. (1999). Expanded lysine acetylation specificity of Gcn5 in native complexes. J Biol Chem *274*, 5895-5900.

Hartwell, L.H., and Unger, M.W. (1977). Unequal division in Saccharomyces cerevisiae and its implications for the control of cell division. J Cell Biol *75*, 422-435.

Helenius, A., and Aebi, M. (2001). Intracellular functions of N-linked glycans. Science *291*, 2364-2369.

Henry, K.W., Wyce, A., Lo, W.S., Duggan, L.J., Emre, N.C., Kao, C.F., Pillus, L., Shilatifard, A., Osley, M.A., and Berger, S.L. (2003). Transcriptional activation via sequential histone H2B ubiquitylation and deubiquitylation, mediated by SAGA-associated Ubp8. Genes Dev *17*, 2648-2663.

Hinnebusch, A.G. (2005). Translational regulation of GCN4 and the general amino acid control of yeast. Annu Rev Microbiol *59*, 407-450.

Huber, A., Bodenmiller, B., Uotila, A., Stahl, M., Wanka, S., Gerrits, B., Aebersold, R., and Loewith, R. (2009). Characterization of the rapamycin-sensitive phosphoproteome reveals that Sch9 is a central coordinator of protein synthesis. Genes Dev *23*, 1929-1943.

Huber, A., French, S.L., Tekotte, H., Yerlikaya, S., Stahl, M., Perepelkina, M.P., Tyers, M., Rougemont, J., Beyer, A.L., and Loewith, R. (2011). Sch9 regulates ribosome biogenesis via Stb3, Dot6 and Tod6 and the histone deacetylase complex RPD3L. EMBO J *30*, 3052-3064.

Huisinga, K.L., and Pugh, B.F. (2004). A genome-wide housekeeping role for TFIID and a highly regulated stress-related role for SAGA in Saccharomyces cerevisiae. Mol Cell *13*, 573-585.

Ji, H., Jiang, H., Ma, W., Johnson, D.S., Myers, R.M., and Wong, W.H. (2008). An integrated software system for analyzing ChIP-chip and ChIP-seq data. Nat Biotechnol *26*, 1293-1300.

Jorgensen, P., Nishikawa, J.L., Breitkreutz, B.J., and Tyers, M. (2002). Systematic identification of pathways that couple cell growth and division in yeast. Science *297*, 395-400.

Jorgensen, P., and Tyers, M. (2004). How cells coordinate growth and division. Curr Biol *14*, R1014-1027.

Kaeberlein, M., Powers, R.W., 3rd, Steffen, K.K., Westman, E.A., Hu, D., Dang, N., Kerr, E.O., Kirkland, K.T., Fields, S., and Kennedy, B.K. (2005). Regulation of yeast replicative life span by TOR and Sch9 in response to nutrients. Science *310*, 1193-1196.

Kim, J.H., Saraf, A., Florens, L., Washburn, M., and Workman, J.L. (2010). Gcn5 regulates the dissociation of SWI/SNF from chromatin by acetylation of Swi2/Snf2. Genes Dev *24*, 2766-2771.

Kohler, A., Schneider, M., Cabal, G.G., Nehrbass, U., and Hurt, E. (2008). Yeast Ataxin-7 links histone deubiquitination with gene gating and mRNA export. Nat Cell Biol *10*, 707-715.

Kurdistani, S.K., Tavazoie, S., and Grunstein, M. (2004). Mapping global histone acetylation patterns to gene expression. Cell *117*, 721-733.

Langer, M.R., Fry, C.J., Peterson, C.L., and Denu, J.M. (2002). Modulating acetyl-CoA binding in the GCN5 family of histone acetyltransferases. J Biol Chem *277*, 27337-27344.
Lee, K.K., and Workman, J.L. (2007). Histone acetyltransferase complexes: one size doesn't fit all. Nat Rev Mol Cell Biol *8*, 284-295.
Liko, D., Conway, M.K., Grunwald, D.S., and Heideman, W. (2010). Stb3 plays a role in the glucose-induced transition from quiescence to growth in Saccharomyces cerevisiae. Genetics *185*, 797-810.
Lin, S.J., Defossez, P.A., and Guarente, L. (2000). Requirement of NAD and SIR2 for life-span extension by calorie restriction in Saccharomyces cerevisiae. Science *289*, 2126-2128.
Lippman, S.I., and Broach, J.R. (2009). Protein kinase A and TOR activate genes for ribosomal biogenesis by inactivating repressors encoded by Dot6 and its homolog Tod6. Proc Natl Acad Sci U S A *106*, 19928-19933.
Liu, Z., and Butow, R.A. (2006). Mitochondrial retrograde signaling. Annu Rev Genet *40*, 159-185.
Longo, V.D., Shadel, G.S., Kaeberlein, M., and Kennedy, B. (2012). Replicative and chronological aging in Saccharomyces cerevisiae. Cell Metab *16*, 18-31.
Martineau, Y., Le Bec, C., Monbrun, L., Allo, V., Chiu, I.M., Danos, O., Moine, H., Prats, H., and Prats, A.C. (2004). Internal ribosome entry site structural motifs conserved among mammalian fibroblast growth factor 1 alternatively spliced mRNAs. Mol Cell Biol *24*, 7622-7635.
Masumoto, H., Hawke, D., Kobayashi, R., and Verreault, A. (2005). A role for cell-cycle-regulated histone H3 lysine 56 acetylation in the DNA damage response. Nature *436*, 294-298.
Mischerikow, N., Spedale, G., Altelaar, A.F., Timmers, H.T., Pijnappel, W.W., and Heck, A.J. (2009). In-depth profiling of post-translational modifications on the related transcription factor complexes TFIID and SAGA. J Proteome Res *8*, 5020-5030.
Novick, A., and Szilard, L. (1950). Description of the chemostat. Science *112*, 715-716.
Pokholok, D.K., Harbison, C.T., Levine, S., Cole, M., Hannett, N.M., Lee, T.I., Bell, G.W., Walker, K., Rolfe, P.A., Herbolsheimer, E., *et al.* (2005). Genome-wide map of nucleosome acetylation and methylation in yeast. Cell *122*, 517-527.
Robert, F., Pokholok, D.K., Hannett, N.M., Rinaldi, N.J., Chandy, M., Rolfe, A., Workman, J.L., Gifford, D.K., and Young, R.A. (2004). Global position and recruitment of HATs and HDACs in the yeast genome. Mol Cell *16*, 199-209.
Rolland, F., Winderickx, J., and Thevelein, J.M. (2002). Glucose-sensing and -signalling mechanisms in yeast. FEMS Yeast Res *2*, 183-201.
Rudra, D., Mallick, J., Zhao, Y., and Warner, J.R. (2007). Potential interface between ribosomal protein production and pre-rRNA processing. Mol Cell Biol *27*, 4815-4824.
Rudra, D., Zhao, Y., and Warner, J.R. (2005). Central role of Ifh1p-Fhl1p interaction in the synthesis of yeast ribosomal proteins. EMBO J *24*, 533-542.

Sandmeier, J.J., French, S., Osheim, Y., Cheung, W.L., Gallo, C.M., Beyer, A.L., and Smith, J.S. (2002). RPD3 is required for the inactivation of yeast ribosomal DNA genes in stationary phase. EMBO J *21*, 4959-4968.

Schawalder, S.B., Kabani, M., Howald, I., Choudhury, U., Werner, M., and Shore, D. (2004). Growth-regulated recruitment of the essential yeast ribosomal protein gene activator Ifh1. Nature *432*, 1058-1061.

Sonveaux, P., Vegran, F., Schroeder, T., Wergin, M.C., Verrax, J., Rabbani, Z.N., De Saedeleer, C.J., Kennedy, K.M., Diepart, C., Jordan, B.F.*, et al.* (2008). Targeting lactate-fueled respiration selectively kills hypoxic tumor cells in mice. J Clin Invest *118*, 3930-3942.

Steffen, K.K., MacKay, V.L., Kerr, E.O., Tsuchiya, M., Hu, D., Fox, L.A., Dang, N., Johnston, E.D., Oakes, J.A., Tchao, B.N.*, et al.* (2008). Yeast life span extension by depletion of 60s ribosomal subunits is mediated by Gcn4. Cell *133*, 292-302.

Suka, N., Suka, Y., Carmen, A.A., Wu, J., and Grunstein, M. (2001). Highly specific antibodies determine histone acetylation site usage in yeast heterochromatin and euchromatin. Mol Cell *8*, 473-479.

Takahashi, H., McCaffery, J.M., Irizarry, R.A., and Boeke, J.D. (2006). Nucleocytosolic acetyl-coenzyme a synthetase is required for histone acetylation and global transcription. Mol Cell *23*, 207-217.

Trievel, R.C., Rojas, J.R., Sterner, D.E., Venkataramani, R.N., Wang, L., Zhou, J., Allis, C.D., Berger, S.L., and Marmorstein, R. (1999). Crystal structure and mechanism of histone acetylation of the yeast GCN5 transcriptional coactivator. Proc Natl Acad Sci U S A *96*, 8931-8936.

Tu, B.P., Kudlicki, A., Rowicka, M., and McKnight, S.L. (2005). Logic of the yeast metabolic cycle: temporal compartmentalization of cellular processes. Science *310*, 1152-1158.

Tu, B.P., and McKnight, S.L. (2009). Evidence of carbon monoxide-mediated phase advancement of the yeast metabolic cycle. Proc Natl Acad Sci U S A *106*, 14293-14296.

Tu, B.P., Mohler, R.E., Liu, J.C., Dombek, K.M., Young, E.T., Synovec, R.E., and McKnight, S.L. (2007). Cyclic changes in metabolic state during the life of a yeast cell. Proc Natl Acad Sci U S A *104*, 16886-16891.

Tu, B.P., and Wang, J.C. (1999). Protein footprinting at cysteines: probing ATP-modulated contacts in cysteine-substitution mutants of yeast DNA topoisomerase II. Proc Natl Acad Sci U S A *96*, 4862-4867.

van den Berg, M.A., de Jong-Gubbels, P., Kortland, C.J., van Dijken, J.P., Pronk, J.T., and Steensma, H.Y. (1996). The two acetyl-coenzyme A synthetases of Saccharomyces cerevisiae differ with respect to kinetic properties and transcriptional regulation. J Biol Chem *271*, 28953-28959.

Wade, J.T., Hall, D.B., and Struhl, K. (2004). The transcription factor Ifh1 is a key regulator of yeast ribosomal protein genes. Nature *432*, 1054-1058.

Wang, Q., Zhang, Y., Yang, C., Xiong, H., Lin, Y., Yao, J., Li, H., Xie, L., Zhao, W., Yao, Y.*, et al.* (2010). Acetylation of metabolic enzymes coordinates carbon source utilization and metabolic flux. Science *327*, 1004-1007.

Warner, J.R. (1999). The economics of ribosome biosynthesis in yeast. Trends Biochem Sci *24*, 437-440.
Wellen, K.E., Hatzivassiliou, G., Sachdeva, U.M., Bui, T.V., Cross, J.R., and Thompson, C.B. (2009). ATP-citrate lyase links cellular metabolism to histone acetylation. Science *324*, 1076-1080.
Wu, M., Newcomb, L., and Heideman, W. (1999). Regulation of gene expression by glucose in Saccharomyces cerevisiae: a role for ADA2 and ADA3/NGG1. J Bacteriol *181*, 4755-4760.
Wu, P.Y., and Winston, F. (2002). Analysis of Spt7 function in the Saccharomyces cerevisiae SAGA coactivator complex. Mol Cell Biol *22*, 5367-5379.
Xu, F., Zhang, K., and Grunstein, M. (2005). Acetylation in histone H3 globular domain regulates gene expression in yeast. Cell *121*, 375-385.
Zaman, S., Lippman, S.I., Schneper, L., Slonim, N., and Broach, J.R. (2009). Glucose regulates transcription in yeast through a network of signaling pathways. Mol Syst Biol *5*, 245.
Zaman, S., Lippman, S.I., Zhao, X., and Broach, J.R. (2008). How Saccharomyces responds to nutrients. Annu Rev Genet *42*, 27-81.
Zhang, W., Bone, J.R., Edmondson, D.G., Turner, B.M., and Roth, S.Y. (1998). Essential and redundant functions of histone acetylation revealed by mutation of target lysines and loss of the Gcn5p acetyltransferase. EMBO J *17*, 3155-3167.
Zhao, S., Xu, W., Jiang, W., Yu, W., Lin, Y., Zhang, T., Yao, J., Zhou, L., Zeng, Y., Li, H.*, et al.* (2010). Regulation of cellular metabolism by protein lysine acetylation. Science *327*, 1000-1004.